SUPRAMOLECULAR DERIVATISATION OF BIOACTIVE MOLECULES VIA CO-CRYSTALLIZATION AND CYCLODEXTRIN INCLUSION COMPLEXATION

Andrea Sala

Dissertation presented for the degree of Master of Science in Chemistry

In the Department of Chemical Sciences, Life Sciences, and Environmental Sustainability of the

University of Parma and Department of Chemistry of the University of Cape Town

February 2018

Supervisors: Professor Mino R. Caira and Professor Alessia Bacchi

ACKNOWLEDGMENTS

My special thanks to:

Professor Mino Caira for his excellent supervision, infinite patience and support. His passion, curiosity and energy for the research, made this experience unique!

Professor Alessia Bacchi for her co-supervision, guidance, encouragement and, always present, great support. Thank you very much for making this adventure possible.

Professor Luigi Nassimbeni for creating a beautiful working atmosphere and for have felt in me the desire to travel across Africa.

All the colleagues at the Centre for Supramolecular Chemistry Research for their kindness and encouragement, mainly Dr Laurelle Joseph for her patience and willingness.

Françoise, Jacky and Ana for the *hard* work in the laboratory and all the international cooking lessons. Without your friendship this experience would not have been the same!

The large group of people with whom I shared my time Anna, Riccardo, Sherpherd, Giaocomo, Marcello, Thato, Olaulu, Dylan and Cody.

Matteo to be my greatest friend and ally, to be my shoulder, my strength and my happiness during this experience and in life.

Giulia, with her adorable madness, that with Davide, Francesco, Valentina, Carlotta and Luca, helped make the world a little smaller making me feel at home all the time.

Nima (with his big hugs and his 'small cokes'), Daniele, Alice, Giulia, Laura, Sara and Federico to be great friends and to always be present by my side.

My family to whom I would like to dedicate this work, to be my biggest support and my guide.

ABSTRACT

The objective of this study was to modify the physicochemical properties of two common drugs *via* supramolecular derivatization. Sulfasalazine is a powerful anti-inflammatory drug and fluconazole has a strong antibacterial and antifungal activity. The common feature is their very low solubility in water. Cyclodextrin (CD) inclusion complexation and co-crystallization were carried out with the aim of ultimately improving the bioavailability of both drugs. Each new crystal phase isolated was analysed using X-ray diffraction, thermal and spectroscopic techniques.

Sulfasalazine presents two tautomeric forms which were isolated using different preparative methods *via* recrystallization from different solvents. Each form was used in combination with nine different co-formers in attempts to form co-crystals. This approach yielded negative results. Cyclodextrin inclusion complexation of sulfasalazine was studied with a variety of cyclodextrins (α-CD, β-CD, γ-CD, dimethylated β-CD and permethylated β-CD). The complexation attempts yielded an inclusion complex between one of the tautomers of sulfasalazine and γ-cyclodextrin. No single crystals were obtained and hence it was impossible to resolve the crystal structure. However, it was possible to analyse the complex thermally and spectroscopically.

The co-crystallization of fluconazole with biocompatible co-formers was not investigated due to the appearance of extensive previous reports on its co-crystal formation in the literature. Thus, only cyclodextrin inclusion complexation (with the same CDs listed above) was studied. Three inclusion complexes with native CDs were successfully prepared. Two crystallographically distinct complexes of β-CD with fluconazole as guest having 2:1 host-guest stoichiometry were isolated. While these two hydrated complexes had been identified recently by previous researchers and the X-ray structure of one of the crystal forms had been partially resolved, their characterization was incomplete. In the present study, significant advances on the previous work included the complete X-ray structural resolution of both crystal forms, designated TBCDFLU (triclinic) and MBCDFLU (monoclinic), as well as a systematic study of the conditions under which these individual forms could be isolated.

The occurrence of these crystal forms was dependent on two variables, namely β-CD concentration in the aqueous mother liquor and the incubation temperature of the solution. Careful examination of the sensitive crystallization equilibrium indicated that, at a solution

concentration of 6.52×10^{-2} M, pure TBCDFLU could be isolated at an incubation temperature of 45 °C or lower, while pure MBCDFLU crystallized at an incubation temperature of 60 °C (for both cases the incubation period is over 48 h). MBCDFLU and TBCDFLU crystals displayed different stabilities with respect to dehydration when exposed to air and hence determination of their respective water contents was performed using thermogravimetry on fresh crystals immersed in silicone oil. From a phase solubility study, it was established that the association constant for complex formation between β-CD and fluconazole in solution was very low (27.2 M^{-1}), implying weak host-guest binding. Finally, a 1:1 inclusion complex between γ-CD and fluconazole was isolated and characterized by thermal and spectroscopic techniques.

TABLE OF CONTENTS

CHAPTER 1

INTRODUCTION

1.1) CRYSTAL ENGINEERING: AN OVERVIEW

The discipline of crystal engineering is strictly connected to crystallography and all the classical branches of chemistry (analytical, inorganic, organic and physical). Since its discovery, various scientists worldwide have been attracted by this young science of the solid-state and in the last two decades the interest in the field has grown exponentially. Crystal engineering studies the nature of molecular interactions in the context of crystal packing and the possibilities of designing new solids with desired physical and chemical properties.

The primary objectives of crystal engineering are crystalline solids, molecular crystals representing a subset of these assemblies. The definition of a molecular crystal was proposed for the first time in a book edited by Kitaigorodsky.[1] A molecular crystal is a solid with molecules packed by intermolecular interactions which may be various in number, energy and type. Several types of bonds or attractive interactions are generally present in these crystals: hydrogen bonds, halogen bonds (where atoms F, Cl, Br or I are present), hydrophobic interactions, π-stacking and van der Waals interactions. It is awesome to think that there exist many crystals which are packed with interactions whose energy is of the order 1-20 kcal mol^{-1} (a little greater than the thermal energy kT under ambient conditions).

The first appearance of the term *crystal engineering* (with the analogous term 'crystal chemistry') goes back to 1955 and it was disputed between two scientists. Ray Pepinsky defined it at a meeting of the American Physical Society[2] and Gerhard M. J. Schmidt published a paper,[3] which referred to a study that commenced in 1950, in which he explained the possibility of applying X-ray diffraction to organic chemistry. For this reason, Schmidt is widely credited to have introduced the crystal engineering term and to have contributed to the birth of organic solid-state chemistry. The first study regarded the solid-state 2+2 photocycloaddition reaction of trans-cinnamic acids to cyclobutanes. The result showed that

the solid-state reactivity in crystals is a characteristic of periodic assemblies of molecules. The reactions studied by Schmidt were called *topochemical* and are reported in *Figure 1.1*.

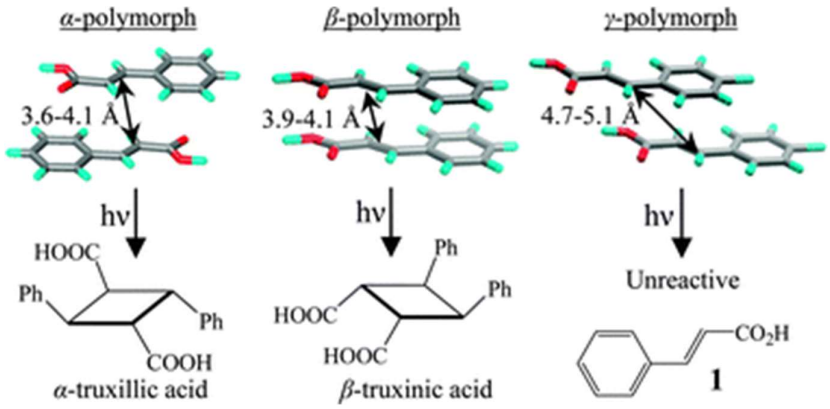

Figure 1.1: Topochemical photodimerization reactions of different polymorphs of cinnamic acid. It is possible to notice the influence of the molecular assembly on the formation of each product.[4]

In the 1970s the concept of *supramolecular chemistry* was defined and in 1988, with the studies of Ermer on the 3D network of the adamantane-1,3,5,7-tetracarboxylic acid,[5] it entered the crystal engineering field. This permitted visualisation of an organic crystal structure as a proper network (until that time it was considered as a union of assembled molecules). A molecular crystal observed with supramolecular analysis is a periodic self-assembly of billions of molecules held together by non-covalent forces; they are therefore supramolecular systems and thus crystal engineering is a form of supramolecular synthesis. The fundamental unit of a molecular crystal is the supramolecular synthon.

"Supramolecular synthons are structural units within the supermolecules which can be formed and/or assembled by known or conceivable synthetic operations involving intermolecular interactions" [G. R. Desiraju].[6]

A supramolecular synthon is a sub-structural unit in a molecular crystal that can be assembled with known synthetic operations. Study of a synthon is fundamental for determination or prediction of an experimental crystal structure. In most cases a synthon is

composed of common functional groups held together by directional interactions (e. g. O-H···O; C-H···O; N-H···O; N-H···N).

Crystal engineering is the process by which crystalline materials with specific properties are designed and synthesized. Reactivity, tautomerism, change of colour, magnetism and solubility represent only a few examples of the properties that depend, chemically or physically, on the crystal structure and that are possible to modify. The final use for these crystals is as wide as the type of properties modified (e.g. sensors, devices, light sensitive materials, catalysts). A recent branch of chemistry, that includes the properties relating to polymers and crystal engineering, is the study of metal-organic frameworks (MOFs). The MOFs field has a wide range of application due to the possibility of encapsulating liquids and gases (these materials have a surface area comparable to, or greater than, those of classical zeolites). For industries involved with explosives, dyestuffs and pharmaceuticals, the change of solid structure should be fundamental. To obtain different crystalline forms of a drug (e.g. solvates, co-crystals or polymorphs) can be of huge commercial interest apart from the possibility of altering the pharmacokinetics of an active pharmaceutical ingredient.

1.2) MULTI-COMPONENT CRYSTALS

As suggested by the name, a multi-component crystal is a crystalline phase that contains more than one type of molecule or ions. The types of interactions and the crystal design within a single-component and a multi-component crystal are the same. It is possible to expand the meaning of a multi-component crystal into six groups: co-crystals, host-guest compounds, mixed crystals (belonging to the widest group of solid solutions), donor-acceptor complexes (it is worth mentioning the example of the TTF-TCNQ semiconductor system),[7] solvates and hydrates. The work described in this dissertation has focused on the first two groups.

1.2.1) CO-CRYSTALS

Co-crystals, according to the FDA definition, are solids that are crystalline single-phase materials composed of two or more different molecular and/or ionic compounds generally in a stoichiometric ratio.[8] It is a very delicate definition and it is necessary to specify that all the chemical species involved in the co-crystal must be neutral. In the case of e.g. a proton

transfer or the presence of solvent inside the structure, it is necessary to refer to a salt or a solvate, respectively. Solvated co-crystals are not uncommon.

For co-crystals, the definition of synthon should be divided into two parts based on the types of functional groups present (usually they are an acid-base pair). Taking as example a carboxylic acid and a primary amide, two types of ring synthons are possible: homosynthons (acid-acid and amide-amide) and heterosynthons (acid-amide). In *Figure 1.2* are represented all the possible ring synthons generated by this pair.

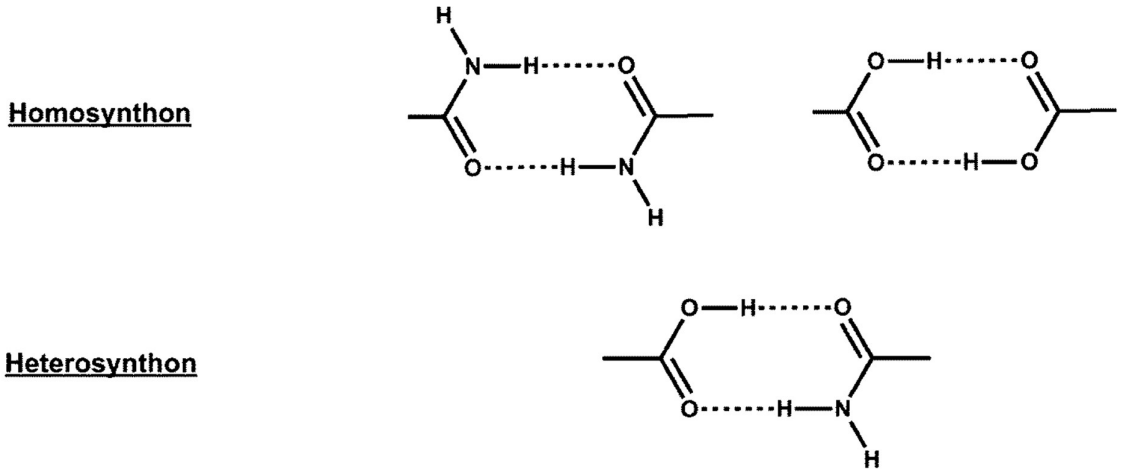

Figure 1.2: Schematic representations of typical ring homosynthons and a heterosynthon generated by carboxylic acid and a primary amide pair.

Zaworotko was the first to suggest this division and to propose a retrosynthetic approach to analyse the structures of co-crystals.[9] He observed that the heterosynthons are more common than the homosynthons. The reason for this behaviour of molecules should be attributed to the robustness of the synthon itself.

The principles of crystal engineering should be applied to co-crystals intended for a pharmaceutical purpose. Drugs are usually sold in solid formulations and for this reason a pharmaceutical co-crystal could be useful. These co-crystals should be prepared with an active pharmaceutical ingredient (API) and a co-former (COF) selected from the US Food and Drug Administration's "generally recognized as safe" (GRAS) database.[10] It is also possible that an API might be used as COF but it is necessary to find it in the WHO's list of

essential medicines.[11] The Combivir[12] case is interesting because it is a commercialized example of an anti-HIV co-crystal formed by two different APIs (lamivudine and zidovudine). The presence of a COF in a co-crystal of an API can result in physicochemical enhancement of the API (e.g. by increasing its solubility, altering its melting point, and providing a phase that is less hygroscopic).

A retrosynthetic[13] or a crystallization path should be followed to design a pharmaceutical co-crystal. Retrosynthesis in crystal engineering is an analysis, analogous to retrosynthesis in organic chemistry except that non-covalent bonds are involved in the former while covalent bonds are involved in the latter. The crystallization, corresponding to the experimental path, is certainly preferable and should be carried out with solution techniques or with mechanochemical methods. The crystallization of the product has poor efficiency and needs long times but is very useful to determine the crystal structure and investigate the effects of different solvents on the crystallization process. Mechanochemical methods are more versatile because they permit grinding of solid-solid or solid-liquid systems with or without solvents (the experimental efficiency is higher but it is impossible to obtain single crystals). The combination of the two methods is advantageous.

The purpose of pharmaceutical co-crystals is the enhancement of the poor solubility of many APIs, whereas previously the primary way to modify the solubility was to convert it into a salt. The co-crystal route is also favourable in that APIs and COFs are not necessarily required to be acids and bases. Nowadays the co-crystallization approach is a good competitor to the old method because, with the improvement of solubility, it leaves the component molecules unchanged and potentially enables preparation of solid formulations starting from liquid[14] or solid APIs without modifying them.

1.2.2) HOST-GUEST COMPOUNDS: CYCLODEXTRINS

The term “cyclodextrin” was used for the first time by Franz Schardinger[15] in 1911. The enzymatic degradation of starch produced the native CDs (illustrated in *Figure 1*.3) which are composed of six, seven or eight D-glucopyranose rings, bonded in α-1,4 linkage (α-, β-, γ-CD respectively). The shape of a CD is a truncated cone with two rims called primary and secondary (corresponding to the narrower and to the wider sides, respectively). All the CDs are soluble in water to different extents: this is due to the presence of a primary hydroxyl group on the primary rim and of two secondary hydroxyl groups on the secondary rim per

D-glucopyranose unit. The cavities have a lipophilic character. The native CDs can be modified to obtain derivatised CDs with different physicochemical properties (such as aqueous solubility) that can be used in pharmaceutical applications. The commonest modified CDs for industrial appications are: heptakis(2,6-di-*O*-methyl)-β-cyclodextrin (DIMEB), heptakis(2,3,6-tri-*O*-methyl)-β-cyclodextrin (TRIMEB), (2-hydroxypropyl)-β-cyclodextrin (HPβCD) and (2-hydroxypropyl)-γ-cyclodextrin (HPγCD).

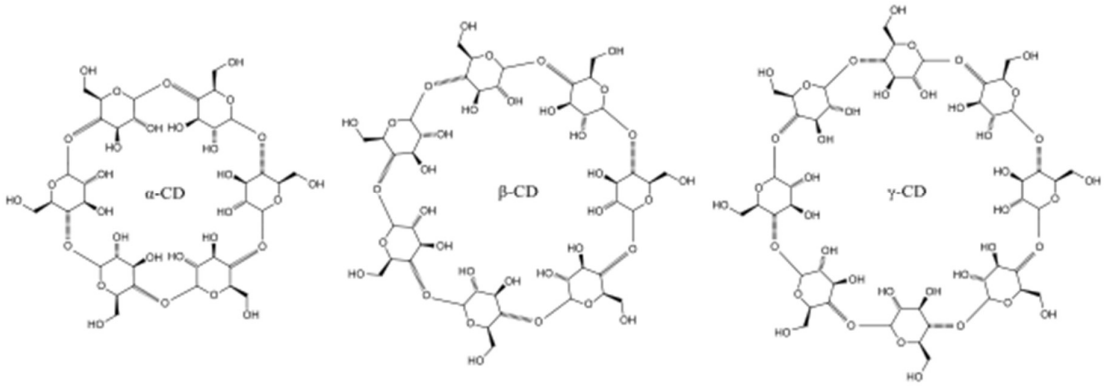

Figure 1.3: Schematic representation of native CDs. It is possible to note the presence of the three hydroxyl groups per D-glucopyranose unit.

The lipophilic molecular cavity, in a pure CD crystal or in an aqueous solution of pure CD, contains water molecules with a high level of enthalpy. If a lipophilic substance is dissolved in the aqueous CD solution, it can enter into the CD cavity, expelling included water molecules and thus reducing the enthalpy while forming a host-guest complex. Cyclodextrin inclusion complexation is a common method employed to modify the physicochemical properties of substances with the principles of crystal engineering explained above.

The CDs have a variable toxicity. A study conducted on rats has shown that β-CD is metabolised by the intestinal flora[16] and does not generate mutations or diseases if the dose is sufficiently low. The types of CDs reported above could be arranged in a general sequence (from the least toxic to the most toxic molecule): HPγCD<γ-CD<α-CD<HPβCD<β-CD. This sequence was adapted from a paper[17] in which the effects of native and derivatised CDs were intensively studied on rat and human bodies. CDs have an extremely wide field of application: food, cosmetics, toiletry, pharmaceutical, agricultural and tobacco[18] industries are only a few examples. Despite their toxicity, all CDs reported above are common in these

fields because the toxic poperties are strongly influenced by their solubility (for this reason, β-CD, that has a low solubility in water, is widely used in industry). Aroma-containing raw materials for foods are stabilised by the action of CDs; the elimination of unpleasant odours and the stabilisation of preservatives to improve the qualities of food are often attributed to the action of these molecules. Recent studies confirmed an important role of CDs in analytical chemistry,[19] and in selective complexation[20] or purification of solutions contaminated by organic pollutants.[21]

1.2.2.1) PHARMACEUTICAL APPLICATIONS OF CDs

The CDs, especially β-CD, are used to make drug formulations for oral and dermal preparations. The conversion of liquids into crystalline solids, the enhancement of bioavailability and the stabilization of labile compounds are desirable characteristics for the pharmaceutical industries. The major part of the β-CD market is consumed by the pharmaceutical industry for the production of tablets.

The advantages for the pharmaceutical industry are similar for some aspects to the applications of CDs explained above. More specifically the advantages are:

- Better drug formulations. Liquid APIs may be complexed in a crystalline form and an eventual bad taste or smell can be eliminated;
- Improvement of physicochemical stability. It is possible to protect APIs with sensitive properties such as evaporation, oxidation by air or decomposition by light;
- Enhancement of bioavailability. Poorly water-soluble substances usually show improved dissolution characteristics if included in a CD complex.

Not all drugs can be complexed by CDs. Three factors can limit the application of CDs in oral formulations: complexability, stoichiometry and required dose of drug. The hydrophobicity, the relative size and the geometry of the drug molecule in relation to the CD cavity are the most important parameters that control the complexability factor (expressed as the stability constant). To be acceptable by the pharmaceutical industry, a CD inclusion compound should have a stability constant of 200-10000 (less stable to very stable). The stoichiometry of CD-drug complexes is predominantly 1:1, 2:1 and 3:2, while other ratios have been reported but they are not common.[22] The required dose of drug is strictly correlated to stoichiometry which indicates the percentage by mass of drug

complexed compared to the total mass of the complex. A complex prepared with a low or a high molecular weight drug can encapsulate the same percentage of molecules. The difference could be reflected in the effective amount of complex that would be large for the first and small for the second case. With this reasoning, it is easy to understand that the stoichiometry influences the effective size of tablets due to the same amount of encapsulated drug being contained in e.g. hundreds of milligrams or tens of milligrams of complex (respectively). For the pharmaceutical industries this is a critical point during the formulation process because it is also well known that the CDs, in high dosages, are toxic.

The CDs are useful drug delivery agents. When drug molecules are encapsulated in CDs they can be considered as dispersed in the oligosaccharide matrix. The hydophobic drug enters into the CD cavity simply by contact, but the aqueous solution of the two substances (host and guest) needs intensive stirring (times vary depending on each case). As explained above, CDs are metabolized in the intestine but they are not absorbed in the gastrointestinal tract.[23] A study has revealed that only the 2-4% of CDs are degraded to simple sugars by α-amalyses, then they are absorbed by gastro-intestinal membranes (an intact CD molecule would be too large to do this).[24, 25] The cyclodextrins are only carrier agents, they transport a hydrophobic guest molecule through an aqueous medium to the lipophilic membrane (which has a greater affinity for the guest than the host).

The criteria for the selection of the studied bioactive compounds, the aims and objectives of the survey are described in Chapters 2 and 3.

1.3) REFERENCES

1. A. I. Kitaigorodsky, *Molecular Crystals and Molecules*, Academic Press, New York, 1973.
2. G.R. Desiraju, J. J. Vittal, A. Ramanan, *Crystal Engineering A Textbook*, World Scientific Publishing Co. Pte. Ltd., Singapore, 1st edn., 2011, ch. 1, pp. 5-7.
3. G. M. J. Schmidt, *Pure Appl. Chem.*, 1971, **27**, 647-678.
4. K. Biradha, R. Santra, *Chem. Soc. Rev.*, 2013, **42**, 950-967.
5. O. Ermer, *J. Am. Chem. Soc.*, 1988, **110**, 3747-3754.
6. G. R. Desiraju, *Angew. Chem. Int. Ed.*, 1995, **34**, 2311-2327.
7. R. Foster, *Organic Charge-Transfer Complexes*, Academic Press, New York, 1969.
8. S. Aitipamula, R. Banerjee, A. K. Bansal, *Cryst. Growth Des.*, 2012, **12**, 2147–2152.
9. Ö. Almarsson, M. J. Zaworotko, *Chem. Commun.*, 2004, 1889-1896.
10. *Generally Recognized as Safe* (GRAS), FDA, Gov. Retrieved 2013-03-17.
11. WHO Model List of Essential Medicines (20th List), http://www.who.int/medicines/publications/essentialmedicines/EML_2015_FINAL_amended_NOV2015.pdf?ua=1, (accessed October 2017).
12. P. M. Bhatt, Y. Azim, T. S. Thakur, G. R. Desiraju, *Cryst. Growth Des.*, 2009, **9**, 951–957.
13. G. R. Desiraju, J. J. Vittal, A. Ramanan, *Crystal Engineering A Textbook*, World Scientific Publishing Co. Pte. Ltd., Singapore, 1st edn., 2011, ch. 6, par. 6.6.2.1, pp. 147-148.
14. A. Bacchi, D. Capucci, M. Giannetto, M. Mattarozzi, P. Pelagatti, N. Rodriguez-Hornedo, K. Rubini, A. Sala, *Cryst. Growth Des.*, 2016, **16**, 6547–6555.
15. F. Schardinger, *Microben. Zentralbl. Bakteriol. Parasitenk. Abt. II*, 1911, **29**, 188-197.
16. J. Szejtli, A. Gerloczy, A. Fonagy, *Arznei-forschung,* 1980, **30**, 808-810.
17. M. E. Brewster, T. Loftsson, *Adv. Drug Deliv. Rev.*, 2007, **59**, 645-666.

18. E. W. Robb, J. J. Wesbrook, A. Baverly, *Tob. Sci.,* 1964, **8**, 3-7.
19. J. L. Atwood, J. E. D. Davies, D. D. MacNicol, *Inclusion compounds,* Vol. 3, Academic Press, 1984, p. 373-375.
20. J. L. Atwood, J. E. D. Davies, D. D. MacNicol, *Inclusion compounds,* Vol. 3, Academic Press, 1984, p. 368.
21. K. L. Salipira, B. B. Mamba, R. W. Krause, T. J. Malefetse, S. H. Durbach, *Environ. Chem. Lett.*, 2007, **5**, 13–17.
22. K. Uekama, *Yakugaku Zasshi*, 1981, **101**, 857-873.
23. T. Irie, K. Uekama, *J. Pharm. Sci.*, 1997, **86**, 147-162.
24. J. Szejtli, *Trends Biotechnol.*, 1989, **7**, 170-174.
25. C. A. Lipinski, F. Lombardo, B. W. Duminy, P. J. Feeney, *Adv. Drug Deliv. Rev.*, 2001, **46**, 3-26.

CHAPTER 2

EXPERIMENTAL

The materials used in this study are listed below with their sources.

The Active Pharmaceutical Ingredients (APIs), which consisted of sulfasalazine ($C_{18}H_{14}N_4O_5S$) and fluconazole ($C_{13}H_{12}F_2N_6O$), were purchased from Sigma-Aldrich Chemie Gmbh (Steinheim, Germany). An extensive description of these compounds is reported in Chapter 3.

Native cyclodextrins such as α-cyclodextrin (α-CD; $C_{36}H_{60}O_{30}$) and γ-cyclodextrin (γ-CD; $C_{48}H_{80}O_{40}$), were purchased from Wacker, Biosolutions (Halle, Germany). β-cyclodextrin (β-CD; $C_{42}H_{70}O_{35}$), heptakis(2,6-di-*O*-methyl)-β-cyclodextrin (DIMEB; $C_{56}H_{96}O_{35}$) and heptakis(2,3,6-tri-*O*-methyl)-β-cyclodextrin (TRIMEB; $C_{63}H_{112}O_{35}$) were purchased from Cyclolab Ltd. (Budapest, Hungary).

Solvents employed in the study were purchased from Sigma-Aldrich (South Africa).

All materials were used without further purification.

2.1) CO-CRYSTAL SCREENING

The co-crystal screening with the drugs was conducted following a precise and systematic procedure. At first, co-formers were selected in order to have the potential to build a well-defined supramolecular synthon with the drug molecule. This study was carried out with the use of the Cambridge Structural Database (CSD)[1] and ConQuest software was the principal program used for this preliminary part of the study. All the co-formers (COFs) used to conduct the experimental attempts appeared in the US Food and Drug Administration's "generally recognized as safe" (GRAS) database[2] or were reported in the World Health Organization's (WHO's) List of Essential Medicines.[3]

After the theoretical study, each co-former was analysed with a powder diffractometer instrument to determine the PXRD pattern of the substance. This expedient is important to

identify the polymorphic form found in the bottle of the chemical substance. The first process to be employed for co-crystallization was co-grinding. All possible binary combinations of drugs and co-formers were co-ground for 10-15 minutes with a mortar and pestle. Two techniques were carried out: neat grinding (i.e. without solvent present) and liquid-assisted grinding (LAG). For both methods, a small quantity of drug (1-5 mg) and an equimolar amount of co-former were added to the mortar. The LAG experiments involved the addition of small drops of an appropriate organic solvent that formed with the reactants a soft paste in the mortar. Usually, for each API-COF pair three LAGs with different solvents and a neat grinding were carried out.

All the products of grinding were analysed using PXRD. The traces were compared with those of the components to try to identify new solid phases. If the co-crystallization do not occur the PXRD trace of the product was the sum of the two PXRD traces of the components (it was therefore unequivocally identified as a physical mixture). Compared to the component traces, if the PXRD pattern of a product of co-grinding displayed new peaks in different positions, it was possible to confirm the presence of a new crystal phase.

Where PXRD indicated the formation of a new phase, co-precipitation experiments were performed. Stoichiometric amounts of drug and co-former were dissolved in an appropriate solvent; the resulting suspension was then heated to enhance the solubilization process. The solution was filtered through a 0.45 μm nylon filter into a clean, pre-heated vial. Vials were left in the fume-hood to allow the solvent to evaporate at room temperature. If suitable crystals were formed, they were fully characterized using single crystal X-ray diffraction and the techniques explained in the paragraphs which follow.

In the case of failure of co-precipitation experiments, different co-crystallization attempts were carried out (the principal techniques used are illustrated in *Figure 2.1*).

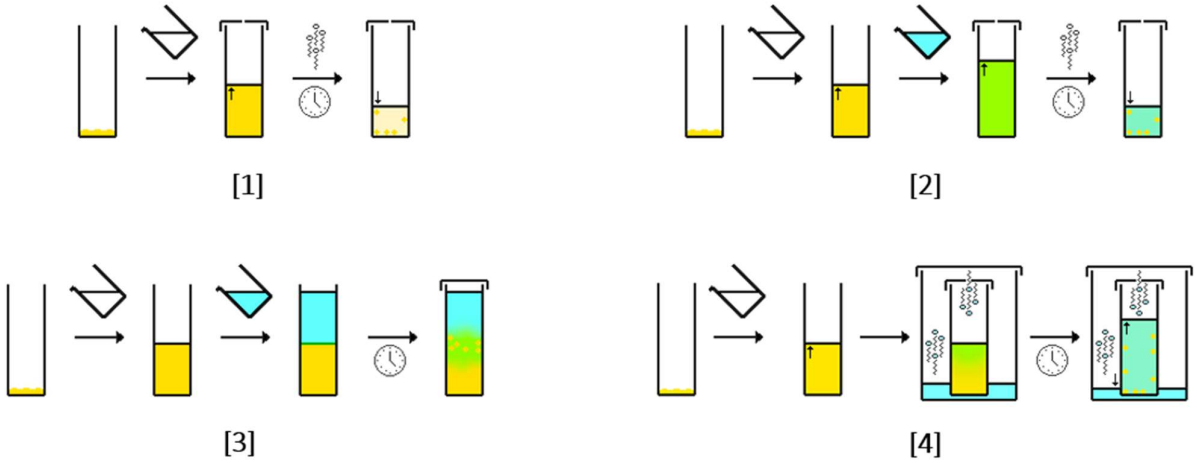

Figure 2.1: Schematic representation of four co-precipitation techniques used to provide single crystals for SCXRD analysis: evaporation of a single solvent [1]; evaporation of a multi-solvent system [2]; liquid-liquid diffusion or slow interface diffusion [3]; vapour-liquid diffusion [4].

The schematic representation of the evaporation of a single solvent [1] shows the typical co-precipitation experiment (explained above); this may be used to explain the seeding technique, as follows. After the dissolution of drug and co-former in the hot solvent, the solution was slowly cooled and a crystal of the desired product (from a previous synthesis) was added to the vial to facilitate the crystallization. The co-precipitation via evaporation of a multi-solvent system [2] involves two or more miscible solvents with different volatilities. The compounds might be more soluble in the most volatile solvent and, after the evaporation of this one, crystals could be formed in the solution of the less volatile solvent. In a liquid-liquid diffusion [3] the raw materials are dissolved in an appropriate solvent and a second one is carefully added on the top to form an interface. It is possible to use this technique with different approaches, such as using a pair of miscible solvents with different densities or completely immiscible solvents (both were used in this study under different thermal conditions). Finally, the vapour-liquid diffusion [4] takes advantage of the same principle as that for liquid-liquid diffusion. In this case the solvents might be completely miscible and the pair might be composed of a volatile solvent and a slightly volatile one.

2.2) CYCLODEXTRINS OVERVIEW

The cyclodextrins (CDs) are oligomeric forms of glucose. The native ones are composed of six, seven or eight units of D-glucopyranose rings, linked in the positions α-1,4. The number of units determines the name of the molecule: six units correspond to an α-cyclodextrin, seven to a β- and eight to a γ-. The truncated conical geometry and the dimensions of each cage are shown in *Figure 2.2*. These data were determinant for a screening with the dimensions of the selected drugs to evaluate the possibilities of formation of an inclusion complex.

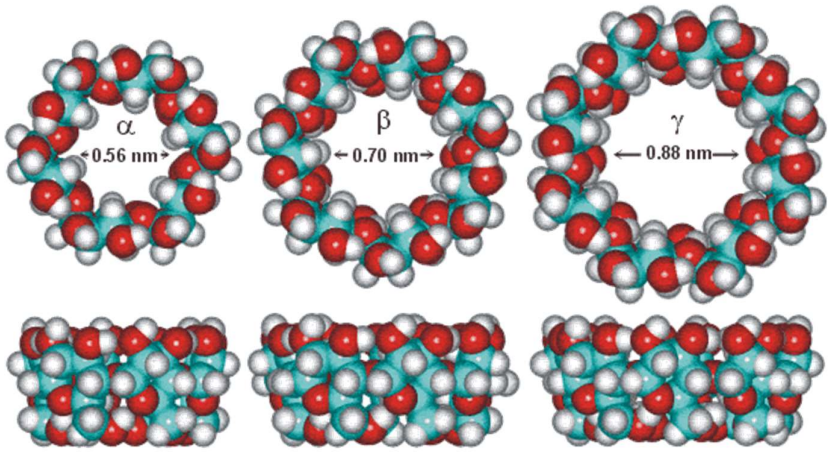

Figure 2.2: Conical morphology and dimensions of the cavities of the native cyclodextrins.

Due to the truncated conical shape, it is possible to identify the presence of two rims: primary and secondary. Three hydroxyl groups are present per glucose unit: a primary hydroxyl group is located on the narrower ('primary') rim in the position labelled as 6 and two secondary hydroxyl groups are located on the wider ('secondary') rim in the 2 and 3 positions. In *Figure 2.3* is shown the schematic representation of a β-CD molecule and a D-glucopyranose unit.

The native cyclodextrins have quite a high content of water inside their structure and their aqueous solubilities are relatively low (see *Table 2.1*).

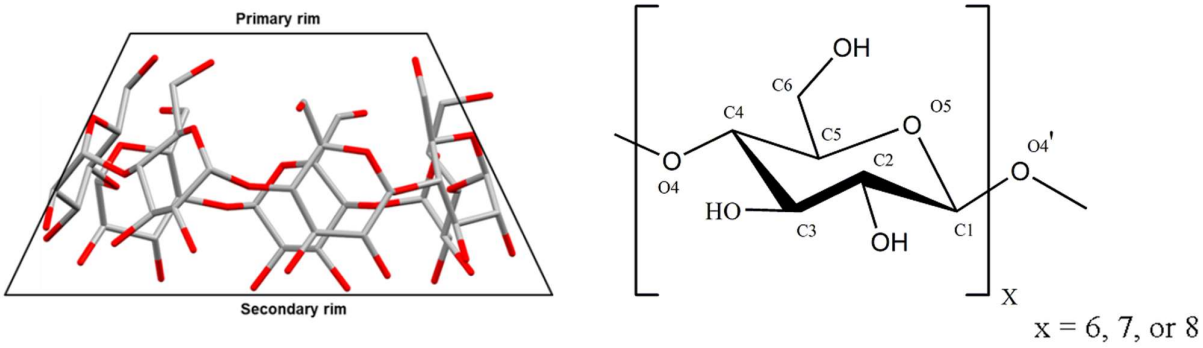

Figure 2.3: Schematic representation of the truncated conical shape of a native cyclodextrin (left) and of a D-glucopyranose unit (right). On the right side are reported the typical labels for the glucoside ring and it is possible to distinguish the positions of the primary and secondary hydroxyl groups in the molecule.

Table 2.1: Aqueous solubility of the native cyclodextrins.[4]

	Aqueous solubility at 25 °C (g/100 ml)
α-CD	14.5
β-CD	1.85
γ-CD	23.2

The low aqueous solubility of β-cyclodextrin is probably related to the strong binding of the CD molecules in a network of O-H···O hydrogen bonds. These interactions are principally intramolecular (forming 'belts' that maintain the round shape of the CD). If the CD hydroxyl groups are substituted by methoxy groups this physicochemical property changes radically (as shown in Chapter 7).

2.2.1) MOLECULAR GEOMETRY

The schematic representation of β-cyclodextrin in *Figure 2.4* shows the parameters useful for describing the modification of its macrocyclic conformation when a guest is present inside the cavity. The geometric parameters are six in number and all are based on the seven O4 glycosidic oxygen atoms taken as a reference plane. For the case of β-CD (and its derivatives), the geometrical figure inscribed in the macrocyclic ring is a heptagon. With this figure, it is possible to define all the geometrical parameters: the distance between each O4

atom and the centroid of the O4-heptagon (**l**), the O4···O4′ distance (**D**), the O4···O4′···O4′′ angle (**φ**) and the O4···O4′···O4′′···O4′′′ torsion angle (**d**). There are three more parameters that are not directly connected to the O4 mean plane. If intramolecular hydrogen bonding is present, it is important to cite the O2···O3′ distance ($\mathbf{D_3}$). The (**α**) parameter measures the deviation of each O4 atom from the O4 mean plane. It is well known that the CDs have a truncated conical shape. The last parameter ($\boldsymbol{\tau_1}$) is related to the deviation of the conical (more accurately 'toroidal') shape of the CD molecule from a hypothetical cylindrical shape. Generally, it is observed that the primary rim of each individual glucose residue is tilted by a characteristic angle $\boldsymbol{\tau_1}$ towards the seven-fold axis of the macrocycle. Therefore $\boldsymbol{\tau_1} = 90° - \theta$, where θ is the angle between (C1, C2, C3, C4, C5, O5) mean plane and the O4 mean plane (*Figure 2.5*).

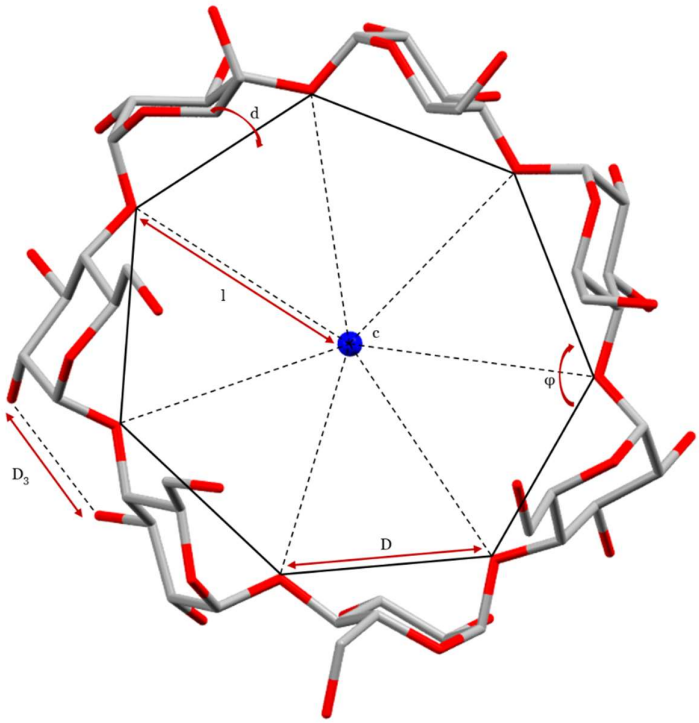

Figure 2.4: Geometrical parameters of the O4-heptagon.

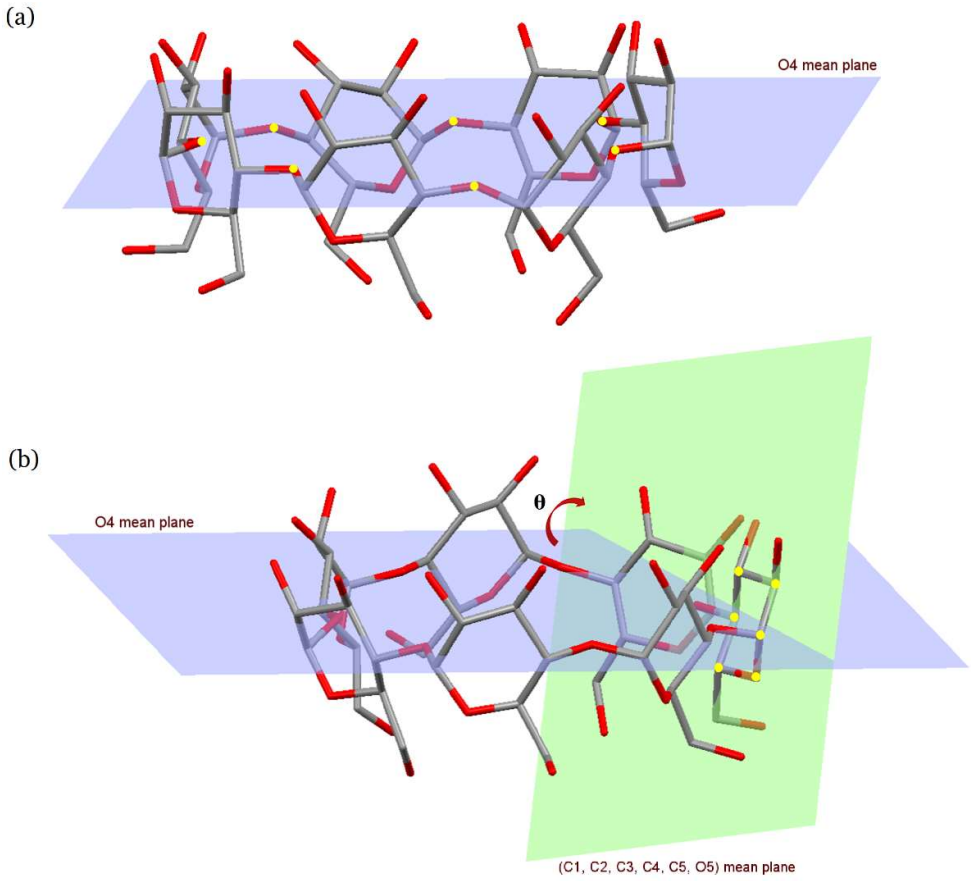

Figure 2.5: (a) O4 mean plane calculated for a β-CD molecule, (b) θ angle between O4 and (C1, C2, C3, C4, C5, O5) mean planes used to calculate parameter τ_1. The yellow dots indicate the atoms used to calculate the planes.

2.2.2) CRYSTAL PACKING ARRANGEMENTS

The packing arrangements for a generic cyclodextrin complex could be monomeric or dimeric with a channel or cage type (*Figure 2.6)*. The channel type packing has the cavities of cyclodextrins aligned and it is possible to distinguish a monomeric arrangement if the primary and the secondary rim are in contact; this arrangement is called head-to-tail (AAAA). If the channels are formed by head-to-head channels, the structure is dimeric (ABAB) and two primary (or secondary) rims are in contact. The most common cage type packing is monomeric and it occurs when the cavities are obstructed. These arrangements are referred to as brickwork or herringbone.

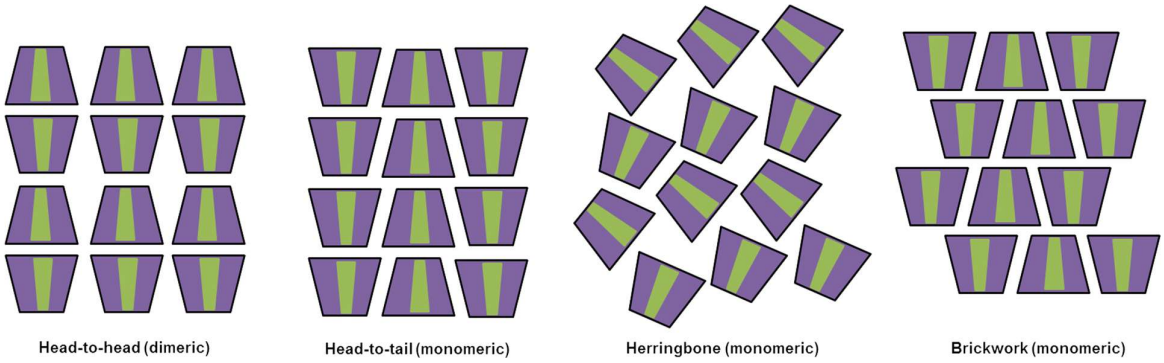

Figure 2.6: Packing arrangements for cyclodextrin complexes.

The similarity between types of crystal packing arrangements raises the need to explain the term 'isostructurality'. Two or more phases (e.g. from a cyclodextrin complexing different guests) that have the same gross packing arrangements or molecular arrangements, as well as a common space group and similar unit cell dimensions, are referred to as isostructural phases.[5] A review by Caira described various isostructural series of PXRD traces for known CD complexes and reported that the PXRD patterns were comparable for CD complexes within any given series.[6] It is now possible to compare the PXRD pattern (or the unit cell parameters from a single crystal) of the crystalline product of a CD inclusion experiment and determine whether complexation has occurred or not.

2.3) CYCLODEXTRIN INCLUSION COMPLEX SCREENING

The cyclodextrin rims are hydrophilic and the cavities lipophilic. A lipophilic molecule (guest) can be complexed by a cyclodextrin (host) in solution with the formation of a precise equilibrium. The equilibrium constant K_C is defined in equation (1) in *Figure 2.7*, which also presents a graphical representation of the formation of a 1:1 complex.[7]

$$K_C = \frac{[G \cdot CD]}{[G][CD]} \qquad (1)$$

To prepare each inclusion complex, both kneading and co-precipitation experimental attempts were carried out with a 1:1 molar ratio of host and guest. The kneading technique is very similar to LAG but it uses water instead of organic solvents. For a kneading attempt, the raw materials were mixed in a mortar and gently kneaded with a pestle for ~15 minutes, the mixture being kept moist with the addition of ~20-25 µl of pure water. The products

were analysed using PXRD and each pattern was compared with the calculated traces from the isostructural series and with the experimental traces of components. If the powder pattern was different from those of the components and matched one of the patterns of the isostructural series ones, it was identified as a new complex.

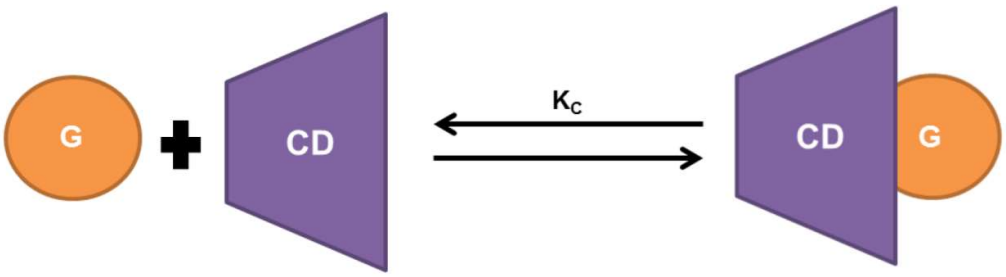

Figure 2.7: Reversible complexation of a guest by a CD in solution.

The co-precipitation experiments took place in different modalities. Each cyclodextrin used for this study presented different properties. For this reason, each experimental procedure will be reported in a separate paragraph at the beginning of the chapters that deal with the study of different CD complexes (Par. 5.1, Par. 6.1 and Par. 7.2.1).

2.4) THERMAL ANALYSIS

All the thermal analyses described in this paragraph were combined to study the thermal behaviour of a new crystal phase or to determine the properties of the drugs. The techniques used were Hot Stage Microscopy (HSM), Thermogravimetric Analysis (TGA) and Differential Scanning Calorimetry (DSC). To determine the conditions for reliable TGA estimation of crystal water content, an empirical test involving timing of the rate of dehydration of the crystal was devised. This test was carried out with HSM instrumentation and was dubbed the Dehydration Timed Test (DTT).

2.4.1) HSM

Hot Stage Microscopy (HSM) was used as a preliminary test to evaluate the behaviour of a crystal with elevated temperatures. Bubbling, colour changes or change of opacity of crystals indicates a thermal event that may be correlated to TGA or DSC traces. Samples were placed on a cover slip with a small drop of silicone oil and monitored using a Nikon SMZ-10 stereoscopic microscope fitted with a Linkam THMS600 hot stage and a Linkam TP92 temperature control unit. The images were captured with a real-time Sony Digital Hyper HAD colour video camera and viewed using analySIS (the Soft Imaging System program).[8]

2.4.2) DEHYDRATION TIMED TEST

The Dehydration Timed Test (DTT) was an experiment that was carried out to promote the success of thermogravimetric analysis (TGA). Some new crystal phases in this study lost water within a few seconds once removed from their mother liquor. The preparation of a TGA experiment needed around two minutes. If the sample lost mass during this period it would be very difficult to have a good set of data for thermogravimetric analysis. To estimate an average time in which the sample lost the solvent contained inside the structure, a single crystal was placed on a slide in a small pool of mother liquor. The sample was monitored with the HSM instrumentation, without heating the system. After a few minutes, the drop of mother liquor had evaporated and the time test began. The images recorded were useful to understand the stability of the crystal on exposure to the open air (time of formation and position of cracks were the prominent empirical behaviours observed). Certainly, important crystal characteristics like shape or thickness could influence the time of formation of cracks, but these aspects were not considered due to the difficulty of analysing them in a statistical sense.

2.4.3) TGA AND DSC

Thermogravimetric analysis (TGA) exposes a solid sample to elevated temperatures. The instrument measures the change in mass of sample as a function of temperature. This analysis is important and it was used extensively during this study in order to quantify the solvent present in crystals. Differential scanning calorimetry (DSC) measures the difference in energy as a function of temperature between a sample pan and a reference pan. During

the analysis it is possible to observe both endothermic and exothermic peaks that are directly correlated to solvent loss, melting, phase transitions or decomposition.

A TA-Q500 Thermogravimetric Analyzer with Universal Analysis software (v4.5A, TA Instruments-Waters LLC) was used. It was operated with a dry nitrogen purge gas flow rate of 60 cm^3 min^{-1} and samples were heated at a rate of 10 K min^{-1}. The samples, in a mass range of 1-5 mg, were removed from their mother liquor, dried on filter paper and placed in an open crucible. For some samples, due to their nature (Par. 5.3.3), a secondary procedure (recording the time for each attempt) was necessary. A small quantity of sample was removed from mother liquor, dried on filter paper and placed inside a tared open crucible. After a second weighing, 1-2 drops of silicone oil were placed inside the crucible and it was weighed a third time.

Differential scanning calorimetry (DSC) was performed on a DSC25 Differential Scanning Calorimeter (TA instruments) with TRIOS software (v4.1.0.3179, TA Instruments-Waters LLC). It was operated using a dry nitrogen purge gas flow rate of 60 cm^3 min^{-1} and samples were heated at a rate of 10-20 K min^{-1}. Samples, with mass range 1.5-3 mg were removed from the mother liquor, dried on filter paper and placed inside a closed vented aluminium pan.

2.5) NMR SPECTROSCOPY

All the crystals analysed were dissolved in deuterated DMSO (DMSO-d_6) for recording their ^1H NMR spectra on a Bruker 300 MHz spectrometer. For the CD inclusion complexes, the peaks were assigned and integrated to determine the host-guest stoichiometry and, in the case of co-crystals, the same integration was done to confirm the stoichiometry. This technique was used also to determine the effective drug purity of all the molecules used in this study.

2.6) FTIR SPECTROSCOPY

Fourier Transform Infrared (FTIR) spectroscopy was used to check if all of the drug employed in the attempted synthesis of a CD inclusion complex was complexed. It was possible to establish this by comparing the spectrum of the crystal complex with those of the

CD and the drug. In the complex spectrum, the absorption bands of the CD were more evident than those of the drug in the case of total complexation due to the larger mass fraction of the CD present. The IR spectra were recorded on a Bruker Tensor27 spectrometer with an ATR platinum Diamond 1 reflectance accessory for solid samples.

2.7) POWDER X-RAY DIFFRACTION (PXRD)

PXRD patterns were recorded to establish if a new crystal phase was obtained following attempted synthesis via co-grinding, co-precipitation and kneading experiments. The recorded pattern was compared with the patterns of the drug and the appropriate co-former. In the case of the presence of cyclodextrins, it was compared also with a library of reference patterns for known series of isostructural inclusion complexes.[6,9] If the pattern did not match any reference pattern, the likelihood of complexation was low, but further investigation of the nature of the product would have to follow. For the co-grinding case, the superimposition of the pertinent PXRD patterns was fundamental to evaluate the emergence of new peaks or the disappearance of any peaks from the patterns of individual components.

Two powder X-ray diffraction instruments were used for the measurements: a BRUKER D8 X-ray diffractometer and a HUBER X-ray diffractometer. Both instruments used a CuKα_1-radiation source (λ = 1.54056 Å). With the Bruker instrument, all the samples were placed on a zero-background sample holder (rotating at 10 rpm) and scanned over the 2θ-range 4° – 40°, with a step size of 0.05° per second. The X-ray generator settings were 30 kV and 40 mA. The HUBER X-ray diffractometer used a Philips PW1120/00 X-ray generator fitted with a Huber long fine-focus tube PW2273/20 and a Huber Guinier Monochromator Series 611/5 to produce the CuKα-radiation specified above. The PXRD patterns were recorded by a Huber Imaging Plate Camera 670 and all the samples were introduced into a silica capillary.

2.8) SINGLE CRYSTAL X-RAY DIFFRACTION (SCXRD)

Single crystals of adequate quality, size and optical uniformity were removed from the mother liquor and immersed in a small pool of Paratone N oil.[10] They were subsequently mounted on a nylon cryoloop.

Two different instruments were used to check the unit cell dimensions or for full intensity data-collections. The unit cell dimension checks were performed on a Nonius KappaCCD (where CCD refers to the Charge Coupled Device detector) single crystal X-ray diffractometer, using graphite-monochromated MoKα radiation (λ = 0.71073 Å) generated by a Nonius FR590 generator operated at 50 kV and 20 mA. The preliminary unit cell refinement was performed using the DENZO and SCALEPACK[11] programs. The data-collections were recorded on a Bruker KAPPA APEX II DUO single crystal X-ray diffractometer using MoKα radiation (λ = 0.71073 Å) generated by a Bruker K780 generator operated at 50 kV and 30 mA.[12] All the samples were maintained at low temperature during the data-collection (usually 173 K and in some cases 100 K) by cooling with a constant flow of N_2 gas (rate of flow 20 cm^3 min^{-1}). The cryostream cooler was an Oxford Cryostream, UK. As in the case of the Nonius instrument, the unit cell refinement and data reduction were performed with the programs DENZO[11] and SAINT.[13] The intensity data were automatically corrected for Lorentz-polarization effects while absorption corrections were based on the multi-scan method using the program SADABS.[14] The observed Laue symmetry of the diffraction pattern was fundamental in assigning the crystal system. The space group was determined from the systematic absences.

The input file for the structure solution was elaborated using the program XPREP.[15] All the crystal structures were solved by direct methods using SHELXS-97[16] and refined by full-matrix least-squares using SHELXL-97.[16] These programs were implemented with the X-Seed[17] interface (versions 2.0 and 4.0).

2.8.1) SHELX-97

The SHELX-97[16] software program uses a full-matrix least-squares fitting to minimize the sum of the squares of the differences between the observed (F_o^2) and calculated (F_c^2) intensities. The residual index R_1 [defined in (2) below] indicates the agreement between the lists of observed (F_o) and calculated (F_c) structure factors. A low R_1 index (typical range

~0.03-0.05 for small molecules) corresponds to a well-refined model. The second residual index is wR_2 [defined in (3)], which indicates the agreement between F_o^2 and F_c^2 for the refinement against F^2. The parameter w, defined in formula (4), refers to the weighting scheme and the parameters a and b appearing in (4) were optimised during the refinement of each structure. The quantity P is defined in (5). The parameter S, defined in expression (6), is commonly called the "Goodness-of-Fit". A well-refined structure has S close to 1.0 and a n/p ratio close to 10 (where n and p are equal to the number of reflections and the total number of parameters, respectively).

$$R_1 = \frac{\sum\left||F_o| - |F_c|\right|}{\sum|F_o|} \qquad (2)$$

$$wR_2 = \left(\frac{\sum w\,(F_o^2 - F_c^2)^2}{\sum w\,(F_o^2)^2}\right)^{\frac{1}{2}} \qquad (3)$$

$$w = [\sigma^2(F_o^2) + (aP)^2 + bP]^{-1} \qquad (4)$$

$$P = \frac{\max(0, F_o^2) + 2F_c^2}{3} \qquad (5)$$

$$S = \left(\frac{\sum w\,(F_o^2 - F_c^2)^2}{n - p}\right)^{\frac{1}{2}} \qquad (6)$$

The program PLATON[18] was used to calculate intramolecular and intermolecular geometrical parameters, with their standard deviations. Images of crystal structures were created with POV-Ray[19] software available in program Mercury.[20] The final crystallographic data files for each crystal structure reported in this study can be found in the Appendix. Table 2.2 lists the file types and information they contain.

Table 2.2: Crystallographic data files available in the Appendix.

Extension	Details
.hkl	Reflection data
.res	SHELX co-ordinate data
.cif	Crystallographic information
.lis	PLATON output
.fcf	Observed and calculated intensities
.xl	SHELX output
.sup	Tabulated supplementary data

To finalise each model obtained by Single Crystal X-ray Diffraction (SCXRD), a PXRD pattern was calculated with the program LAZY PULVERIX[21]. From the comparison of the calculated PXRD pattern with an experimental one (based on material obtained via co-grinding or co-precipitation) it was possible to confirm the correspondence between the model and the bulk material.

2.9) PHASE SOLUBILITY STUDIES

The calibration curves for the drugs were constructed by preparing a stock solution of known concentration and diluting it to have a set of solutions with varying concentrations. The drugs studied have very poor aqueous solubility and therefore, to encourage the dissolution process, a small amount of ethanol was added to the solutions. All the phase solubility studies were performed in a 1% ethanol/water [v/v] medium. To determine the concentration of the drug in solution UV-Visible spectroscopy was used. The fundamental equation used to quantify the drug present in each solution was the Beer-Lambert law (7). The expression below describes the relation between the absorbance (A) and concentration (c) of an absorbing species with a constant path length (l) and a molar absorption coefficient (ε_0).

$$A = \varepsilon_0 lc \qquad (7)$$

The absorbance readings were recorded on a Cintra 20 UV-Visible spectrometer and data were processed using the GBC Spectral computer program (v1.70, December 1998). The

readings were plotted as a function of the molar concentration of the drug to construct the calibration curve.

For the phase solubility studies, a set of dilutions of a cyclodextrin solution were prepared and an excess of the drug was added to each solution (the volume of solution in each vial was 3 ml). The vials were sealed and stirred (500 rpm) at constant temperature (25.5 ± 1.0 °C) for 36 hours. The solutions were filtered through a 0.45 μm nylon filter, diluted 20-fold and analysed with the UV-Visible spectrometer. Using the respective calibration curve, the concentration of the drug was determined.

2.10) REFERENCES

1. Cambridge Structural Database and Cambridge Structural Database system, Version 5.36 (updates to May 2017), Cambridge Crystallographic Data Centre, University Chemical Laboratory; Cambridge, England, 2014.
2. SCOGS (Select Committee on GRAS Substances), http://www.accessdata.fda.gov/scripts/fdcc/?set=SCGOS (accessed October 2017).
3. 20th WHO Essential Medicines List (EML), http://www.who.int/medicines/publications/essentialmedicines/20th_EML2017_FINAL_amendedAug2017.pdf?ua=1 (accessed October 2017).
4. E.M. Martin Del Valle, *Process Biochem.,* 2004, **39**, 1033-1046.
5. A. Kálmán and L. Párkányi, Advances in Molecular Structure Research, JAI Press Inc., Greenwich, USA, 1997, **3**, 189-226.
6. M. R. Caira, *Rev. Roum. Chim.*, 2001, **46**, 371-386.
7. T. Higuchi and K. A. Connors, *Adv. Anal. Chem. Instrum.*, 1965, **4**, 117-212.
8. Soft Imaging System GmbH, Digital Solutions for Imaging and Microscopy, Version 3.1 for Windows (Copyright 1987-2000).
9. M. R. Caira, S. A. Bourne, H. Samsodien, E. Engel, W. Liebenberg, N. Stieger and M. Aucamp, *Cryst. Eng. Comm.*, 2012, **14**, 2541-2551.
10. Paratone N oil (Exxon Chemical Co., Texas, USA).
11. Z. Otwinowski and W. Minor, *Method Enzymol.*, 1997, **276**, 307-326.
12. Bruker AXS Inc., APEX2, Version 1.0-27, Bruker AXS Inc., Madison, Wisconsin, USA.
13. Bruker AXS Inc., Program SAINT, Version 7.60a, Bruker AXS Inc., Madison, WI, USA, 2006.
14. G. M. Sheldrick, Program SADABS, Version 2.05, University of Göttingen, Germany, 2007.

15. Bruker AXS Inc., XPREP, Version 5.1, Bruker AXS Inc., Madison, WI, USA, 1997.

16. G. M. Sheldrick, *Acta Crystallogr. A.*, 2008, **64**, 112-122.

17. L. J. Barbour, *J. Supramol. Chem.*, 2001, **1**, 189-191.

18. A. L. Spek, *Acta Crystallogr. D.*, 2009, **65**, 148-155.

19. C. Cason, T. Froehlich, N. Kopp and R. Parker, POV-Ray for Windows, Version 3.6.1a.icl8.win32, The Persistence of Vision Raytracer Pty. Ltd., 2003.

20. C. F. Macrae, I. J. Bruno, J. A. Chisholm, P. R. Edgington, P. McCabe, E. Pidcock, L. Rodriguez-Monge, R. Taylor, J. van de Streek and P. A. Wood, Mercury CSD 2.0, *J. Appl. Cryst.*, **41**, 466-470, 2008.

21. K. Yvon, W. Jeitschko and E. Parthé, *J. Appl. Crystallogr.*, 1977, **10**, 73-74.

CHAPTER 3

AIM OF THE STUDY, COMPOUNDS AND EXPERIMENTAL ATTEMPTS

3.1) AIM OF THIS WORK

The study motivation focused on the change, via supramolecular intervention (co-crystallization or cyclodextrin inclusion complexation) of two active pharmaceutical ingredients (APIs) that are commonly available on the market. Both targets are slightly soluble in water and the final purpose was to improve this physicochemical property for possible enhancement in drug delivery. In the first place, it was necessary to check by PXRD if a new crystal form was identified. In the second place, it was necessary to further characterize it with thermal and spectroscopic analysis and, where possible, to determine its crystal structure with SCXRD.

3.2) SULFASALAZINE

Sulfasalazine (5-[4-(2-pyridylsulfamoyl) phenylazo] salicylic acid; $C_{18}H_{14}N_4O_5S$) is a powerful anti-inflammatory drug finding application in chronic diseases like rheumatoid arthritis,[1] Crohn's disease,[2] ulcerative colitis and pancreatic cancer.[3] An image of sulfasalazine (SSZ) should read in *Figure 3.1,* it is a powerful API, derivatised by the 5-aminosalicylic acid with a moderate effect on these problematic diseases. Nowadays, the commonest way to administer SSZ is via oral tablets, such as the registered products Salazopyrin or Azulfidine. The solubility of SSZ in water at the temperature of 25 °C is 0.0464 mg/ml.[4] It is an orange, crystalline powder that melts at 265-266 °C.

Figure 3.1: Group of sulfasalazine crystals photographed at the microscope.

The peculiarity of SSZ is the presence of two recognized tautomers[5] with different crystalline forms. The procedure to obtain them is long and has a low yield: 50 mg of raw material solubilized in 10 ml of a first solvent, heated at 50-60 °C (depending on the boiling point of the solvent itself) to have the maximum concentration possible and stirred overnight. After the complete evaporation of the liquid, a second recrystallization must be set up with a different solvent under the same conditions as the first one. It is necessary to evaporate the second solvent slowly and, if possible, perform seeding with a crystal of the desired tautomer to encourage the crystallization of the entire sample. The specific types of tautomers and solvents are explained below (the CCDC refcodes for the respective molecular and crystal forms are given in parentheses).

- Amine (QIJZOY). This tautomeric form exists as a solid-state dimeric structure with hydrogen bonds as principal interaction between the molecules of the dimer (*Figure 3.2*). The units are bonded only with an offset-π-stacking interaction of the phenyl groups. The solvents used to obtain this tautomer (orange crystalline powder) are absolute ethanol 98% (EtOH) or 2-butanone (methyl ethyl ketone, MEK). Henceforth, this molecule will be designated A-SSZ, to denote the amine group that characterizes the tautomer.
- Imine (QIJZOY01). The solid-state X-ray analysis shows a structure with chains and the same type of interactions as found in the amine tautomer (*Figure 3.3*). The relationship of the phenyl groups with an offset stacking is significantly different from that in the other tautomer. In the A-SSZ case, all the phenyl rings are stacked in the same way, while in this one, successive pairs of chains are inclined at 46.4°. The imine

tautomer of sulfasalazine (I-SSZ) is a crystalline dark orange powder and it is obtained by recrystallization from acetone and tetrahydrofuran (THF).

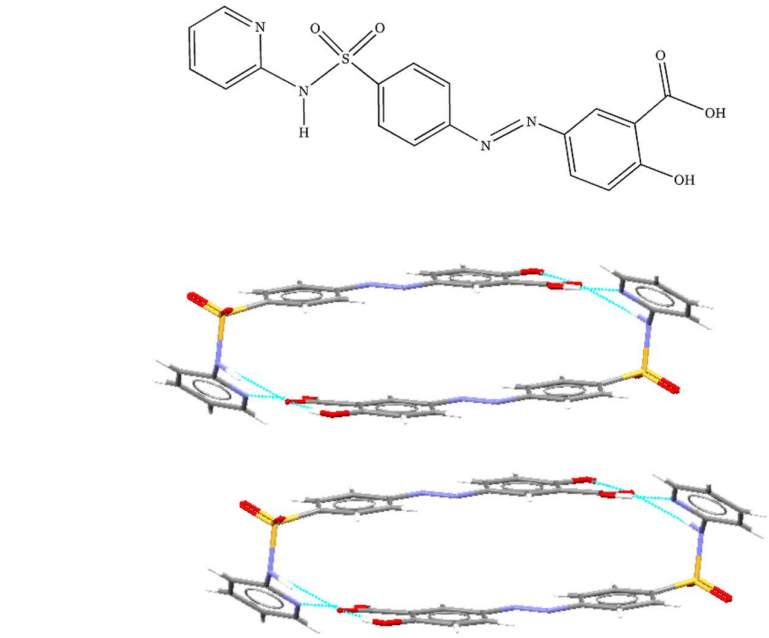

Figure 3.2: Schematic and solid-state aspect of A-SSZ (two dimers are included in the figure).

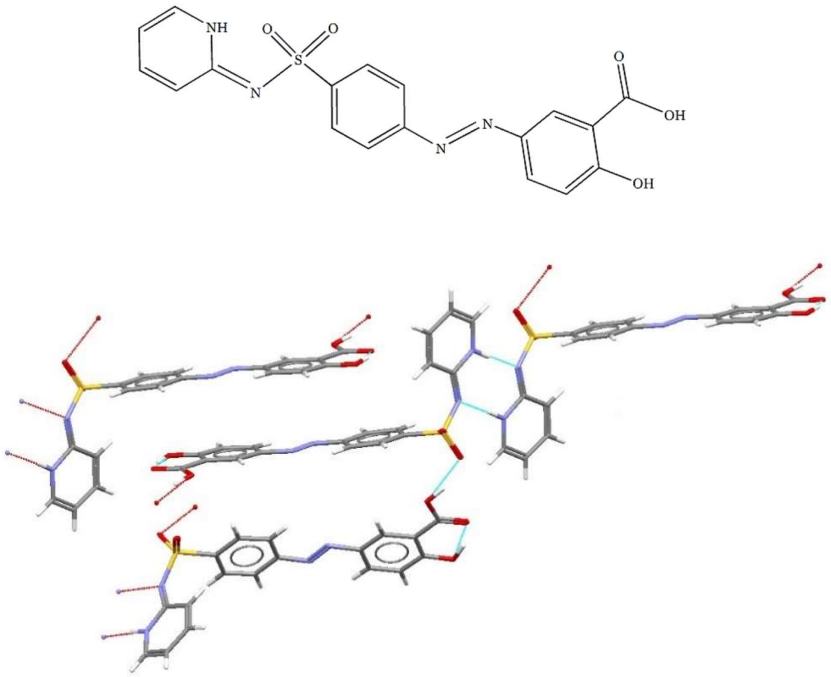

Figure 3.3: Schematic and solid-state aspect of I-SSZ.

3.3) FLUCONAZOLE

Fluconazole (2-(2,4-difluorophenyl)-1,3-bis(1H-1,2,4-triazol-1-yl) propan-2-ol), is an antifungal drug in commercial use since 1988[6] and has high potency against these microorganism infections (*Figure 3.4*). It is enumerated in the List of Essential Medicines of the World Health Organization[7] and the demand for its use is rising rapidly.

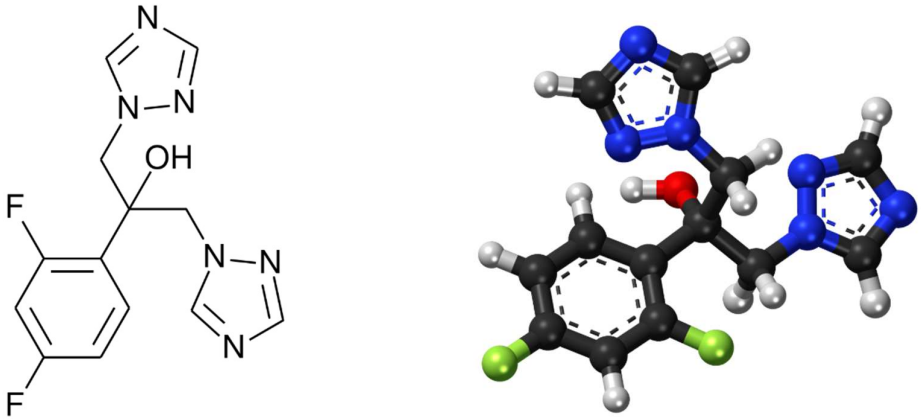

Figure 3.4: Representations of the fluconazole molecule.

Fluconazole ($C_{13}H_{12}F_2N_6O$) is a solid, white, azole API, that is formulated as tablets, creams or solutions. The melting point range is 138-140 °C and the solubility in water is very low (< 0.001 mg/ml[8]). The most common forms of fluconazole in commerce are tablets like Diflucan, Flucamed or Forcan (principally formed with salts of API). The research on co-crystals that contain this API is very extensive, principally with carboxylic acids as co-formers.[9,10] For this reason, all the work reported in the present study with this target molecule is on cyclodextrin inclusion complexes.

Using solid-state characterization techniques, it is possible to observe the presence of five polymorphic anhydrous forms and one hydrate. The raw fluconazole used in this work corresponds to an anhydrous form (CCDC refcode IVUQOF02) with orthorhombic symmetry (space group Pbca). The principal interaction in this structure is O-H···N hydrogen bonding between the hydroxyl group and the nitrogen atom of a triazole group. Describing the crystal packing is simple due to the formation of chains of molecules along the direction shown in *Figure 3.5*.

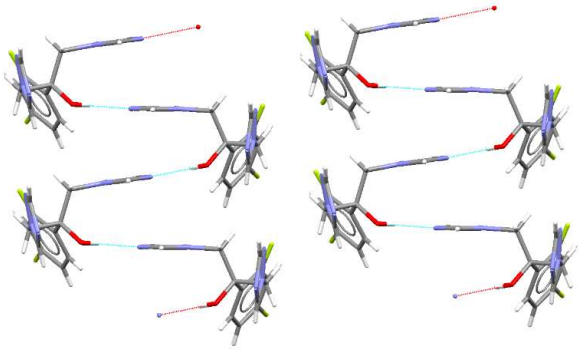

Figure 3.5: Solid-state representation of IVUQOF02.

3.4) CO-FORMERS FOR SSZ

The research on the co-crystallization of SSZ was carried out with the intention of eventually forming a hydrogen-bonded synthon with a series of co-formers, using first a literature study to explore this possibility, then an experimental attempt. All potential co-former compounds chosen were biocompatible (enumerated in the GRAS list[11] or in the WHO's List of Essential Medicines[7]). After the period of study and selection, small amounts of co-former and API (in a 1:1 molar ratio) were combined with an appropriate technique of crystallization (dry grinding, liquid assisted grinding or LAG, kneading, co-precipitation and liquid-liquid diffusion). The product of each attempt was analysed with PXRD to distinguish a possible new crystalline phase between its components. Only in the case that this analysis confirmed a new phase, were other types of analyses performed (primarily thermoanalytical techniques). Below, in *Table 3.1*, is reported the list of all co-formers used. All the substances were in a crystalline form.

Table 3.1: Co-formers for the-attempts to form co-crystals with SSZ.

Name	Formula	Description
Nicotinic acid	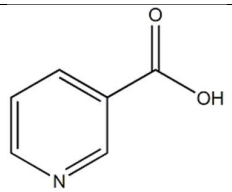	Known also as niacin, it is a component, with nicotinamide, of Vitamin B_3.[12] It is classified as one of the essential human nutrients.
Pyrazinecarboxamide	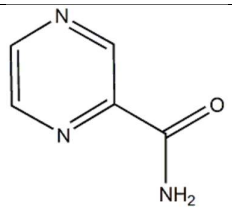	It is a strong antiuricosuric[13] API commonly used against tuberculosis,[14] and is included in the WHO's List of Essential Medicines.
Fumaric acid	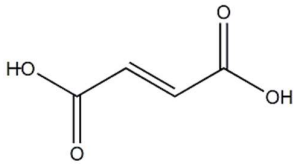	In the past it was used for the treatment of psoriasis; today it is used as food additive (an acidity regulator), commercialized with the name E297.[15]
Citric acid	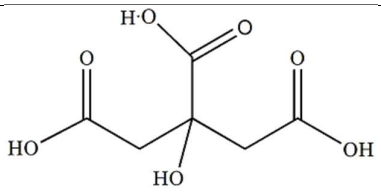	Fundamental in biochemistry. The annual production for industrial applications like food and cosmetics is more than a million tons.[16]
Lidocaine	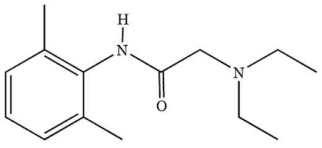	This is classified in the WHO's List of Essential Medicines as a local anaesthetic and antiarrhythmic drug.
D-Tartaric acid	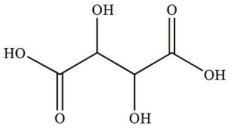	Naturally present in wine, it is used in food preparations and it is an excipient for effervescent drug formulations.

Urea	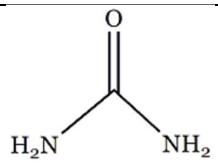	Secreted by organisms and industrially synthesized, it is used mostly for fertilization of plants and other technological applications.
L-Ascorbic acid (Vitamin C)	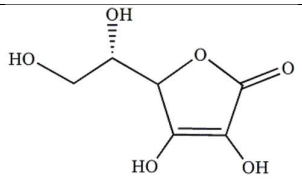	Essential nutrient for certain animals (like humans). It has an enormous field of application in areas such as medicine, chemistry and biology.

3.5) EXPERIMENTAL ATTEMPTS

In the next sections of this work, the aspects of results will be discussed. In the *Tables 3.2* and *3.3* are reported all the attempts made with the APIs (SSZ and Fluconazole respectively), co-formers and cyclodextrins. In these tables, the first column lists labels identifying specific experiments. Co-crystallization/inclusion complex formation attempts that yielded possible new solid forms have labels *in italic type* and the respective partner molecules appear in *italic underscored* type in the two succeeding columns.

Table 3.2: Experimental attempts to form co-crystals/CD inclusion complexes with SSZ.

LABEL	API	CO-FORMER	RATIO	CRYSTALLIZATION TECHNIQUES	SOLVENTS
1 AS	I-SSZ*	Nicotinic acid	1:1	Neat grinding, LAG	Acetone, Acetonitrile, THF
2 AS	I-SSZ	Pyrazinecarboxamide	1:1	Neat grinding, LAG	Acetone, Acetonitrile, THF
3 AS	I-SSZ	Fumaric acid	1:1	Neat grinding, LAG	Acetone, Acetonitrile, THF
4 AS	I-SSZ	Citric acid	1:1	Neat grinding, LAG	Acetone, Acetonitrile, THF
5 AS	*I-SSZ*	*Lidocaine*	1:1	Grinding, LAG, Seeding, Co-precipitation, Vapour diffusion, Liquid-liquid interface diffusion	Acetone, Acetonitrile, THF, DMSO, Hexane, DMF, Methanol, Cyclohexane, Ethyl acetate

6 AS	I-SSZ	D-Tartaric acid	1:1	Neat grinding, LAG	Acetone, Acetonitrile, THF
7 AS	I-SSZ	Urea	1:1	LAG, Co-precipitation, Neat grinding	Acetone, Acetonitrile, THF
8 AS	I-SSZ	L-Ascorbic acid	1:1	Neat grinding, LAG	Acetone, Acetonitrile, THF
9 AS	I-SSZ	β-cyclodextrin	1:1	Kneading, Co-precipitation	H_2O
10 AS	*A-SSZ**	*Citric acid*	1:1	Co-precipitation, LAG	EtOH, MEK
11 AS	*A-SSZ*	*Urea*	1:1	Co-precipitation, LAG	EtOH, MEK
12 AS	*A-SSZ*	*Lidocaine*	1:1	Co-precipitation, LAG, Neat grinding	EtOH, MEK, Acetonitrile
13 AS	*I-SSZ*	*γ-cyclodextrin*	1:1	Kneading, Co-precipitation	H_2O
14 AS	A-SSZ	γ-cyclodextrin	1:1	Kneading, Co-precipitation	H_2O, EtOH
15 AS	A-SSZ	β-cyclodextrin	1:1	Kneading, Co-precipitation	H_2O
16 AS	A-SSZ	Nicotinic acid	1:1	LAG	EtOH
17 AS	A-SSZ	Fumaric acid	1:1	LAG	EtOH
18 AS	A-SSZ	Pyrazinecarboxamide	1:1	LAG	EtOH
19 AS	A-SSZ	L-Ascorbic acid	1:1	LAG	EtOH
20 AS	A-SSZ	D-Tartaric acid	1:1	LAG	EtOH
21 AS	I-SSZ	α-cyclodextrin	1:1	Kneading, Co-precipitation	H_2O
22 AS	A-SSZ	α-cyclodextrin	1:1	Kneading, Co-precipitation	H_2O
23 AS	I-SSZ	TRIMEB	1:1	Co-precipitation	H_2O
24 AS	A-SSZ	TRIMEB	1:1	Co-precipitation	H_2O
25 AS	I-SSZ	DIMEB	1:1	Co-precipitation	H_2O
26 AS	A-SSZ	DIMEB	1:1	Co-precipitation	H_2O

*I-SSZ and A-SSZ refer to the sulfasalazine tautomers (imine and amine respectively).

Table 3.3: Experimental attempts to form CD inclusion complexes with Fluconazole.

LABEL	API	CYCLODEXTRIN	RATIO	CRYSTALLIZATION TECHNIQUE	SOLVENTS
50 AS	*Fluconazole*	*β-cyclodextrin*	1:2	Kneading, Co-precipitation	H_2O
51 AS	*Fluconazole*	*γ-cyclodextrin*	1:1	Kneading, Co-precipitation, Seeding	H_2O
52 AS	Fluconazole	α-cyclodextrin	1:1	Kneading, Co-precipitation	H_2O
53 AS	Fluconazole	TRIMEB	1:1	Co-precipitation	H_2O
54 AS	Fluconazole	DIMEB	1:1	Co-precipitation	H_2O

The total number of experiments performed was 165.

If the first LAG or kneading experiment with a particular co-former did not yield a PXRD pattern indicating a possible new product (e.g. 18 AS), a new co-former was immediately introduced for further experiments. In certain cases (e.g. 5 AS and 12 AS for SSZ, and 50 AS and 51 AS for fluconazole), where positive results were identified at an early stage, a large number of further experiments followed in order to obtain better definition of the new product and to isolate single crystals for X-ray structural studies. These examples will be discussed in the next chapters.

3.6) REFERENCES

1. M. C. Stuart, M. Kouimtzi, S. R. Hill, *WHO Model Formulary 2008*, World Health Organization, Geneva, 2009.
2. Sulfasalazine, https://www.drugs.com/monograph/sulfasalazine.html, (accessed October 2017).
3. M. Lo, V. Ling, C. Low, Y. Z. Wang, P.W. Gout, *Curr. Oncol.*, 2010, **17**, 9–16.
4. Sulfasalazine, www.drugbank.ca/sulfasalazine, (accessed October 2017).
5. L. A. Filip, M. R. Caira, *Acta Cryst*., 2001, **C57**, 435-436.
6. J. Fischer, C. R. Ganellin, *Analogue-based Drug Discovery*, IUPAC, John Wiley & Sons, USA, 2006, p. 503.
7. WHO Model List of Essential Medicines (20th List), http://www.who.int/medicines/publications/essentialmedicines/EML_2015_FINAL_amended_NOV2015.pdf?ua=1, (accessed October 2017).
8. Fluconazole, http://www.pubchem.ncbi.nlm.nih.gov, (accessed October 2017).
9. J. Kastelic, Z. Hodonik, P. Sket, J. Plavec, N. Lah, I. Leban, M. Pajk, O. Planinsek, D. Kikelj, *Cryst. Growth Des.*, 2010, **10**, 4943-4953.
10. J. Kastelic, N. Lah, D. Kikelj, I. Leban, *Acta Cryst*., 2011, C**67**, 0370-0372.
11. *Generally Recognized as Safe* (GRAS), F. da. Gov. Retrieved **2013-03-17**.
12. J. Krutmann, P. Humbert, *Nutrition for Healthy Skin: Strategies for Clinical and Cosmetic Practice*, Springer Science & Business Media, Berlin, p. 153.
13. S. Spaia, I. Magoula, G. Tsapas, G. Vayonas, *Perit. Dial. Int*., 2000, **20**, 47–52.
14. Pyrazinamide, *https://www.drugs.com/monograph/pyrazinamide.html, (accessed October 2017).*

15. Current EU approved additives and their E Numbers, https://www.food.gov.uk/science/additives/enumberlist, (accessed November 2017).
16. M. Berovic, M. Legisa, *Biotechnology Annual Review*, 2007, **13**, 303–343.

CHAPTER 4

STUDIES ON SULFASALAZINE: CO-CRYSTALLIZATION AND CYCLODEXTRIN INCLUSION COMPLEXATION

The differences between functional groups on the two tautomers of sulfasalazine (SSZ) *(Figure 4.1)* are fundamental for the formation of a new crystalline phase. Aminic sulfasalazine (A-SSZ) presents a 2-aminopyridine group and imine sulfasalazine (I-SSZ) has a 1-hydropyridine-2-imine group. The synthons that each molecule should build with a co-former are similar but different for this portion of the molecule. The second portion, that could already form synthons, is a salicylic acid-diazenide group both in A-SSZ and I-SSZ.

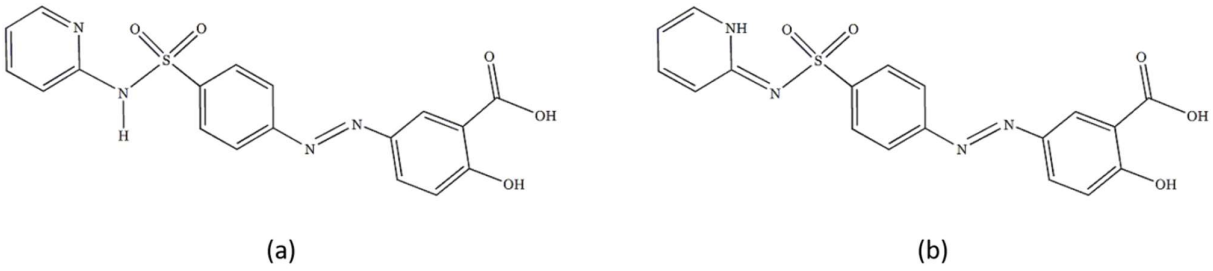

Figure 4.1: Schematic representations of A-SSZ (a) and I-SSZ (b).

The difference between each tautomer should be distinguishable also by PXRD analysis. In *Figure 4.2* are reported the PXRD patterns of A-SSZ and I-SSZ.

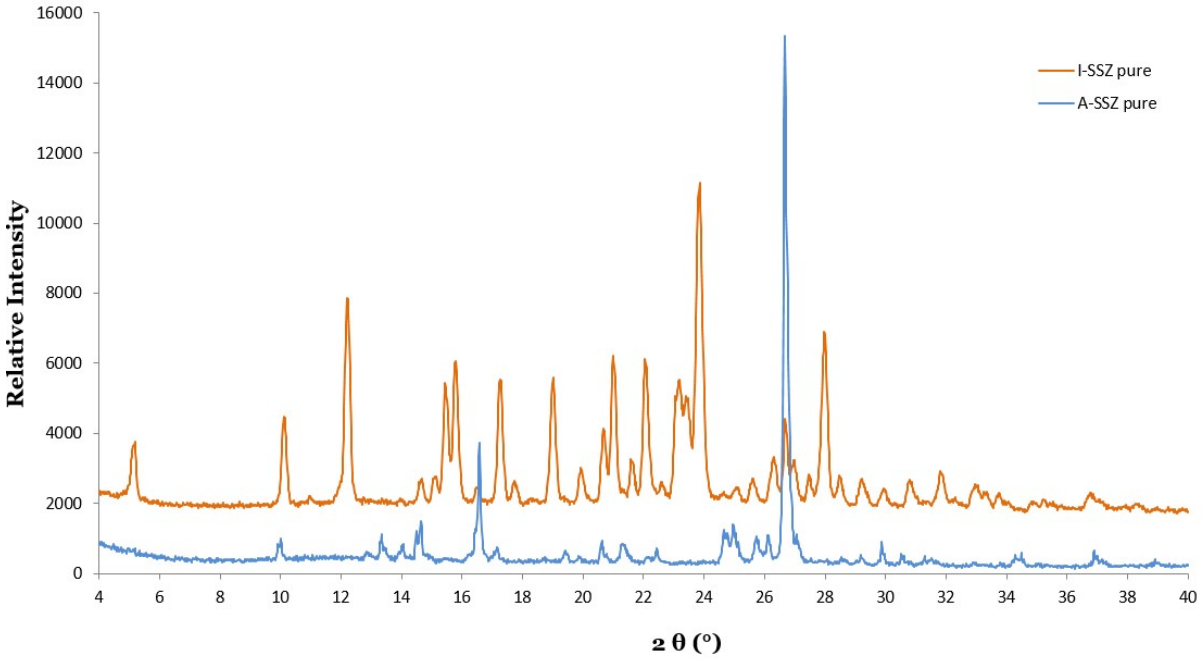

Figure 4.2: PXRD pattern comparison between A-SSZ (blue trace) and I-SSZ (orange trace) to underline the difference between the two crystalline structures. A-SSZ trace has been mathematically rescaled to facilitate the comparison.

Given these structural differences, it was expected that some co-formers (COFs) and cyclodextrins (CDs) could react preferentially with only one tautomer. *Table 4.1* shows the results obtained for the attempts underscored in *Table 3.2* of Chapter 3.

Table 4.1: Experimental results with SSZ tautomers and different co-formers.

	I-SSZ	**A-SSZ**
LIDOCAINE	New crystalline phase	New crystalline phase
UREA	Physical mixture	New crystalline phase
CITRIC ACID	Physical mixture	New crystalline phase
γ-CYCLODEXTRIN	Inclusion complex	Physical mixture

For all the positive results reported in *Table 4.1*, it was impossible to determine the product crystalline structures due to the absence of single crystals. It was instead possible to study them with other types of analysis such as powder X-ray diffraction (PXRD), thermal techniques (HSM, DSC, TGA) and spectroscopy (^{1}H-NMR, IR).

4.1) SULFASALAZINE CO-CRYSTALLIZATION EXPERIMENTS

4.1.1) SSZ AND LIDOCAINE (Expts. 5 AS AND 12 AS, Chapter. 3)

The experiments were carried out in a considerable number for the possibility of obtaining a new crystalline phase with two drugs. The lidocaine interacted with both the sulfasalazine tautomers but it was not clear *how* it did so. The physical state was amorphous for all the products (28 in total) and it was impossible to determine their formulae or structures. All the crystallization techniques were tried: neat grinding, liquid-assisted grinding (LAG), vapour diffusion, liquid-liquid diffusion (with miscible and immiscible solvents), co-precipitation and seeding. The first physical property that changed in the products was the *colour*. A-SSZ and I-SSZ have, respectively, an orange and a dark orange colour, the finely powdered lidocaine is colourless and the LAG or ground products were orange-red. This evidence, revealed again with more solvents and sometimes with diffusion or co-precipitation, suggested that a new phase might have formed by combining these substances. The problem was the *amorphous character*, which hampered their characterization. All the co-precipitation attempts were carried out in an adapted Pasteur pipette, tapered to form a small and long vial. The small surface area of liquid reduced the evaporation rate significantly, preventing the formation of the amorphous red paste. The results were not encouraging. *Figure 4.3* shows the images of the tautomers of sulfasalazine and COF powders and the results of grinding processes. The PXRD patterns of the two products (*Figures 4.4* and *4.5*) are very different: the first product, with I-SSZ, was prepared by LAG in THF and it is completely amorphous; the second, with A-SSZ, was obtained via dry co-grinding and it was the only one product, from the complete set of attempts, that presents a crystalline character (albeit low). *Figure 4.5* were very useful for understand the loss of crystallinity but the traces were not easily comparable. For these reasons, the data of *Figure 4.5* were mathematically rescaled and *Figure4.5A* was added.

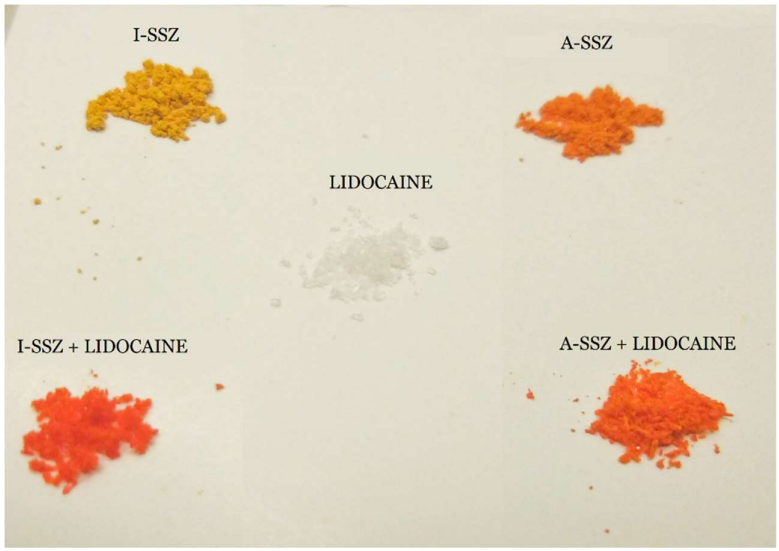

Figure 4.3: Difference in the colours of the SSZ tautomers and colour changes which occurred with the experimental co-grinding attempts of the individual tautomers with lidocaine.

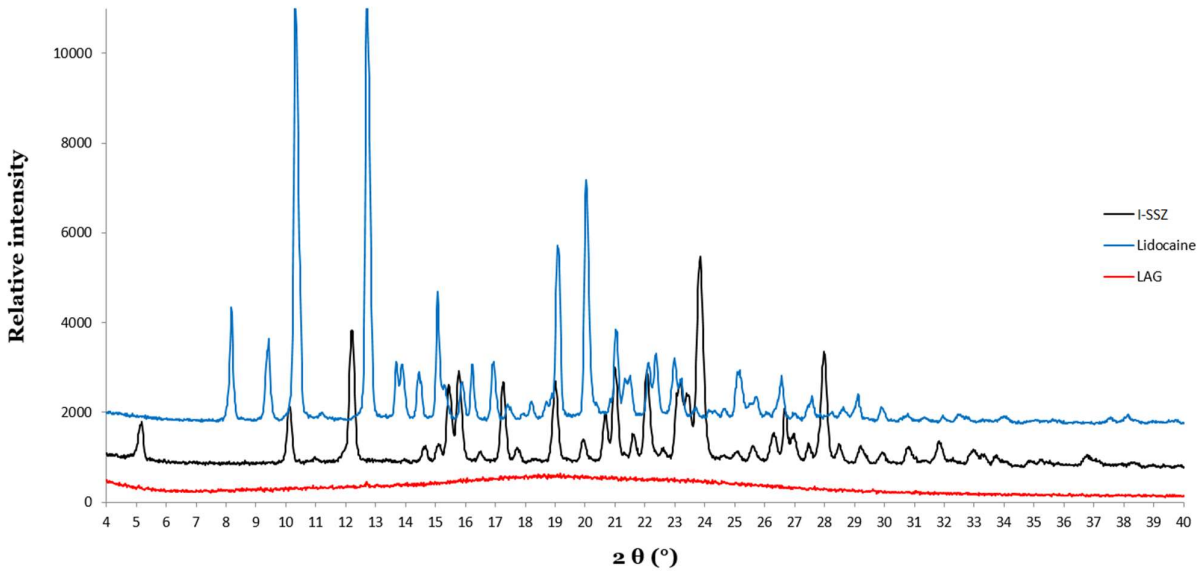

Figure 4.4: PXRD traces of I-SSZ (black), Lidocaine (blue) and the amorphous product of LAG using THF (red).

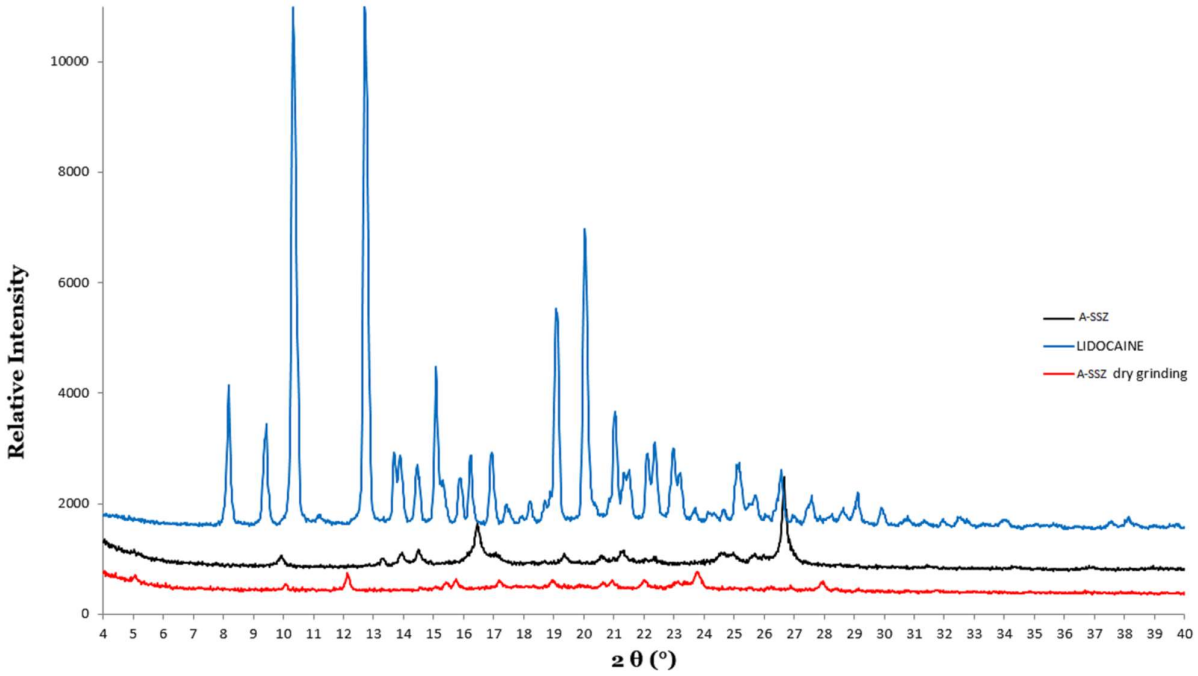

Figure 4.5: PXRD confirmation of a new crystalline phase (red trace) obtained from dry co-grinding of A-SSZ (black trace) and lidocaine (blue trace).

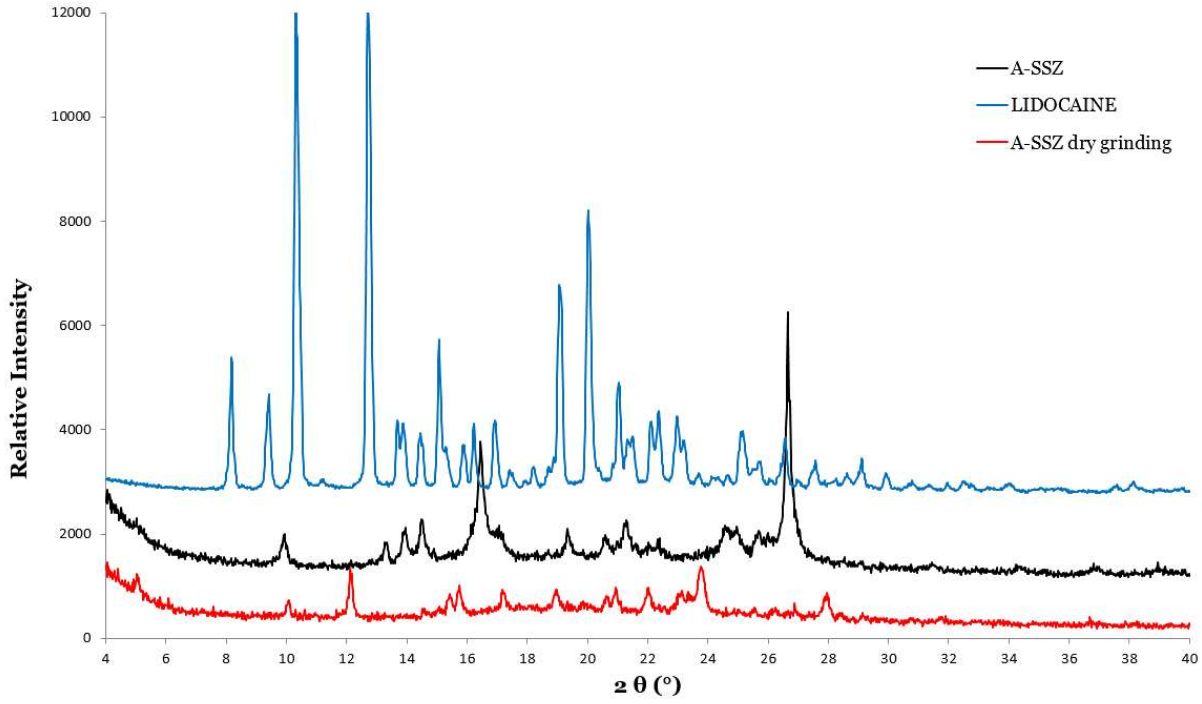

Figure 4.5A: Figure 4.5 mathematically rescaled to facilitate the comparison between traces.

The importance of the red pattern, in *Figure 4.5* and *Figure 4.5A,* would become very significant later. It corresponded to *the only product that had presented a low crystalline character*. The procedure to obtain the amine tautomer in an adequate quantity to proceed with the crystallization attempts had a low yield. For this reason, the quantities of A-SSZ were always meagre and the author was often forced to use small quantities of powders for the attempts. The intention was to prepare other samples shortly after (unfortunately all subsequent attempts with the same operating procedure yielded products that were completely amorphous).

4.1.2) A-SSZ AND UREA (Expt. 11 AS, Chapter 3)

After some grinding studies on both tautomers of SSZ, it was discovered that only the A-SSZ interacts with urea. All the compounds used for these experiments are shown in *Figure 4.6* and all samples are fine powders except the one at the bottom right. At a glance, it is possible to see the difference of physical state between the two product powders. The LAG, done in EtOH, produces a paste if conducted for a long time (~ 15 min) and with vigour. On the contrary, if the force used and the duration of LAG (~ 10 min) are both less, the product is more crystalline. It is possible to notice the loss of crystallinity in *Figure 4.7,* where the PXRD patterns of A-SSZ, urea and the ground products are reported.

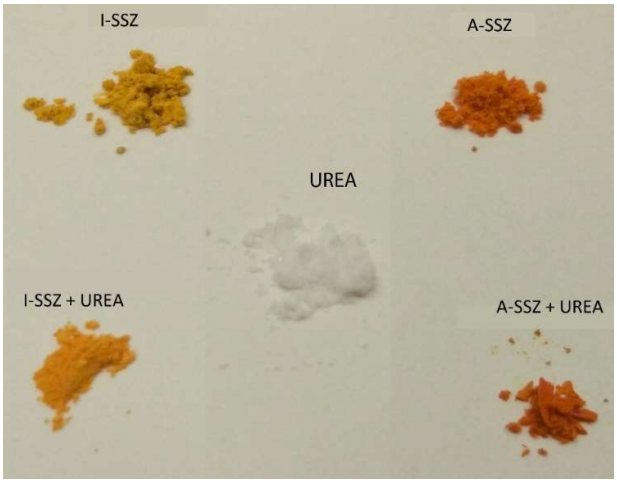

Figure 4.6: Powder samples of the tautomers of SSZ, urea and the respective LAG products.

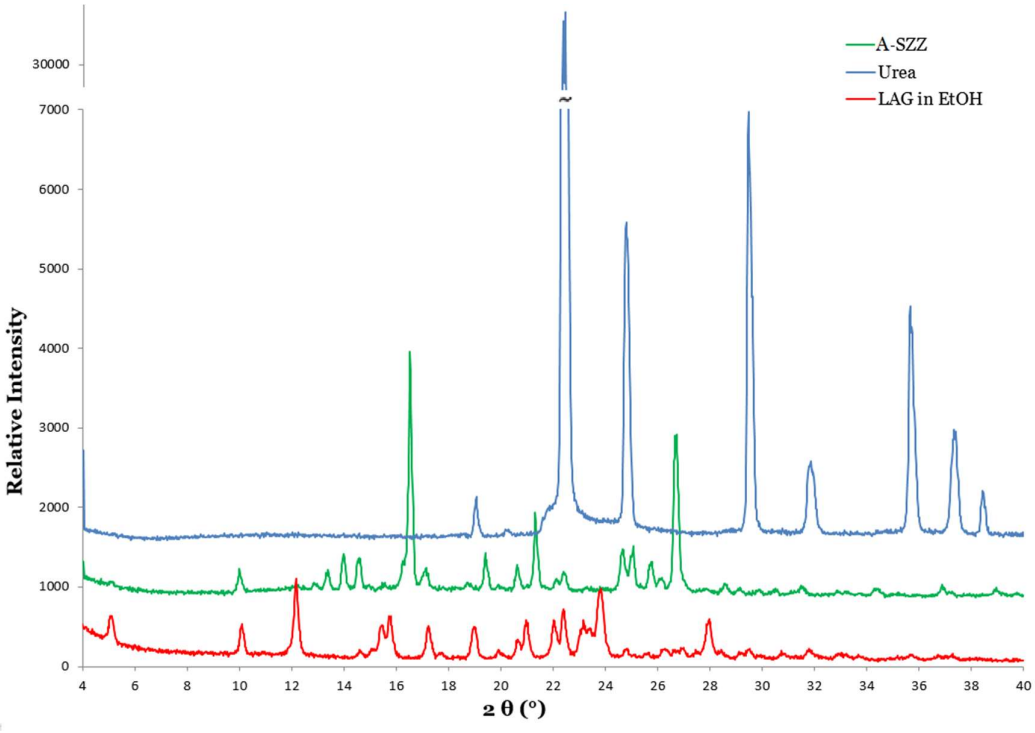

Figure 4.7: PXRD pattern of new crystal phase A-SSZ-urea (red) compared with urea (blue) and pure A-SSZ (green) PXRD traces. Notice the loss of crystallinity of the A-SSZ-urea pattern compared to the pure urea one.

All the attempts at co-precipitation failed, resulting in separate crystallization of each substance in vials.

4.1.3) A-SSZ AND CITRIC ACID (Expt. 10 AS, Chapter 3)

For lack of time, the study on this attempt produced only a PXRD confirmation of the presence of a new crystal phase (red PXRD trace in *Figure 4.8*). It was prepared with a LAG in methyl ethyl ketone (MEK) for ~10 minutes. No other studies were carried out.

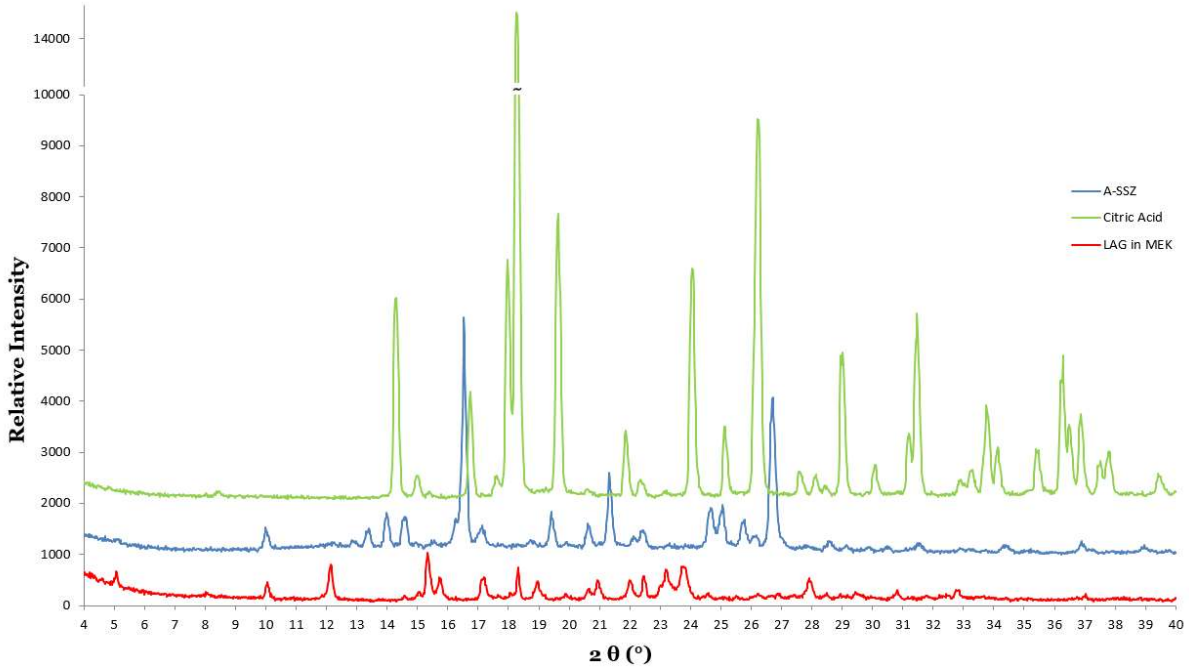

Figure 4.8: PXRD pattern of the new A-SSZ-citric acid crystal phase (red trace), compared with PXRD patterns of pure citric acid (green trace) and A-SSZ (blue trace). The red trace has been mathematically rescaled for clarity.

4.1.4) A COMMENTARY ON PXRD TRACES AND CONCLUSIONS

It is known that the grinding process can modify the solid-state of the components in the mortar. A polymorph[1] or a tautomer[2] might be generated with a different time of grinding, energy or type of solvent. Observing the PXRD patterns relative to the new crystal phases (A-SSZ-lidocaine, A-SSZ-urea and A-SSZ-citric acid) of *Figures 4.5, 4.5A, 4.7* and *4.8,* it was possible to notice an isostructural characteristic and a possible similarity with the I-SSZ PXRD profile. In *Figure 4.9* is reported a PXRD pattern comparison of all new crystal phases and the SSZ tautomers. The result is an elevated level of agreement of the three crystal phases and the I-SSZ pattern (the reader is reminded that the starting tautomer for these attempts was A-SSZ). Therefore A-SSZ, during each LAG experiment, was evidently involved in the tautomerization process to become I-SSZ and each co-former changed its physical state from crystalline to amorphous. This should be considered uncommon but it is the only explanation possible for the result reported below.

This unexpected effect undermined efforts to achieve the desired reactions. To obtain a single crystal, many attempts were carried out with very slow crystallization techniques (low

temperatures or evaporation rates of solvents) trying to avoid the formation of the amorphous phase observed with the mechanochemical approach. A slow phase diffusion is a good example. The experiment was carried out with both SSZ tautomers and lidocaine (1:1). The system was left undisturbed in the refrigerator at 4 °C for 3 months but no crystals formed at the interphase between immiscible solvents. A large number of other experiments were carried out for a total of 68. The formation of a single-crystal was not observed, only amorphous aggregates were present. No other attempts of co-crystallization with SSZ were carried out.

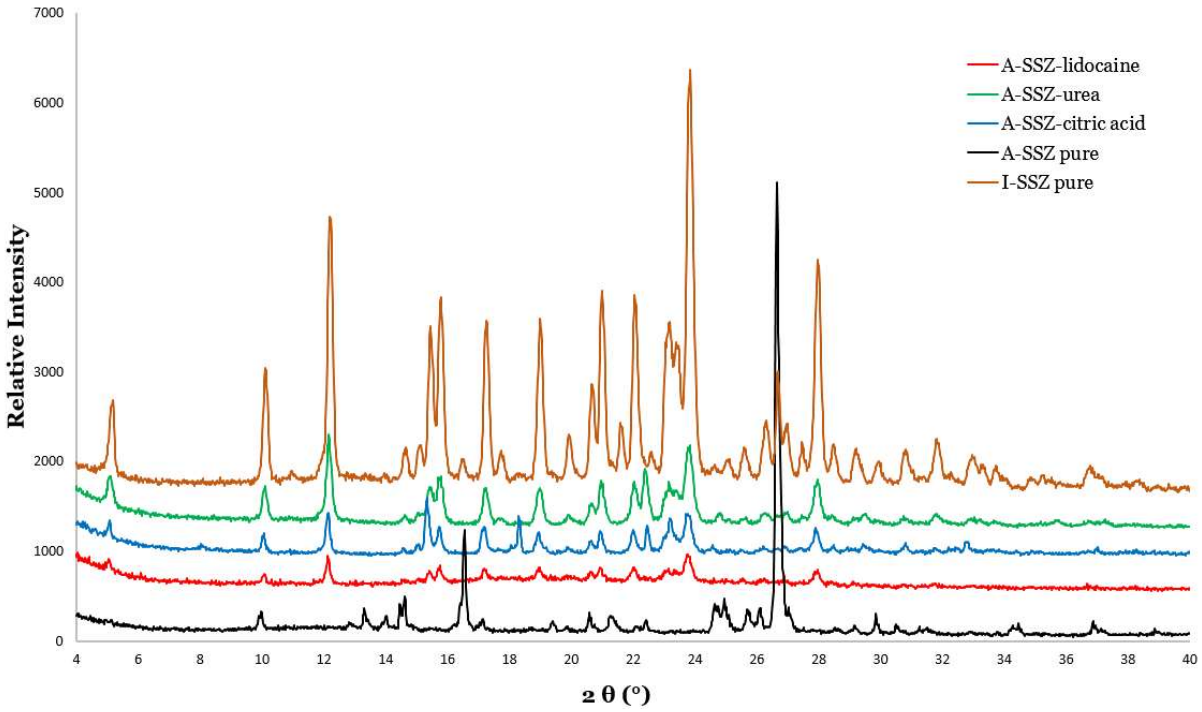

Figure 4.9: PXRD pattern comparison of A-SSZ-lidocaine (red), A-SSZ-urea (green), A-SSZ-citric acid (blue), A-SSZ (black) and I-SSZ (orange). Notice the elevated degree of agreement of each product with I-SSZ, evidence for the tautomerization process which had occurred during all the LAG experiments.

4.2) I-SSZ AND γ-CD (Expt. 13 AS, Chapter 3)

A new crystal phase between I-SSZ and γ-CD was obtained by means of delicate kneading (~15 min) with 25 μl of Milli-Q® water. The powders of host and guest were in a 1:1

stoichiometric ratio. Other attempts with the same experimental conditions were carried out with A-SSZ as guest without any encouraging result. The appearance of I-SSZ-γ-CD was a light orange powder. After the preliminary attempt and the analysis using-PXRD (*Figure 4.10*), other crystallization techniques were explored.

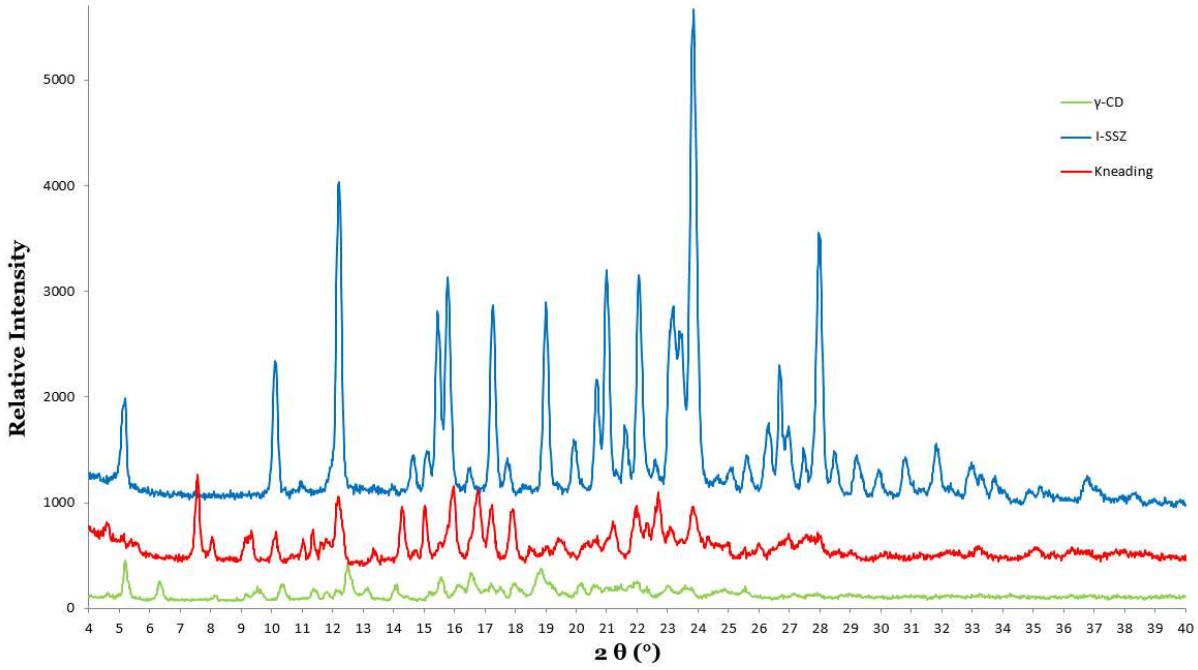

Figure 4.10: PXRD pattern of new crystal phase I-SSZ-γ-CD (red) compared with PXRD traces of pure I-SSZ (blue) and γ-CD (green).

The confirmation of the presence of a new inclusion complex was obtained by showing that the red PXRD trace in *Figure 4.10* matched the reference PXRD pattern for known γ-CD inclusion complexes reasonably well.[3] Using the principle of isostructurality, this implies that the structural arrangement of the host γ-CD molecules in the new inclusion complex is known, but the precise location of the guest molecules within the channel created by the stacked host molecules is not.

No co-precipitation or seeding (using a bit of powder as seeds) attempts gave encouraging results and no single crystals of the complex were prepared (all vials presented a separate crystallization of I-SSZ and γ-CD). For these reasons, all possible analyses (thermal and

spectroscopic) were carried out but it was impossible to determine the structure of the complex using singe crystal X-ray diffraction.

The first thermal analysis was HSM. The images below (*Figure 4.11*) show the best series of micrographs from a set of three experiments with this instrument to determine the behaviour of the complex with increasing temperature until its degradation.

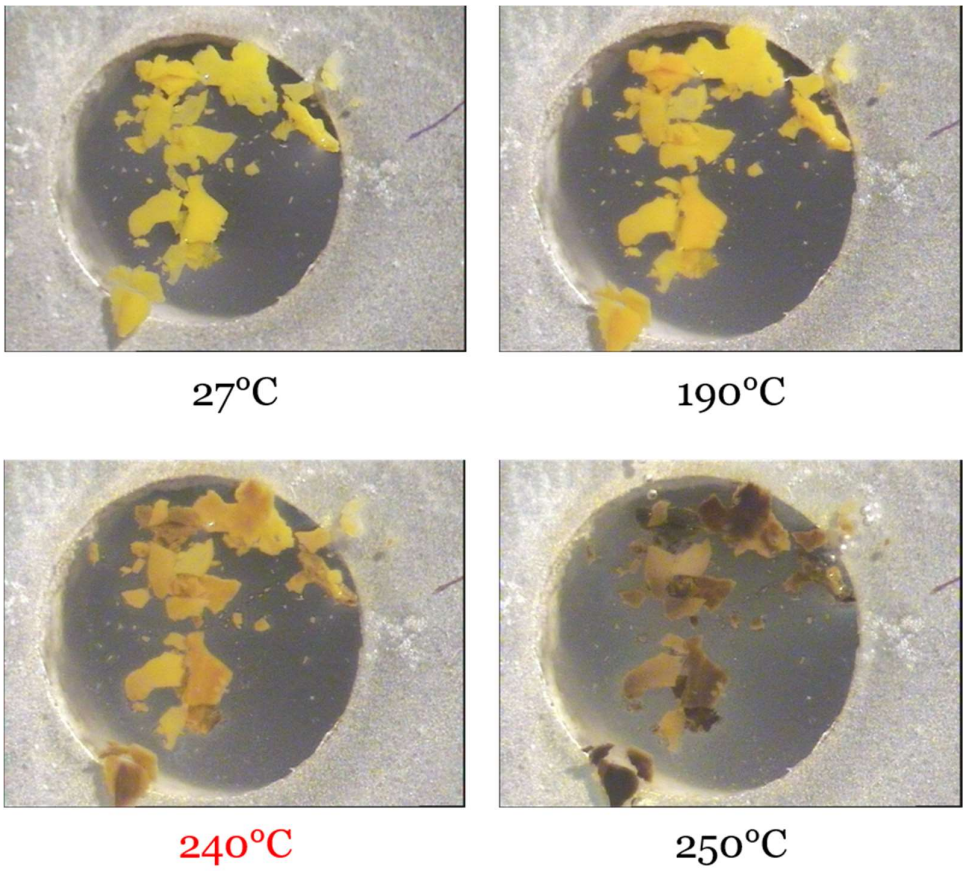

Figure 4.11: HSM on the inclusion complex I-SSZ-γ-CD.

It is important to recall the melting range of I-SSZ (265-266 °C) and the degradation point of γ-CD (267 °C). Progressively from 27 °C to 190 °C the complex in powder form became a bit darker, which could be a sign of dehydration (in the picture relative to 190 °C, two small bubbles are present. No vigorous bubbling was observed but the dehydration phenomenon is underscored by TG and DSC analyses that present a signal variation around 100 °C. The solvent used to carry out the kneading process was water only; no other solvents were used

to prepare this sample. The decomposition began at 240 °C and it was complete at 250 °C. The relatively low temperature of degradation, compared with I-SSZ and γ-CD melting points, confirmed the new crystalline phase. The bubbles visible in the last picture (250 °C) are caused by the formation of CO_2.

The ^{1}H-NMR spectrum in DMSO-d_6 is reported in *Figure 4.12*. It was used to check if the stoichiometric ratio between I-SSZ and γ-CD was different from the one used to prepare the sample (host and guest were inserted in the mortar in a 1:1 molar ratio). In *Table 4.2* all the integration peaks for this analysis are summarized. The data indicate that the stoichiometry remained 1:1.

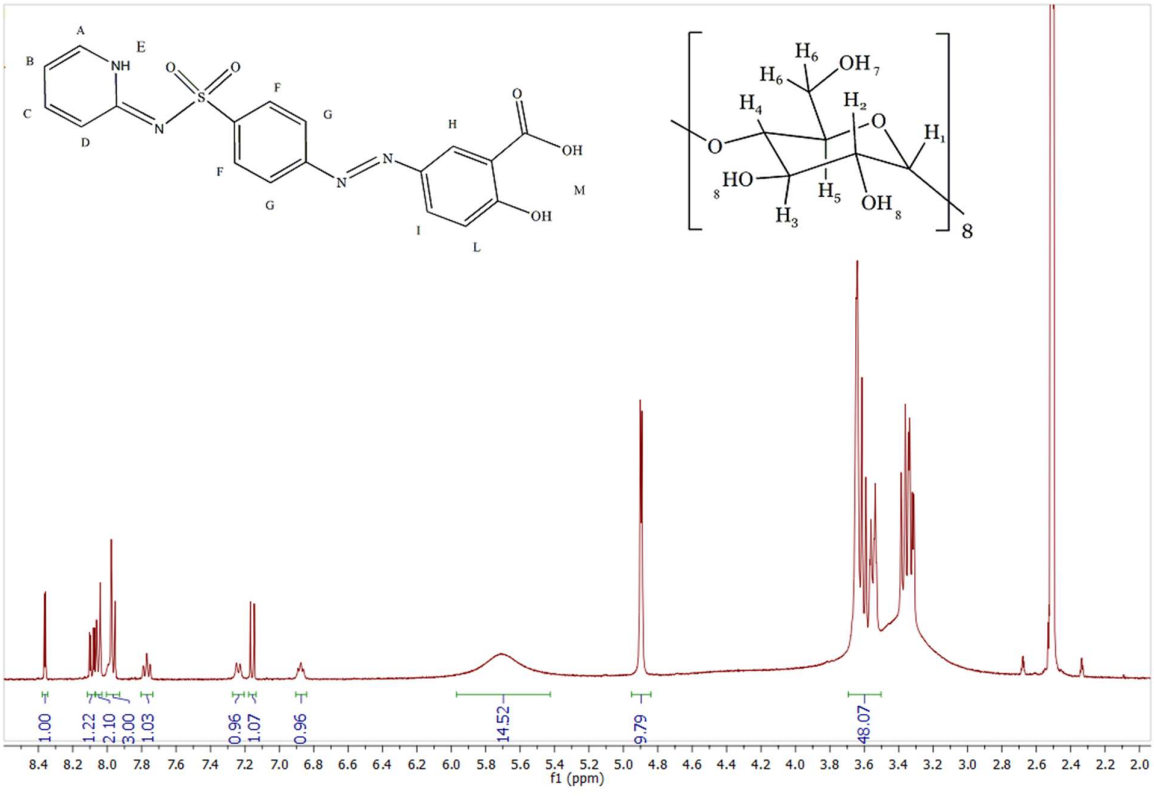

Figure 4.12: ^{1}H-NMR for inclusion complex I-SSZ-γ-CD.

Table 4.2: ^{1}H-NMR integration peaks for inclusion complex I-SSZ-γ-CD.

Proton	δ (ppm)	Multiplicity	J (Hz)	Integration	Experimental/ Theoretical
H_H	8.35-8.37	d	2.1	1.00	1.00
H_F, H_G, H_A, H_I, H_L	7.94-8.11	m	/	6.32	0.90
H_C	7.73-7.80	m	/	1.03	1.03
H_E	7.26-7.27	d	6.3	0.96	0.96
H_D	7.14-7.17	d	6.9	1.07	1.07
H_B	6.85-6.90	t	4.8	0.96	0.96
H_8	5.71	s	/	14.5	0.91
H_1	4.87-4.95	d	3	9.79	1.22
H_2, H_3, H_4, H_5, H_6	3.51-3.69	m	/	48.07	1.00

*reference integral

Three hydroxyl protons (H_M and H_7) are absent from the spectrum. This could be explained assuming a signal overlap with the broad water peak of the solvent at 3.3 ppm. The peaks at 2.5 ppm and 3.3 ppm were not analysed because they were referable to the signals of DMSO and water, respectively.

In the Appendix section it is possible to find the ^{1}H-NMR spectra of pure γ-CD and pure I-SSZ (*Figures A1* and *A2,* respectively). The analysis and the comparison of these results were useful to clarify the commentary written above. In *Figure A1*, the hydroxyl proton H_7 was present. Therefore, it was possible to conclude that the overlap in *Figure 4.12* is a realistic hypothesis. The effects of complexation were clear for three more signals:

- the H_8 signal in the complex spectrum, *Figure 4.12*, it was a broad peak and in *Figure A1* it was a well resolved peak:
- the axial protons of γ-CD H_2 and H_4 are completely overlapped with H_3, H_5 and H_6 signals in *Figure 4.12* while, in *Figure A1*, it was possible to observe two, separate and well resolved, multiplets.

In *Table A2* of the Appendix, it was evident that the H_B proton was a multiplet instead of a triplet, as reported in *Table 4.2*. The reason for this alteration is probably related to the low concentration of complex inside the NMR tube.

To determine the water content of the complex, TG and DSC investigations were performed in a set of three attempts per type of analysis. The results were consistent but they did not fully confirm the HSM test (vigorous bubbling in the dehydration temperature range evidenced by TGA was not observed in HSM). The combined TG and DSC curves are reported in *Figure 4.13*. It was possible to find the average percentage of water lost during the TG experiment (13.4% ± 0.1 %) and, with equation *(8)*, the corresponding number of water molecules (n=15 ± 0.3) has been calculated. It was thus possible to state the full stoichiometric chemical formula of the 1:1 complex, namely $C_{48}H_{80}O_{40}{\cdot}C_{18}H_{14}O_5N_4S{\cdot}15H_2O$.

$$\% = \frac{n \times MW_{H_2O}}{MW_{\beta-CD} + MW_{I-SSZ} + (n \times MW_{H_2O})} \qquad (8)$$

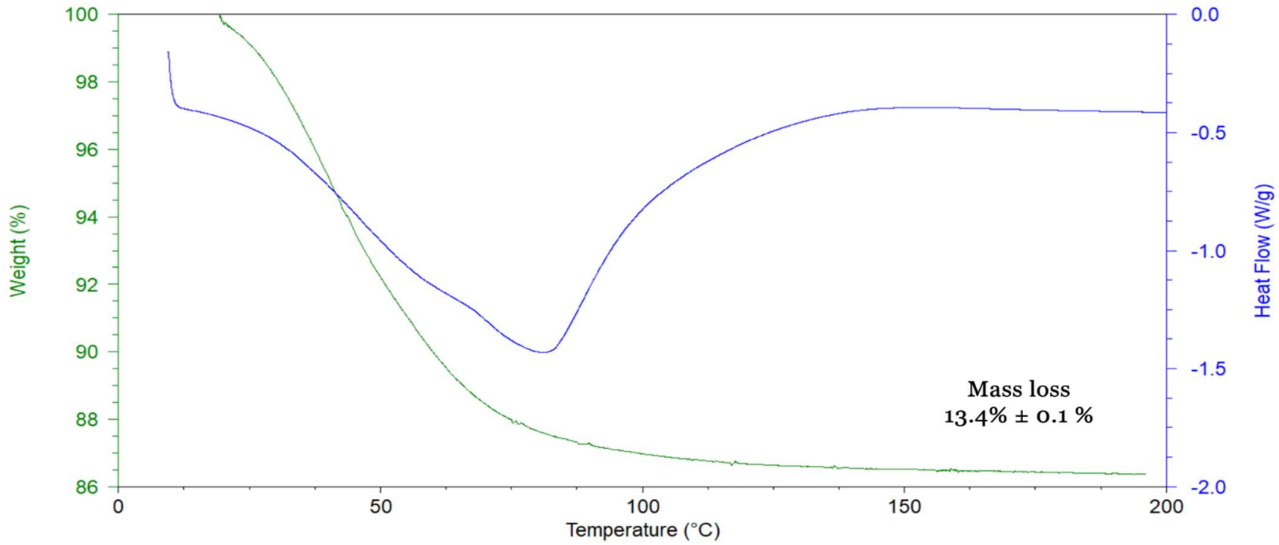

Figure 4.13: Overlaying of TGA (blue trace) and DSC (green trace) for the I-SSZ-γ-CD inclusion complex.

To conclude, it is possible to state that only the I-SSZ tautomer could interact with the host to form an inclusion complex. Some experimental attempts to form a complex between γ-CD and the tautomer A-SSZ were carried out and the results were all negative. This result is consistent with an earlier study in which it was reported that only the imide tautomer of SSZ

formed inclusion complexes with both β- and γ-CD via kneading, while neither of the two tautomers could include in α-CD.[4]

4.4) REFERENCES

1. M. S. Hoard and S. D. Elakovic, *Phytochemistry*, 1996, **43**, 1129-1133.
2. A. J. Cruz-Cabeza and C. R. Groom, *CrystEngComm*, 2011, **13**, 93-98.
3. M. R. Caira, *Rev. Roum. Chim.*, 2001, **46**, 371-386.
4. S. Lubhelwana, Crystal isostructurality and X-ray diffraction studies of cyclodextrin inclusion compounds, 2005, MSc dissertation, University of Cape Town, South Africa, p.87. (https://open.uct.ac.za/handle/11427/6324, accessed Nov 2017).

CHAPTER 5

β-CYCLODEXTRIN INCLUSION OF FLUCONAZOLE: TWO NOVEL FORMS OF AN ANTIFUNGAL DRUG.

Fluconazole, as anticipated in Chapter 3, is an antifungal drug of wide use in pharmacy. Its low solubility in water (~1 mg/l at 25 °C)[1] could be improved via complexation with cyclodextrins, as explained in the introductory chapters.

5.1) EXPERIMENTAL

With an accurate procedure explained below, two forms of an inclusion complex between fluconazole and β-CD (*Figure 5.1*) were isolated: the first crystallizes in a monoclinic space group (MBCDFLU) and the second crystallizes in a triclinic space group (TBCDFLU). The aspects related to their structural analyses by X-ray diffraction will be explained later.

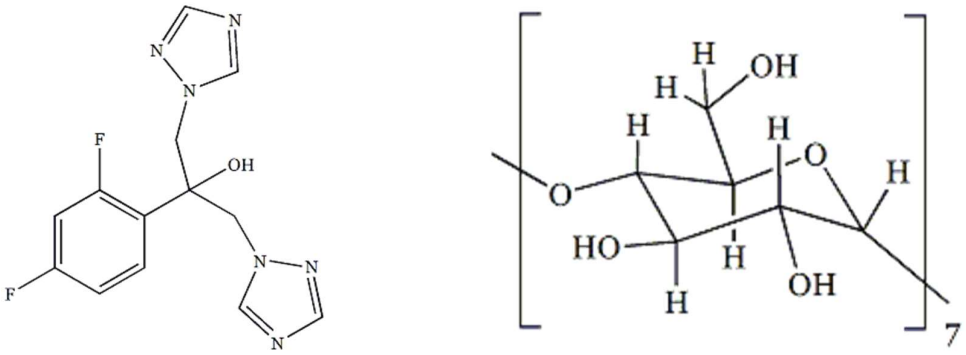

Figure 5.1: Schematic representations of fluconazole (left) and of β-cyclodextrin (right).

A concentrated solution of β-cyclodextrin was prepared by adding ~37 mg (0.1208 mmol) to 0.5 ml of pure water. Keeping the solution stirred, the temperature was raised to 60 °C. The fluconazole was added slowly into the vial (~1 mg every hour for a total of ~5 mg) and then the solution was stirred for a period of 20-24 h, keeping the temperature constant. The solution was then filtered through a 0.45 μm filter into a clean, pre-heated vial. A Dewar

flask was filled with hot water and the vial was immersed in the flask. The system was covered with tinfoil and hydrophilic cotton to isolate it from the surroundings and it was left to incubate, followed by slow cooling for two days. Large, colourless crystals were obtained.

The temperature of incubation was critical to differentiate the crystal forms. If the process started at 60 °C the only form obtained was the monoclinic one, whereas if it started at 45 °C or less, only the triclinic form was obtained. Together with the incubation temperature, the concentration of the solution of β-cyclodextrin was the second variable for the formation of these crystals. In an attempt without incubation, with slow evaporation and low concentration of β-cyclodextrin (2.95×10^{-3} M), the result was a mixture of triclinic and monoclinic forms. The difference between them is their degree of hydration, and thus they are not polymorphs.

In *Table 5.1* are reported two sets of incubation data with different concentrations and the types of forms obtained (M = monoclinic, T = triclinic). To determine which type of complex had crystallized inside each vial, three crystals were casually selected from each batch and their unit cells were determined by single crystal XRD. To ensure homogeneity of crystal form, all the remaining crystals were subsequently analysed by PXRD.

Table 5.1: Experimental conditions for the preparation of TBCDFLU and MBCDFLU.

Name	V H_2O (ml)	Fluconazole (mg)	β-CD (mg)	Concentration (M)	Incubation T.	Crystals	Type of form
50-4 AS	0.5	5	37	6.52×10^{-2}	60 °C	√	**M**
SET No. 1	0.5	4	29.6	5.21×10^{-2}	60 °C	√	**M + T**
	0.5	3	22.2	3.91×10^{-2}	60 °C	√	**M + T**
	0.5	2	14.8	2.61×10^{-2}	60 °C	√	**M + T**
	0.5	1	7.4	1.3×10^{-2}	60 °C	√	**T**
	0.5	0.5	3.7	6.52×10^{-3}	60 °C	×	×
50-10 AS	0.5	5	37	6.52×10^{-2}	45 °C	√	**T**
SET No.2	0.5	4	29.6	5.21×10^{-2}	45 °C	√	**M + T**
	0.5	3	22.2	3.91×10^{-2}	45 °C	√	**T**
	0.5	2	14.8	2.61×10^{-2}	45 °C	√	**T**
	0.5	1	7.4	1.3×10^{-2}	45 °C	√	**T**
	0.5	0.5	3.7	6.52×10^{-3}	45 °C	×	×

The inclusion complex can be prepared also via kneading. The same amounts of raw materials used for the co-precipitation attempts were mixed in a mortar and kneaded for ~15 minutes with ~20 µl of pure water. The powder obtained (called 50-1 AS) was analysed by PXRD. The pattern of 50-1 AS is reported in *Figure 5.2* and it is compared with the PXRD traces of pure host and guest. It was used only to check the presence of an inclusion complex.

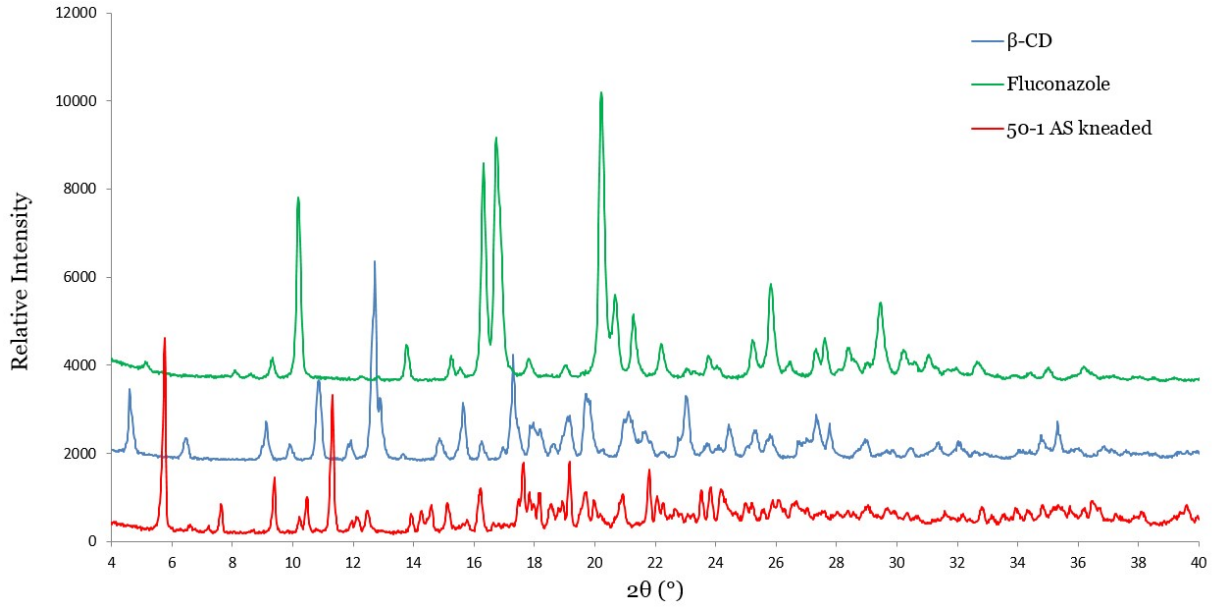

Figure 5.2: Powder pattern of 50-1 AS kneaded (red) compared with those of β-CD (blue) and fluconazole (green).

The 50-1 AS powder was recrystallized with an incubation at 60 °C and analysed again by PXRD. A subsequent analysis on this aspect was carried out after the completion of the study. The PXRD patterns of 50-1 AS before and after the recrystallization were compared with the two calculated patterns of TBCDFLU and MBCDFLU (*Figure 5.3*) based on their single crystal XRD structures (described later). The kneading process, that excludes the incubation procedure, leads to the complexation of raw materials in the triclinic form. If the powder is recrystallized by the incubation procedure, a form can be preferentially obtained (in this case the monoclinic, because the incubation temperature was 60° C).

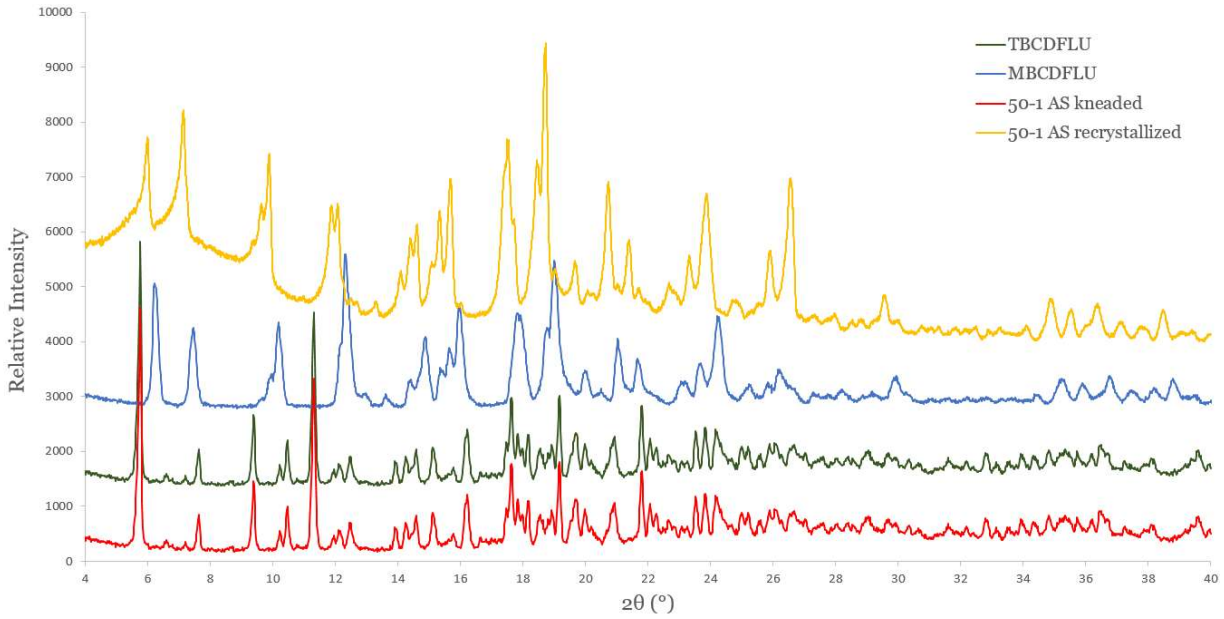

Figure 5.3: Comparison of 50-1 AS kneaded (red) and recrystallized (yellow) powder patterns. In the middle of the figure are reported, as references, the calculated PXRD traces of MBCDFLU (blue) and TBCDFLU (green).

It is possible to conclude that the preferred way to produce the monoclinic form is via the co-precipitation method that involves the incubation at the temperature of 60 °C. It is also possible to confirm that both forms could be prepared by a simple recrystallization, paying due attention to the concentration and temperature of the solution.

5.2) NUCLEAR MAGNETIC RESONANCE SPECTROSCOPY

Only a single ^{1}H-NMR spectrum is reported here (namely that for MBCDFLU) because both MBCDFLU and TBCDFLU have the same host-guest stoichiometry and the only expected change visible with nuclear magnetic resonance spectroscopy would be a different peak for water. The MBCDFLU spectrum is reported in *Figure 5.4* and in *Table 5.2* the relative integrations of peaks are presented. The underlined peaks in the spectrum (green) are those for water (3.30 ppm) and DMSO-d_6 (2.50 ppm).

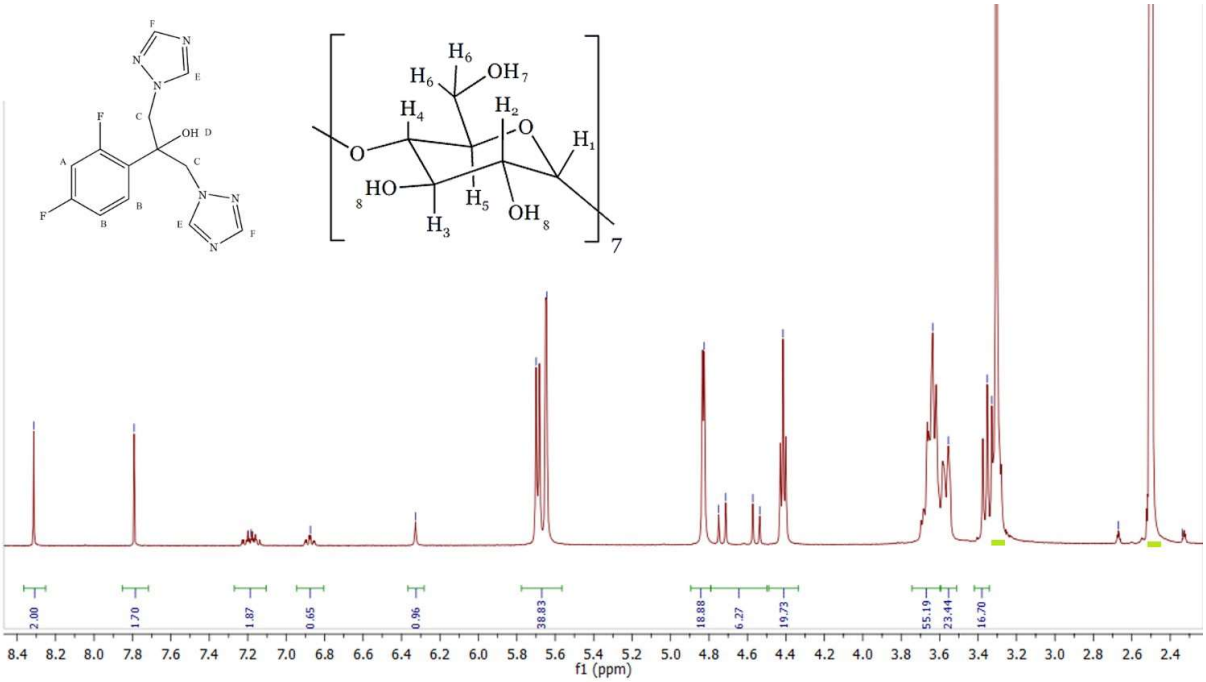

Figure 5.4: [1]H-NMR spectrum of MBCDFLU in DMSO-d_6.

Table 5.2: [1]H-NMR integration peaks for MBCDFLU.

Proton	δ (ppm)	Multiplicity	J (Hz)	Integration	Experimental/ Theoretical
H_E	8.31-8.32	s	/	2.00*	1.00
H_F	7.79	s	/	1.70	0.85
H_B	7.12-7.24	m	/	1.87	0.96
H_A	6.84-6.92	d of t	1.8, 6	0.65	0.65
H_D	6.32-6.33	s	/	0.96	0.96
H_8	5.58-5.74	d x 2	5.1, 1.8	38.83	1.39
H_1	4.79-4.87	d	2.7	18.88	1.34
H_C	4.50-4.78	q	12, 54	6.27	1.56
H_7	4.35-4.46	t	3	19.73	1.41
H_3, H_5, H_6	3.60-3.73	m	/	55.19	0.99
H_4	3.51-3.60	d	9	23.44	1.67
H_2	3.34-3.40	d	6.9	16.70	1.19

*reference integral

Crystals of both forms were dissolved in DMSO-d_6. After the integration, the results confirmed the ratio β-CD:fluconazole of 2:1. The protons used to define the ratio were H_1 for the cyclodextrin and H_E for the fluconazole. The signals of all protons of the cyclodextrin suffer overlap and it was thus impossible to establish a perfect integration in every case.

5.3) THERMAL ANALYSIS

To evaluate the differences and the similarities between MBCDFLU and TBCDFLU, their thermal analyses are reported together. They were carried out using Hot Stage Microscopy (HSM), Thermogravimetric Analysis (TGA), Differential Scanning Calorimetry (DSC) and an empirical test called herein Dehydration Timed Test (DTT). The last analysis was set up specifically to evaluate the loss of solvent as a function of time for both forms and facilitate the consistency of thermogravimetric analysis.

5.3.1) HSM

Crystal samples were removed from the vials and rapidly immersed in a small drop of silicone oil. The two forms had a similar stability at elevated temperatures. MBCDFLU cracks due to water loss at 54°C and TBCDFLU at 50°C. These complexes have a somewhat different degradation point that could be seen at 308°C for MBCDFLU and at 320°C for TBCDFLU. Both experiments, reported in *Figures 5.5* and *5.6,* were recorded at a heating rate of 10 °C/min to a maximum temperature of 400 °C.

MBCDFLU

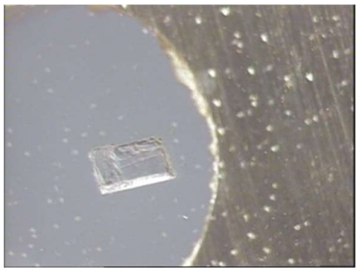

25°C

TBCDFLU

24°C

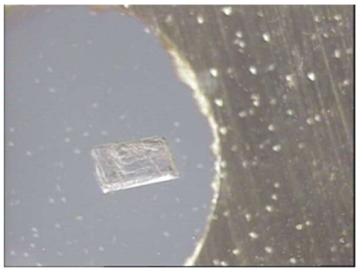

54°C

50°C

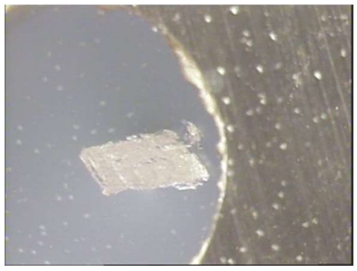

151°C

100°C

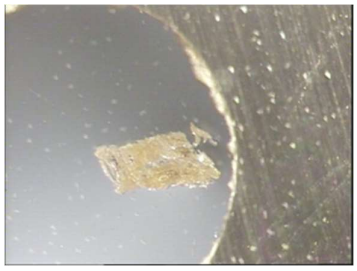

308°C

320°C

Figures 5.5 and 5.6: HSM of MBCDFLU (left column) and TBCDFLU (right column).

5.3.2) DEHYDRATION TIMED TESTS

After the HSM study, both forms were analysed by thermogravimetry. The results were very different for samples taken from the same vial and having similar masses. It was necessary to do a preliminary test to evaluate the time of dehydration of both forms without the silicone oil used for subsequent HSM experiments.

Two crystals (*Figure 5.7,* triclinic, at the top, and monoclinic, below it) were placed on a microscope slide in their mother liquor and allowed to dry spontaneously in order to determine, qualitatively, the stability of the forms with respect to dehydration. The first image (0 seconds) corresponds to the instant at which the mother liquor has evaporated completely.

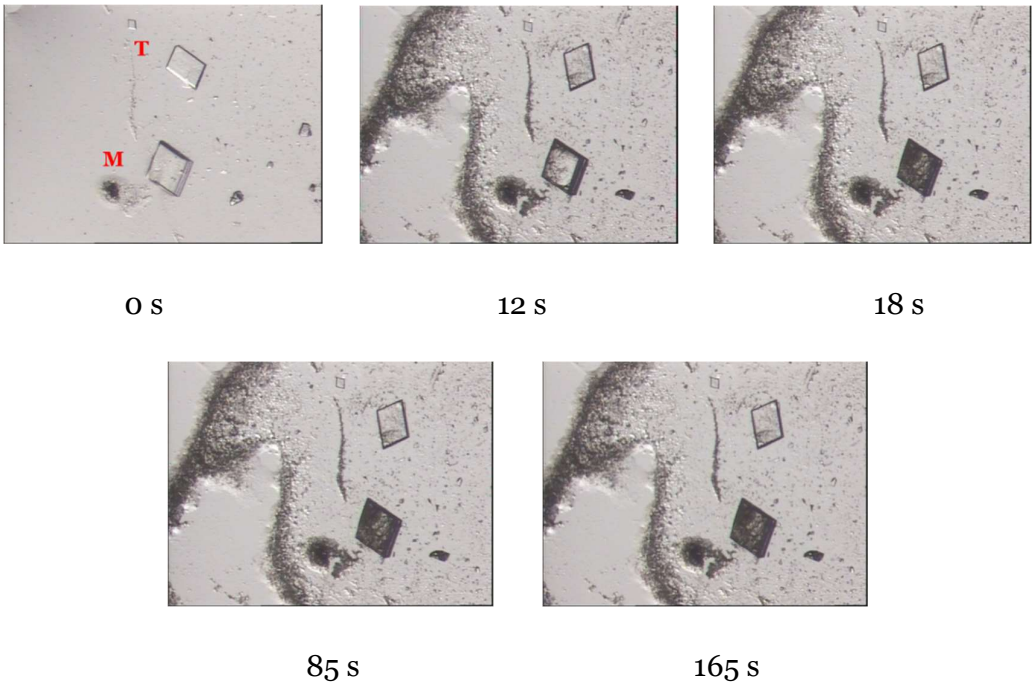

Figure 5.7: Dehydration of MBCDFLU and TBCDFLU.

After 12 seconds, MBCDFLU had developed cracks due to its dehydration. The cracks became very visible after six more seconds (18 s). With this empirical test, it was possible to conclude that MBCDFLU is more unstable when exposed to the atmosphere than TBCDFLU.

5.3.3) THERMOGRAVIMETRY ANALYSIS WITH SILICONE OIL

This type of analysis is fundamental to estimate the content of water inside the crystals and to eventually correlate the results with the respective crystallographic models obtained by single crystal X-ray diffraction (section *5.5*).

The operational times for preparing a sample for a TG analysis had an average of 1-2 minutes. Due to the rapid dehydration of MBCDFLU, this operational time was too long to

obtain a consistent set of data for the mass loss. This instability on exposure to the atmosphere was related primarily to the location of the water molecules in the crystals. Other potential causes could also contribute to instability but assessment of these would require an advanced computational approach to take in account e.g. the morphology and surface features of the crystals. The latter could change the total area in contact with the air and for a macroscopic system this would yield erroneous measurements because some crystals should dehydrate earlier or later proportionally to the surface area. The shape of the crystals is a secondary source of error because, taking as an example a MBCDFLU crystal, it is easy to understand that a thin crystal would lose water faster than a thick crystal. The first set of analyses showed a very wide range of results, namely a mass loss ranging from 8% to 25%. In order to avoid the problems related to the variable water loss of MBCDFLU, all the thermogravimetric experiments were conducted with the crystals in silicone oil. TBCDFLU was treated in same way for consistency between data. The software of the instrument was programmed for a small sample (~5 mg) which, with the oil added gave a total mass of ~40 mg. The instrumental error was larger but this was the only way to try to ensure reproducible results.

Each clean platinum crucible used for analysis was calibrated with both TG instrument and a laboratory scale. After this check, the samples were removed from the mother liquor, dried quickly on filter paper and placed inside the crucible. The weight was recorded quickly and the crystals were covered with 1-2 drops of silicone oil. The weight data was recorded again, the crucible was inserted into the TG instrument and the analysis was started. The procedure was repeated for all experiments (30 in total) and the average time for these operations was 52 seconds. A run without crystals was carried out in order to study the behaviour of silicone oil under the applied temperature program. This experiment was carried out but not recorded because the oil was inert (only instrumental variations of the profile were present).

Figure 5.8 presents the most consistent data in a set of fifteen analyses performed on MBCDFLU. The average mass loss was 16.6 ± 1.6 %.

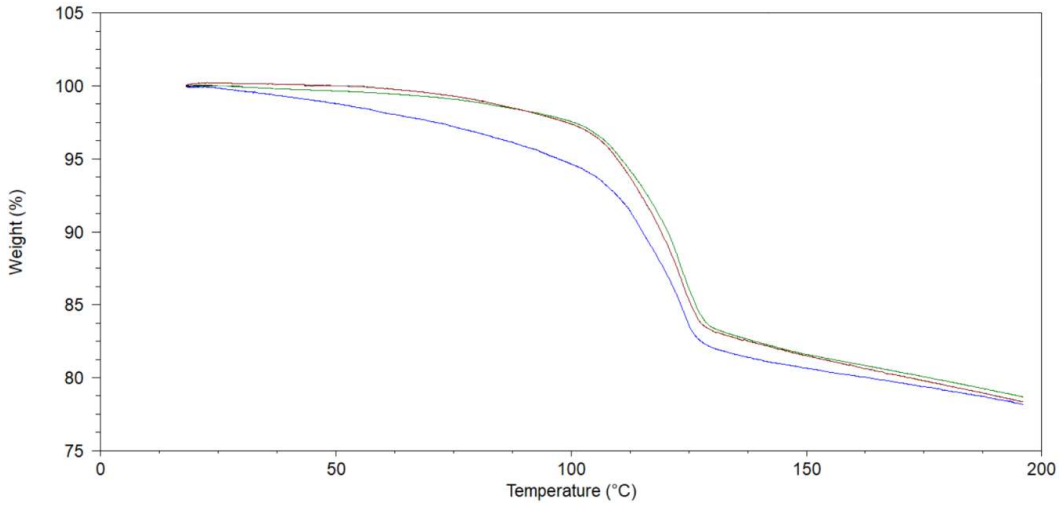

Figure 5.8: TG curves for MBCDFLU.

The formula (9) shows the operational method used to calculate the average number (n) of water molecules per complex unit inside the crystal. For the host-guest stoichiometric ratio 2:1, $n = 28.4 \pm 2.8$.

These thermogravimetric analyses were very consistent because they limited the uncontrolled crystal water loss, minimising the experimental error. The only problematic points were the increase in the instrumental error and the necessity for calculating the curves to remove quantitatively the effects of the oil on the sample. This was carried out with a simple subtraction through Microsoft Excel. The data collected *before* each TG experiment were useful to establish exactly the amount of silicone oil present in the crucible. The calculated data were used to revise the curves obtained by the TG experiments with oil. In these raw profiles, the total mass was composed of crystals and oil. The oil mass values were mathematically removed from each point of the curves with the aim of obtaining the profile for the crystals only. In *Figure 5.9* are reported the overlapped best curves for TBCDFLU.

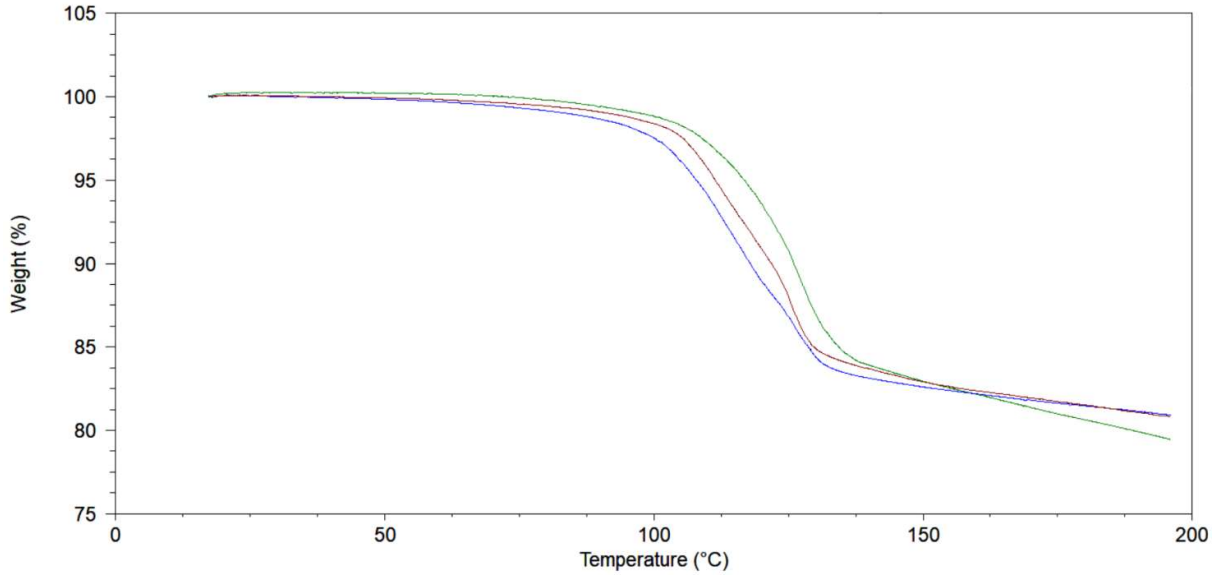

Figure 5.9: TG curves for TBCDFLU.

Using the same formula (9), the number (n) of water molecules per 2:1 host-guest unit of TBCDFLU was calculated. The percentage mass loss was 15.3 ± 0.8 % and n = 25.8 ± 1.1.

$$\%\ mass\ loss = \frac{n \times MW_{H_2O}}{2 \times MW_{\beta-CD} + MW_{FLU} + (n \times MW_{H_2O})} \times 100 \qquad (9)$$

5.3.4) DIFFERENTIAL SCANNING CALORIMETRY

To facilitate reading, in this chapter, TG and DSC curves were separated. In *Figure 5.10* and *5.11* are reported the DSC traces for MBCDFLU and TBCDFLU, respectively. No oil was added to the DSC pan but the operational times were recorded.

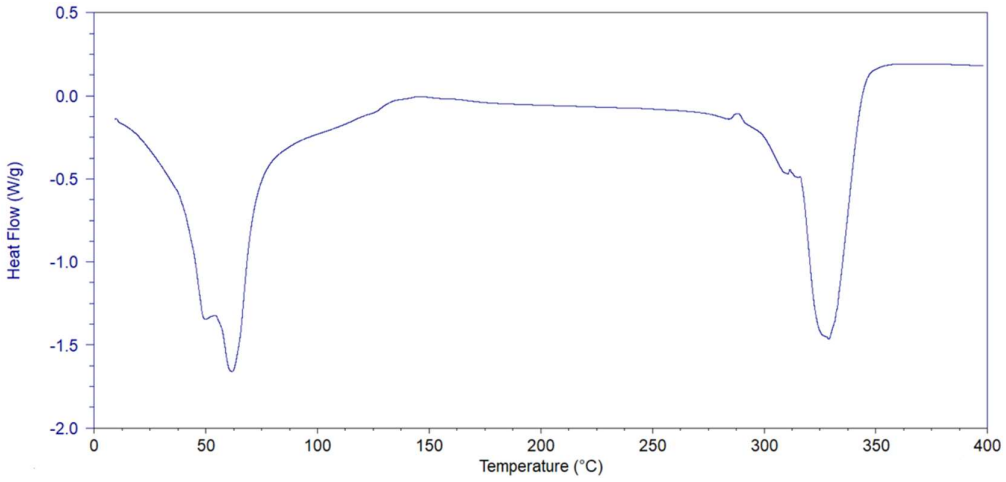

Figure 5.10: DSC curve of MBCDFLU.

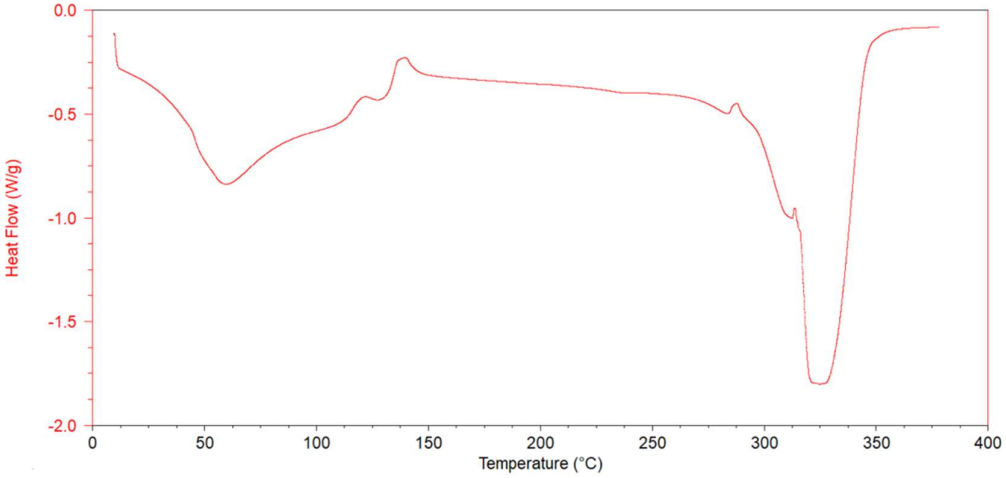

Figure 5.11: DSC curve of TBCDFLU.

The two profiles are different for the dehydration peaks: both are present but the MBCDFLU peak is sharper than that for TBCDFLU. This difference is due to the different structures of the crystals (as reported in the paragraphs describing the crystal structures in Chapters 5.5 and 5.6; the MBCDFLU channel crystal packing can explain the rapid dehydration, whereas the TBCDFLU dehydration is instead slower due to a brick-cage crystal packing). Between 200 °C and 400 °C the curves are identical (the decomposition peak is at 325 °C).

5.4) FOURIER TRANSFORM INFRARED SPECTROSCOPY

The FT-IR spectrum was recorded with an ATR instrument only on the MBCDFLU complex. The peak at 1023 cm^{-1} is characteristic of the glycosidic C-O bonds in the cyclodextrin, while the triazole groups of fluconazole are responsible for the peak at 1625 cm^{-1} and the broad peak at 2960-3760 cm^{-1} (νO-H) is due to the presence of a large quantity of water within the complex crystal. The spectrum of TBCDFLU was not recorded.

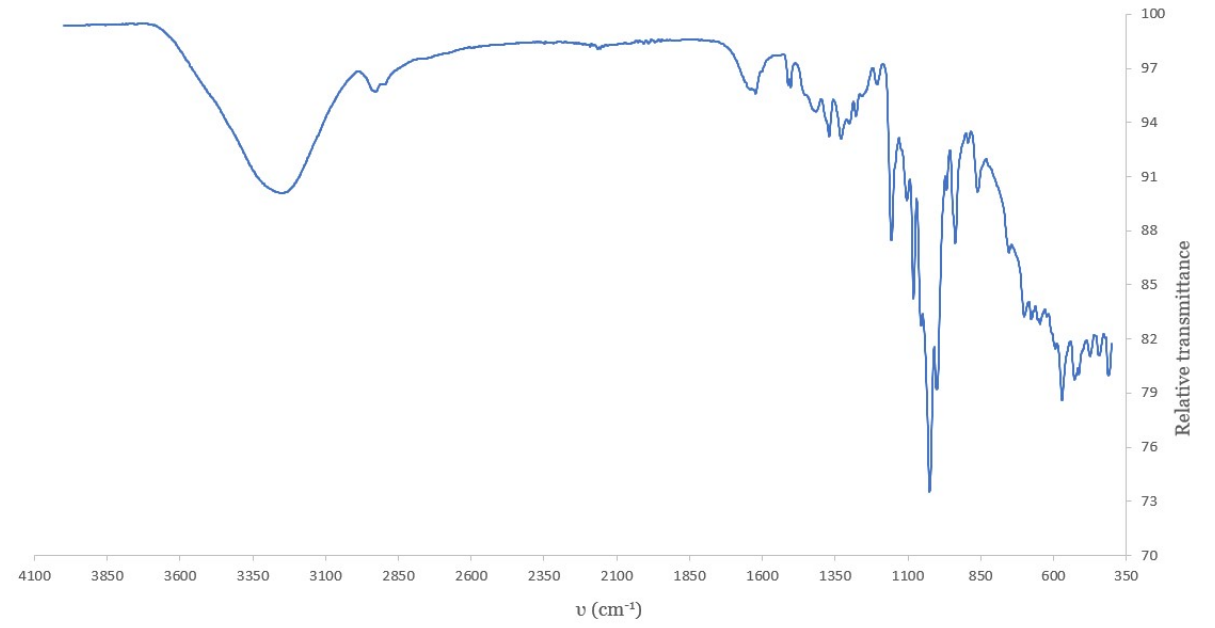

Figure 5.12: IR spectrum of MBCDFLU.

5.5) SOLID-STATE X-RAY ANALYSIS OF MBCDFLU

5.5.1) DATA-COLLECTION AND SPACE GROUP DETERMINATION

The intensity data-collection for MBCDFLU was recorded in a previous study[2] (at the temperature of 173 K). The dimeric host structure was well-resolved but it was impossible to determine the structure and precise location of the guest molecule due to the presence of only weak difference Fourier peaks within the host cavity. During the present study, a data-collection using a freshly-prepared crystal of MBCDFLU was performed at the temperature

of 100 K. The higher-quality data obtained at the low temperature were determinant in resolving the structure completely by revealing the guest molecule inside the cavity of the host.

The reflection intensities were collected with a Bruker KAPPA APEX II DUO single crystal X-ray diffractometer using MoKα-radiation (λ = 0.71073 Å). After the integration of the frames with the Bruker SAINT[3] software, absorption corrections based on the multi-scan method were applied using the SADABS[4] software. The crystal system, confirmed by the program XPREP[5] was found to be monoclinic (from Laue symmetry 2/m) and the space group was identified as C2 from the conditions limiting possible reflections [hkl: h + k = 2n; hol: (h = 2n); oko (k = 2n)], the alternative space groups Cm and C2/m being eliminated since the host is chiral. Crystal data and structural refinement results are shown in *Table 5.3*.

Table 5.3: Data-collection and refinement parameters for MBCDFLU.

Abbreviated formula	2 β-CD · FLUCONAZOLE · 21.28 H_2O
Complex formula	$(C_{42}H_{70}O_{35})_2 \cdot C_{13}H_{12}ON_6F_2 \cdot 21.28\ H_2O$
Formula weight (g mol^{-1})	2908.49
Data-collection temperature (K)	100(2)
Crystal system	monoclinic
Space group	C2
a (Å)	18.879(5)
b (Å)	24.408(5)
c (Å)	15.375(5)
α (°)	90
β (°)	109.862(5)
γ (°)	90
V ($Å^3$)	6663(3)
Z	2
ρ_{calc} (g/cm^3)	1.450

μ (mm^{-1})	0.133
F (000)	3048
Crystal size (mm)	0.23 x 0.16 x 0.06
Radiation wavelength (MoKα) (Å)	λ = 0.71073
Range scanned θ (°)	1.408 to 27.541
Index ranges ±*h*, ±*k*, ±*l*	$-24 \leq h \leq 23$, $-31 \leq k \leq 31$, $-19 \leq l \leq 18$
Reflections (total)	29872
Independent reflections	15223
Completeness (%)	99.5
Reflections with $I>2\sigma(I)$	10937
Parameters	810
R_{int}	0.0361
R_1 [$I>2\sigma(I)$]	0.0861
wR_2 [$I>2\sigma(I)$]	0.2221
Goodness-of-fit, S	1.031
a, b in $w = 1/[\sigma^2(F_o^2)+(aP)^2+(bP)]$	a = 0.1427, b = 13.807
$\Delta\rho_{min,\ max}$ ($eÅ^{-3}$)	-0.97 and 1.06

All the elements useful for this dissertation have been carefully set, but it is necessary to note that the model is not complete. Some changes in the future will be taken into account (e.g. the calculation of hydrogen atoms on water molecules and their correct agreement in a network of hydrogen bonds with that already present).

5.5.2) STRUCTURE SOLUTION AND REFINEMENT

The β-CD molecule from the isomorphous complex with CSD[6] refcode *AJUVEG* was used as a trial model. After removal of the guest molecule (methylparaben) and the freely rotating primary hydroxyl groups, the remaining rigid fragment was refined isotropically and the remaining atoms were located in successive difference Fourier maps. The structure of the complex, including host, guest and water molecules, was refined using full-matrix least-

squares with program SHELXL-97.[7] This model was challenging due to the partial overlap of two disordered components of the fluconazole guest molecule related by the crystallographic twofold axis. The PART command was used extensively, principally on the guest and water molecules, to eliminate false atom connectivities. The phenyl ring geometry was maintained using a regular rigid hexagon model (AFIX 66 command) and ten DFIX restraints were used to maintain reasonable geometry of the triazole groups.

In *Figure 5.13* two representations of the guest molecule are shown: on the right, the partially-overlapped components of guest disorder related by the twofold axis (each with site-occupancy factor (s.o.f.) 0.5), and on the left, a single component of guest disorder.

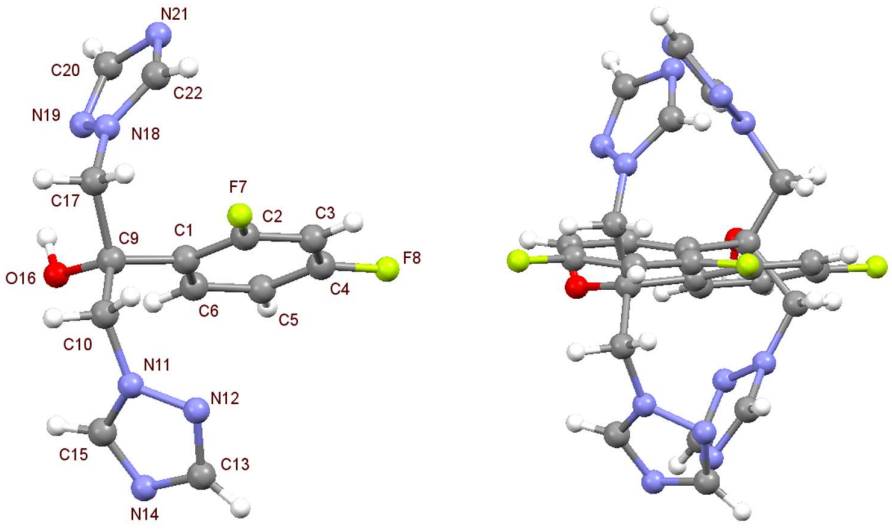

Figure 5.13: Representation of the guest with PART command (left) and without it (right). In the image on the right labels were omitted for clarity.

The glucose units are labelled 1 to 7 and each atom has a label 'XnYm'. 'X' is C, O or H; 'n' is a number from 1 to 8 that represents the atom position; 'Y', in this case, is 'G' and is the label of the cyclodextrin ring; 'm' is a number from 1 to 7 and it references the glucose residue. The host presented disorder in two primary hydroxyl groups. Those atoms were labelled differently for a fast identification (e.g. XnYH and XnYI). In *Figure 5.14*, the primary oxygen atom at C6G2 is disordered over two positions with s.o.f.s of 0.57 for O6GH and 0.43 for O7GH. It was possible to find a comparable situation for the atom C6G6 of the glucose unit G6. The s.o.f.s of atoms O6GI and O7GI in residue G6 refined to the same values as in the case of the disordered component atoms in glucose unit G2. The C-O bond lengths for these

two pairs of atoms were fixed with a DFIX restraint at 1.440(2) Å. The large residual electron density peak of 1.06 e $Å^{-3}$ was located near O7GH, but it had no chemical significance.

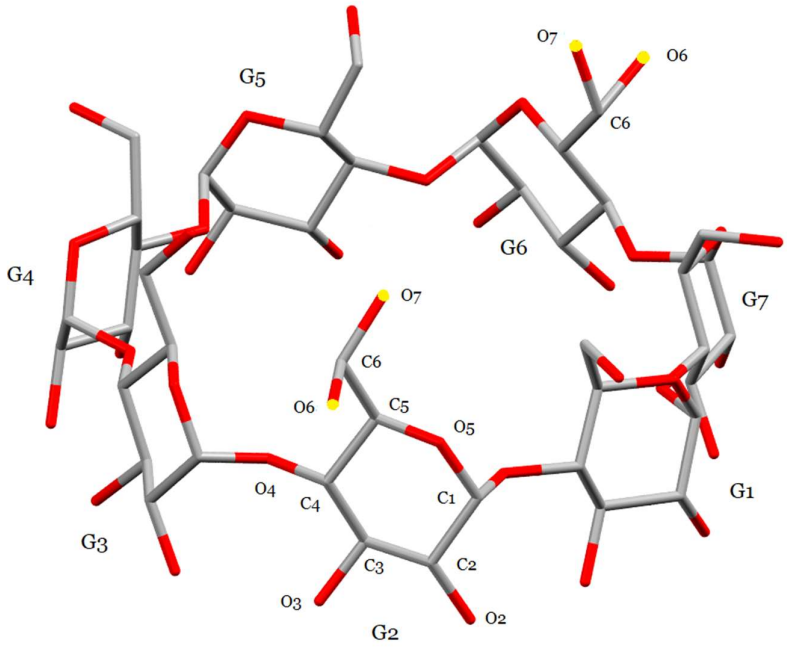

Figure 5.14: Graphical representation of disordered primary hydroxyl oxygens in the MBCDFLU host structure (yellow spots). For simplicity, all hydrogen atoms and water molecules have been omitted.

The hydrogen atoms for host and guest were placed geometrically with the 'generate HFIX' command of the X-Seed interface[8] and their U_{iso} values were maintained in the range 1.2-1.5 times the thermal parameters of their parent atoms. The O-H bond length of the drug molecule was restrained at 0.84(5) Å using the DFIX command. The hydrogen atoms on water molecules were not located in difference Fourier syntheses nor completely generated due to a high degree of disorder of most of the water oxygen atoms.

The sum of the s.o.f.s of all the oxygen atoms of water molecules did not agree with the TGA result. For this reason, a fixed U_{iso} value equal to the average of the fully-occupied water oxygen atoms was assigned to the atoms with a significantly low electron density. With this expedient, the s.o.f. parameters were marginally modified by refinement and the sum of the s.o.f.s increased accordingly. The final sum of the s.o.f.s for water oxygen atoms was 10.6 per asymmetric unit (i.e. corresponding to 21.2 molecules of water per dimeric complex unit)

whereas the thermal analysis yielded a value of 14.2 ± 1.4 per asymmetric unit and thus 28.4 per dimeric complex unit. As explained above, in paragraph 5.3.3, the more reliable result was that obtained by TGA.

5.5.3) DESCRIPTION OF THE STRUCTURE

The asymmetric unit of MBCDFLU is composed of a single β-CD molecule, one half of a fluconazole molecule and 10.6 water molecules (while the TGA result, as explained above, yielded 14.2). The guest molecule is positioned in the host cavity *via* entry of one of the triazole groups from the secondary rim (*Figure 5.15*). A large cavity is generated by two cyclodextrin molecules which are linked at their secondary faces by O-H···O hydrogen bonds. The phenyl and the hydroxyl groups of the drug molecule are located in the middle of the cavity generated by the two CD molecules, the former group lying at the interface between the secondary rims.

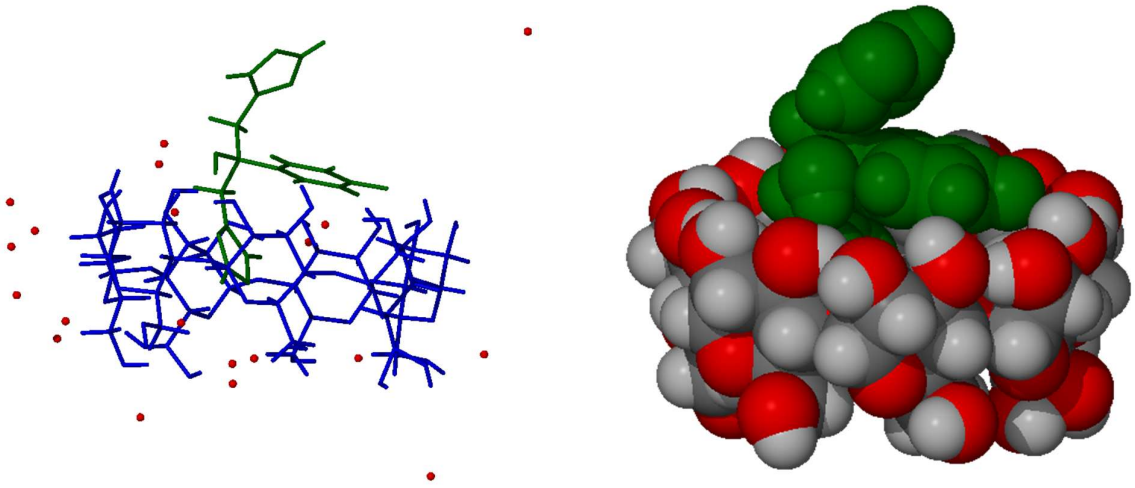

Figure 5.15: The asymmetric unit of MBCDFLU. In the space-filling structure (right) the water oxygens were removed for simplicity.

5.5.4) HOST CONFORMATION

In *Table 5.4* are listed all the geometric parameters of the host molecule. The parameter ***l*** measures the distance between each glycosidic atom (O4) and the centroid of the O4-heptagon. In a regular heptagon, all these distances, must be equal and any variation in their values can be attributed to distortion by the encapsulated guest molecule. Similarly,

parameters such as **D** (O4···O4′distance), **Φ** (O4···O4′···O4′′ angle) and **d** (O4···O4′···O4′′···O4′′′ torsion angle) are also useful for understanding the effect of distortion on the host ring.

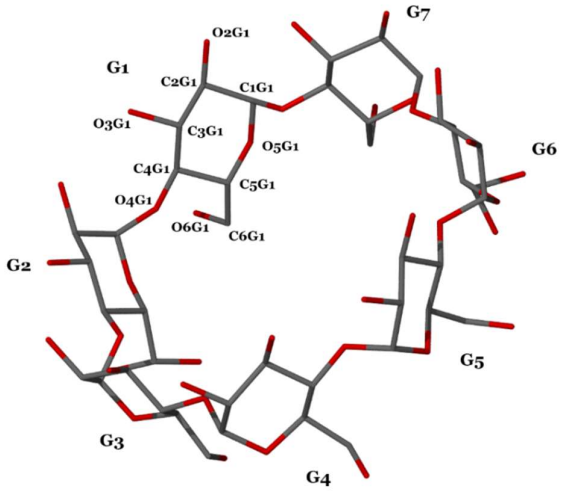

Figure 5.16: β-CD structure in the inclusion complex. For simplicity, all the hydrogen atoms have been removed and only one glucoside unit was completely labelled.

Table 5.4: Geometric parameters of the host molecule in MBCDFLU.

Residue	*l* (Å)	D (Å)	Φ (°)	d (°)	α[a] (Å)	D_3[b] (Å)	τ_1[c] (°)
G1	4.878	4.383	127.8	-3.3	-0.071	2.830	10.2
G2	5.097	4.310	124.5	1.6	-0.041	2.787	11.1
G3	5.194	4.275	132.9	4.5	0.090	2.795	8.5
G4	4.833	4.534	130.4	-5.5	0.012	2.786	1.6
G5	4.951	4.294	122.1	0.4	-0.115	2.760	10.5
G6	5.292	4.336	131.3	3.6	0.062	2.786	12.6
G7	4.957	4.437	130.0	-0.7	0.064	2.964	7.6

[a] mean e.s.d. 0.004 Å; [b] mean e.s.d. 0.0077 Å; [c] mean e.s.d. 0.17°

The deviations of the O4 atoms from the O4 mean plane, listed in the **α** column, clearly indicate that the O4-heptagon has conserved a high degree of planarity. The $\mathbf{D_3}$ parameter measures the distances O2···O3′ involved in intramolecular O-H···O hydrogen bonding on the secondary rim of the cyclodextrin. The last parameter is the tilt angle ($\boldsymbol{\tau_1}$) of each glucose ring from a hypothetical cylindrical host geometry. The values show that G4 is less tilted than other residues. The proximity of G4 to a triazole group of fluconazole could generate a repulsion between the electron densities of the two moieties, modifying the inclination of

the glucose residue. This statement was verified through a comparison between the τ_1 data listed above and those related to an uncomplexed β-CD molecule.

5.5.5) HYDROGEN BONDING

In *Figure 5.17* are reported the representations of the intramolecular hydrogen bonds of the MBCDFLU complex. It is possible to identify twelve contacts in total:

- Seven intramolecular H-bonds, located on the secondary rim of cyclodextrin (they serve to maintain the 'round' macrocyclic-ring shape);
- Four intermolecular host-host H-bonds that maintain the stability of the crystal structure;
- An intramolecular guest-guest H-bond located between the hydroxyl group and the N atom of a triazole group of the fluconazole molecule.

These interactions are listed in *Table 5.5* with their respective labels, distances and angles.

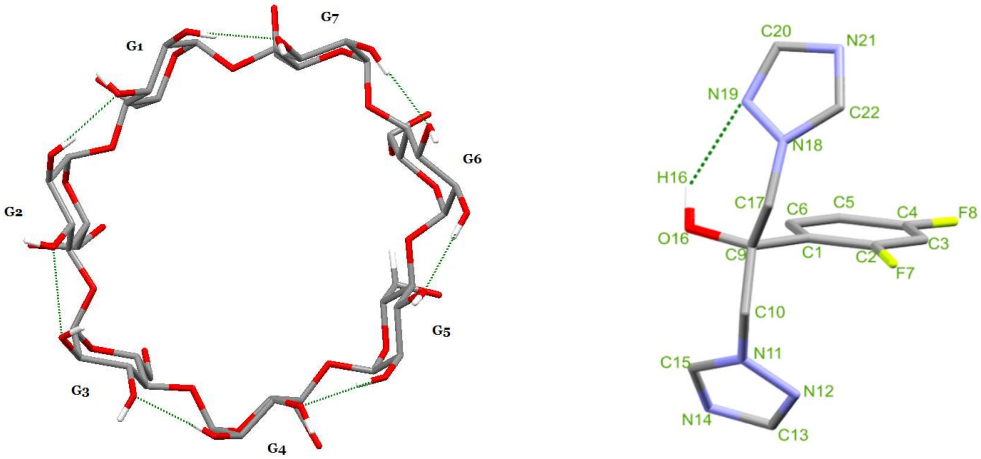

Figure 5.17: Intramolecular hydrogen bonds for the MBCDFLU complex (hydrogen atoms not involved in an intramolecular bond have been removed for clarity).

Table 5.5: Hydrogen bonding interactions in the MBCDFLU inclusion complex.

Interaction	D-H (Å)	H···A (Å)	D···A (Å)	D-H···A (°)
Intramolecular H-bonds				
O2G1-H9G1···O3G7	0.84	2.00	2.830(8)	168
O2G2-H9G2···O3G1	0.84	1.96	2.787(8)	167
O2G3-H9G3···O3G2	0.84	1.98	2.795(8)	165
O2G4-H9G4···O3G3	0.84	1.96	2.786(7)	168
O2G5-H9G5···O3G4	0.84	1.96	2.760(8)	160
O2G6-H9G6···O3G5	0.84	1.95	2.786(8)	170
O2G7-H9G7···O3G6	0.84	2.13	2.964(7)	172
Intermolecular H-bonds				
O3G5-H3G5···O3G4[a]	0.84	1.95	2.779(6)	170
O3G6-H3GF···O3G3[a]	0.84	2.04	2.858(8)	164
O3G7-H3GG···O3G2[a]	0.84	2.03	2.739(7)	142
O6G5-H8G5···O6G7[b]	0.84	1.98	2.759(9)	153
Guest				
O16-H16···N19	0.84	2.24	2.92(2)	140

[a] 1-x, y, 1-z; [b] ½-x, ½+y, -z.

5.5.6) CRYSTAL PACKING

The complex units are packed in a head-to-head type arrangement. The channels are extended along the *c*-axis and are slightly offset. In *Figure 5.18* are reported two representations of crystal packing diagrams (the hydrogen atoms have been hidden for clarity).

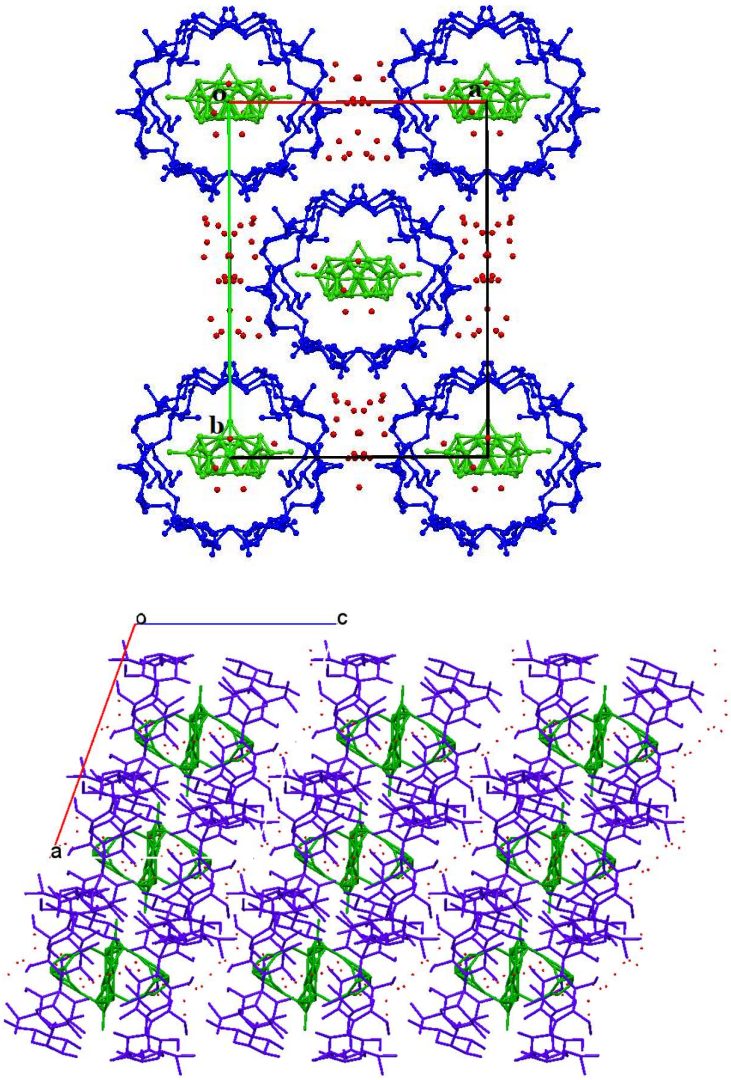

Figure 5.18: Packing diagrams for the MBCDFLU complex: projection along the c-axis [001] projection (top) and along the b-axis (bottom). The guest is coloured in green, the host in blue and the water oxygen atoms in red.

On the upper section of *Figure 5.18* it is possible to see the effects of the C2 space group symmetry on the guest molecule. The two-fold axis passes exactly through a fluorine atom (F7).

Evaluating the structure, principally the host-guest interactions and the packing of the molecules, it is possible to understand the fast dehydration that characterizes the complex. A high degree of disorder is present and very few direct hydrogen bonds are observed between the neighbouring CD dimers, thus water positioned between the columns of CD

dimers can leave easily from the crystal on its removal from the mother liquor. These structural aspects give only a superficial explanation of this propriety; other factors are surely concomitant but this aspect of the study has not been thoroughly investigated.

In *Figure 5.19* is reported the asymmetric unit in space-filling representation with two glucosidic units of the cyclodextrin omitted to emphasise the filling of the cavity by the fluconazole molecule.

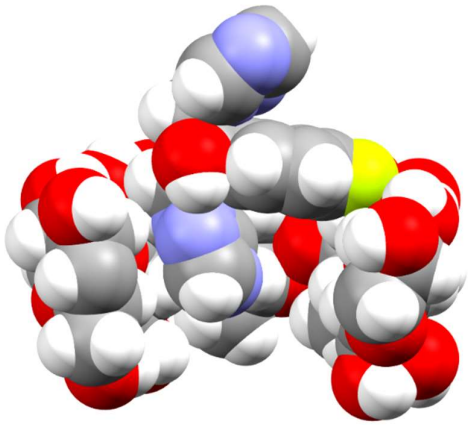

Figure 5.19: Space-filling representation of the asymmetric unit of MBCDFLU with a sectioned view of the host.

5.5.7) COMPARATIVE PXRD

In *Figure 5.20* is reported the comparison between an experimental PXRD pattern of MBCDFLU and the one calculated using the program LAZY PULVERIX[9] with the data of the model. The traces match with a high level of agreement. The slight shift of the red pattern towards higher angular values in *Figure 5.20* could be attributed to the collapse of the crystals during the PXRD analysis and contraction of their unit cells due to their gradual dehydration. The sample used to record the experimental trace was obtained by the co-precipitation method explained in Par. 5.1, as was the specimen used for the SCXRD data-collection.

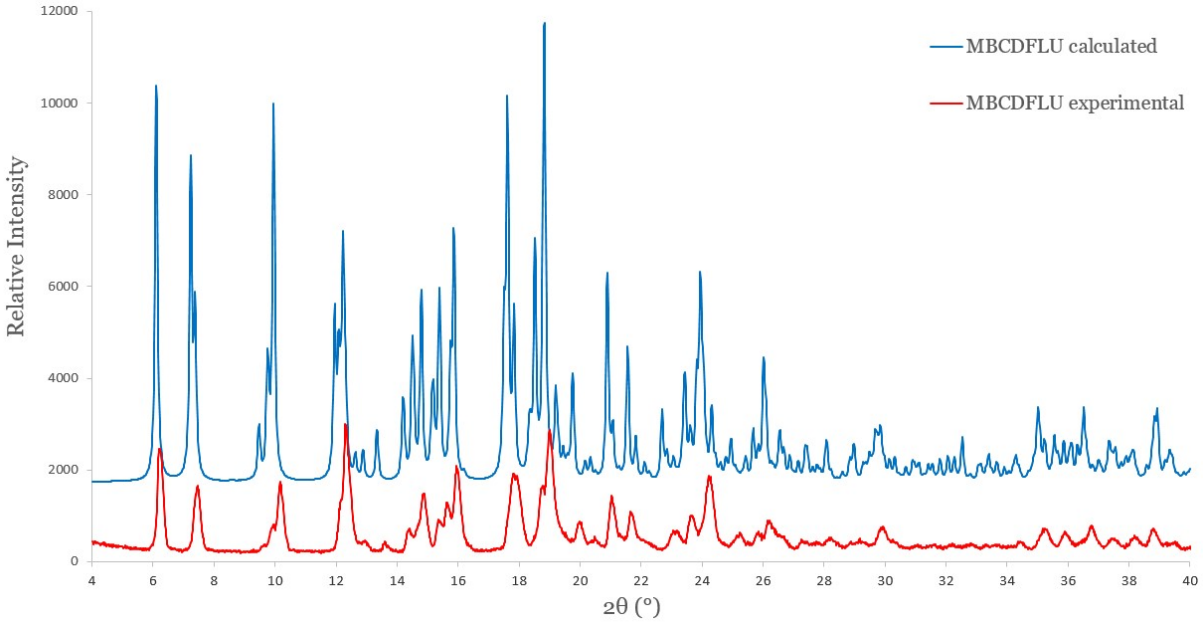

Figure 5.20: Calculated and experimental PXRD patterns for MBCDFLU.

5.6) SOLID-STATE X-RAY ANALYSIS OF TBCDFLU

5.6.1) DATA- COLLECTION AND SPACE GROUP DETERMINATION

The data-collection on this crystal was previously performed at the temperature of 173(2) K by the Chemistry Honours student Ms Zakiena Hoossen in 2016.[2] The complex structure was resolved with a good final residual factor (R_1 ~0.07) but poorly-matching experimental and calculated PXRD traces, mainly due to the small mass of the complex sample available. In the present study, the work of Ms Hoossen was replicated and, as shown in this chapter, the β-cyclodextrin inclusion complexes with fluconazole were considerably more thoroughly investigated. The data-collection on TBCDFLU was recorded at the temperature of 173(2) K.

The crystal intensities were collected with a Bruker KAPPA APEX II DUO single crystal X-ray diffractometer. The frames were integrated with SAINT[3] and the multi-scan method was used to calculate the absorption corrections using software program SADABS.[4] The data were analysed with XPREP;[5] the crystal system was found to be triclinic and the space group P1, since the host molecule is chiral.

5.6.2) STRUCTURE SOLUTION AND REFINEMENT

A trial model for structure solution was obtained by isomorphous replacement using the rigid skeleton of the β-CD dimer extracted from the crystal structure of a complex (CSD[8] refcode VUYGUT) crystallizing in P1 with unit cell parameters very similar to those of the new fluconazole complex. The intensity data displayed a small level of twinning which was overcome during refinement of the structural model using full-matrix least-squares implemented in SHELXL-97.[7] The remaining atoms of the host molecule, as well as the guest and water molecules were revealed in subsequent difference electron density Fourier maps. Non-hydrogen atoms were refined isotropically initially and after convergence of the U_{iso} values, anisotropic refinement followed. The residual factor (R1), with this procedure and the fixing of water molecules, was very good (8.08%) for a structure of this complexity. All the data-collection and refinement parameters are reported in *Table 5.6*.

This structure did not present all the modelling difficulties caused by the disorder or symmetry encountered with MBCDFLU. In TBCDFLU the only slight degree of disorder was associated with water molecules. The hydrogen atoms were refined isotropically with a U_{iso} value in the range 1.2-1.5 times those of their parent atoms. The hydrogen bond network between the host structure and the water molecules was partially fixed with DFIX restraints to avoid problems caused by disorder.

The total count of the water molecules of the model agreed with the estimate from TGA. The thermoanalytical study revealed the presence of 25.8 ± 1.1 water molecules per asymmetric unit (two host molecules, one guest molecule and water molecules). The total sum of the site-occupancy factors (s.o.f.s) of the water oxygen atoms in the model was 27.3. The two results were consistent within experimental error and for this reason it was possible to accept the complex formula derived by the crystallographic model.

Table 5.6: Data-collection and refinement parameters for TBCDFLU.

Abbreviated formula	2 β-CD · FLUCONAZOLE · 27.3 H_2O
Complex formula	$(C_{42}H_{70}O_{35})_2 \cdot C_{13}H_{12}ON_6F_2 \cdot 27.3\ H_2O$
Formula weight (g mol^{-1})	3067.48
Data collection temperature (K)	173(2)
Crystal system	triclinic

Space group	P1
a (Å)	15.331(3)
b (Å)	15.392(3)
c (Å)	17.972(3)
α (°)	113.613(3)
β (°)	99.410(3)
γ (°)	102.597(3)
V (Å^3)	3640.0(12)
Z	1
ρ_{calc} (g/cm^3)	1.3992
μ (mm^{-1})	0.128
F (000)	1636
Crystal size (mm)	0.21 x 0.15 x 0.05
Radiation (Mo Kα) (Å)	λ = 0.71073
Range scanned θ (°)	1.29 - 25.7
Index ranges ±*h*, ±*k*, ±*l*	-18 ≤ *h* ≤ 18, -16 ≤ *k* ≤ 18, -21 ≤ *l* ≤ 0
Reflections (total)	26399
Independent reflections	13586
Reflections with *I* > 2σ(*I*)	11090
Parameters	1887
R_{int}	0.0617
R_1 [*I*>2σ(*I*)]	0.0646
wR_2 [*I*>2σ(*I*)]	0.1595
Goodness-of-fit, S	1.029
a, b in $w = 1/[\sigma^2(F_o^2)+(aP)^2+(bP)]$	a = 0.1050, b = 3.4655
$\Delta\rho_{min, max}$ (e Å^{-3})	-0.44, 0.79

5.6.3) DESCRIPTION OF THE STRUCTURE

The TBCDFLU complex is composed of a dimeric unit forming a head-to-head cage with the two cyclodextrins hydrogen bonded via their secondary rims (*Figure 5.21*). The molecules that comprise the unit are two β-CD molecules, one molecule of fluconazole and 27.3 molecules of water. The TGA revealed the presence of 25.8 ± 1.1 water molecules per

asymmetric unit. The triazole groups are inserted inside the hydrophobic cavities of the cyclodextrins, having entered from the wider secondary rims.

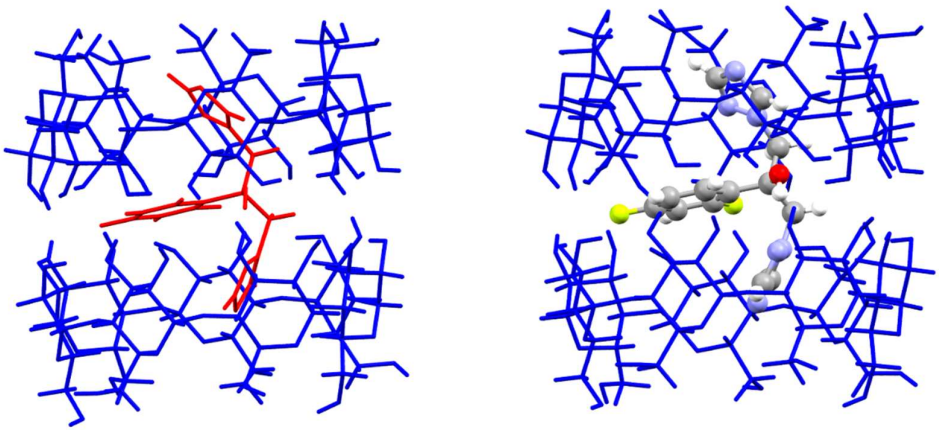

Figure 5.21: Two representations of the asymmetric unit of TBCDFLU (water molecules are omitted for simplicity).

5.6.4) HOST CONFORMATION

In the case of TBCDFLU, the dimer is formed by two crystallographically independent cyclodextrin rings that are designated A and B. Such as MBCDFLU example, the glucose units are labelled 1 to 7 and each atom has a label 'XnYm', as in the example shown in *Figure 5.14*. 'X' is C, O or H; 'n' is a number from 1 to 8 that represents the atom position; 'Y', in this case, is A or B and is the label of the cyclodextrin ring; 'm' is a number from 1 to 7 and it references the glucose residue. The graphical representation of the host dimer is reported in *Figure 5.22*.

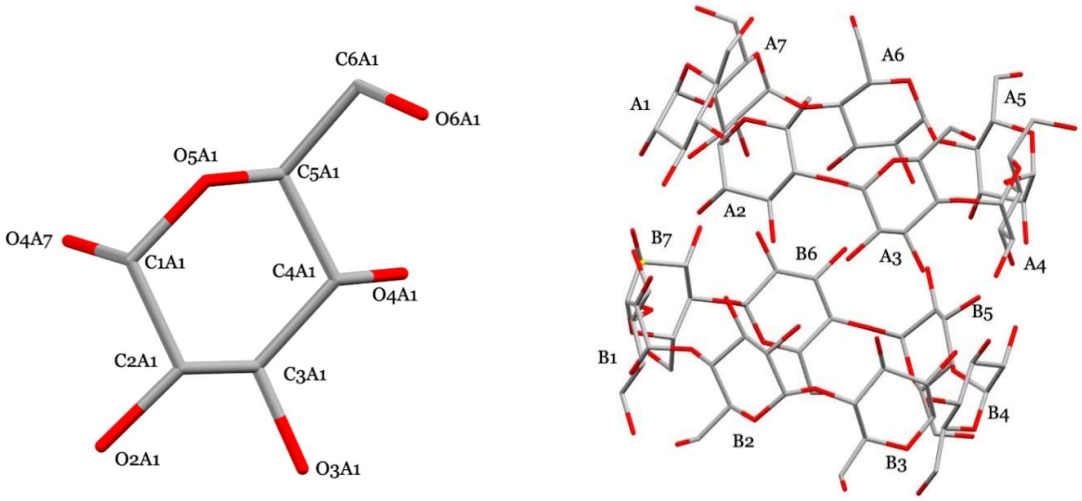

Figure 5.22: Schematic representation of the 'XnYm' system of labelling for TBCDFLU (a single glucose residue on the left and the host dimeric unit on the right). Hydrogen atoms and water molecules are omitted for simplicity.

Table 5.7: Geometric parameters of the host molecule in TBCDFLU.

Residue	*l* (Å)	D (Å)	Φ (°)	d (°)	α[a] (Å)	D_3 (Å)	τ_1[b] (°)
A1	5.017	4.531	132.95	0.53	-0.016	2.84(1)	8.5
A2	4.817	4.300	126.74	0.08	-0.007	2.79(1)	3.7
A3	5.124	4.415	124.75	-1.54	0.016	2.70(1)	4.9
A4	5.230	4.246	130.85	2.07	0.008	2.81(1)	11.0
A5	4.899	4.555	134.07	-0.71	-0.031	2.84(1)	7.8
A6	4.844	4.302	120.60	-0.46	0.020	2.82(1)	12.7
A7	5.351	4.293	130.01	0.19	0.010	2.79(1)	4.8
B1	5.030	4.391	130.14	0.68	0.000	2.71(1)	12.7
B2	4.900	4.401	129.92	0.18	-0.009	2.75(1)	3.3
B3	5.005	4.377	123.23	-1.76	0.012	2.79(1)	6.1
B4	5.240	4.215	132.00	2.74	0.008	2.82(1)	7.8
B5	4.898	4.569	130.98	-1.97	-0.031	2.82(1)	6.9
B6	4.903	4.265	124.27	0.96	0.029	2.80(1)	14.3
B7	5.209	4.324	129.42	-0.70	-0.010	2.88(1)	5.7

[a] mean e.s.d. 0.004 Å; [b] mean e.s.d. 0.8°

The distance between each O4 atom and the centroid of each cyclodextrin ring (***l***) and the **Φ** angles are consistent with those in the MBCDFLU case: the encapsulation of the guest distorted the host rings. However, the torsion angles (**d**) are smaller than in the MBCDFLU case (see *Table 5.4*). For these reasons, it is possible to confirm that the host ring is distorted but the O4-heptagon remains planar and this should be confirmed by **α**, the parameter that represents the deviation of a O4 atom from the mean O4-plane, that does in fact have a very small range (from -0.031 to 0.029 Å). The $\mathbf{D_3}$ parameter, that measures the O2···O3′ distances, is always consistent with the average length for a theoretical hydrogen bond interaction. Compared to the MBCDFLU glucose tilt angles, the $\boldsymbol{\tau_1}$ parameters for TBCDFLU are quite similar.

5.6.5) HYDROGEN BONDING

In *Figure 5.23* the representations of the molecular moieties in TBCDFLU's asymmetric unit are reported (for clarity the labels of host molecules are not shown). The hydrogen bond network for the host dimer includes all the interactions with the 27.3 water molecules found in the model; they were not reported in the figures of this subparagraph for underlining better the host-host interactions. The guest is bonded to the host only with weak interactions; no host-guest hydrogen bonds were found in the model. The intramolecular host hydrogen bonds are very important for the complex: those between O2 and O3′ atoms maintain the round shape of the two cyclodextrin molecules and the intermolecular bonds between the secondary rims of the two macrocycles are fundamental in stabilising the dimeric unit (in *Figure 5.23* all these bonds are represented with blue dotted lines). In *Table 5.8* are reported all the hydrogen bond interactions with their bond lengths and bond angles.

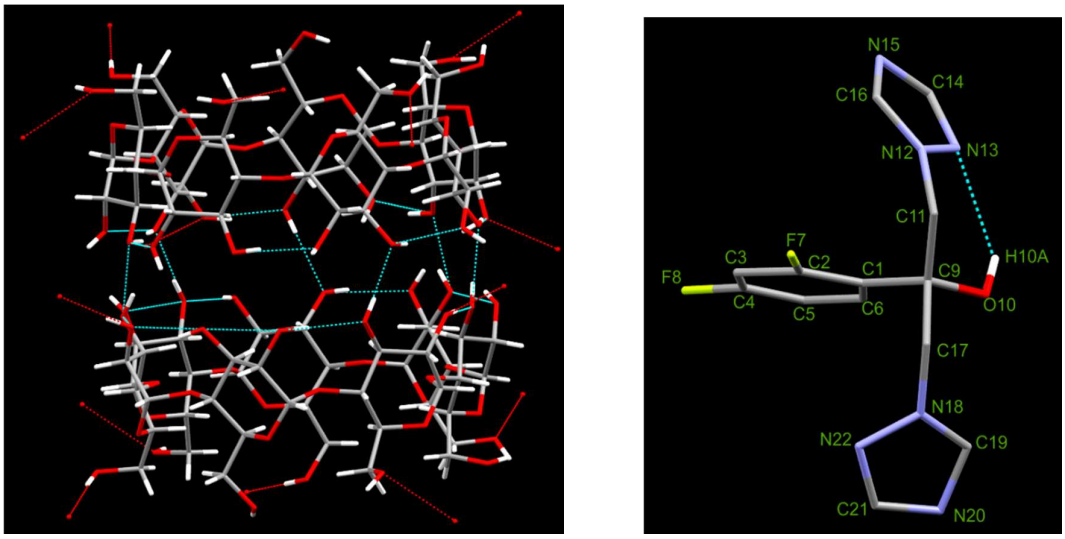

Figure 5.23: Intramolecular and intermolecular hydrogen bonds for the TBCDFLU complex (host on the left side and guest on the right side). Blue dotted lines indicate the hydrogen bonds of the asymmetric unit and red dotted lines represent the hydrogen bonds between the dimeric cages. For simplicity labels were removed.

Table 5.8: Hydrogen bonding interactions in the TBCDFLU inclusion complex.

Interaction	**D-H[i] (Å)**	**H···A[ii] (Å)**	**D···A (Å)**	**D-H···A[iii] (°)**
Intramolecular host H-bonds				
O2A1-H2A1···O3A7	0.84	2.06	2.84(1)	154
O3A1-HAA1···O2A2	0.80	1.90	2.79(1)	162
O2A3-H9A3···O3A2	0.84	1.88	2.70(1)	171
O2A4-H2A5···O3A3	0.84	2.04	2.80(1)	152
O3A4-HAA4···O2A5	1.00	1.80	2.84(1)	160
O3A5-HAA5···O2A6	1.00	1.80	2.83(1)	175
O3A6-HAA6···O2A7	0.85	1.96	2.79(1)	164
O2B2-H2B2···O3B1	0.80	1.80	2.71(1)	165
O3B2-H3B2···O2B3	0.84	2.12	2.76(1)	133
O3B3-H3B3···O2B4	0.80	2.03	2.79(1)	160
O3B4-H11···O2B5	0.84	1.99	2.83(1)	174
O3B5-H12···O2B6	0.84	2.10	2.82(1)	144
O3B6-H15···O2B7	0.80	2.01	2.80(1)	169
O3B7-H17···O2B1	0.80	2.18	2.88(1)	146

Intermolecular host-host H-bonds				
O2A2-H9A2···O3B2	0.84	1.91	2.74(1)	169
O3A3-H3A3···O2B7[a]	0.84	1.96	2.78(1)	165
O2A5-H4···O3B5	0.80	1.90	2.70(1)	175
O2A6-H7···O3B6	0.84	1.97	2.80(1)	167
O2A7-H8···O3B7	0.80	1.97	2.73(1)	159
O3A7-H9···O3B7	0.80	2.43	3.17(1)	152
O3B1-H9B1···O2A1	0.80	2.28	3.00(1)	149
O2B4-H10···O2A4	0.80	2.40	3.13(1)	151
O6A1-H8A1···O6B4[b]	0.84	1.87	2.74(1)	172
O6A3-H8A3···O6A7[a]	0.80	2.02	2.82(1)	174
O6B2-H8B2···O6B5[c]	0.80	1.94	2.74(1)	176
Intramolecular guest H-bond				
O10-H10A···N13	0.84	2.22	2.85(1)	133

[i] mean e.s.d. 0.005 Å; [ii] mean e.s.d. 0.005 Å; [iii] mean e.s.d. 2.5°; [a] x, -1+y, z; [b] 1+x, 1+y, 1+z;

It is possible to observe that all the D···A contact distances are similar with the exception of three intermolecular host H-bonds that have an average value > 3.00 Å (O3A7-H9···O3B7, O3B1-H9B1···O2A1 and O2B4-H10···O2A4). As in the MBCDFLU case, host-guest H-bond interactions are totally absent and an intramolecular guest H-bond is present, with comparable parameter values.

5.6.6) CRYSTAL PACKING

The cyclodextrin dimers are assembled in the 'intermediate' packing arrangement ('brick-work' or 'brick-cage' arrangement).[10] Two representations are shown in *Figure 5.24*. Hydrogen atoms were removed for clarity but the oxygen atoms of water molecules were included. Each primary side of the cyclodextrin cavities is blocked by a second unit.

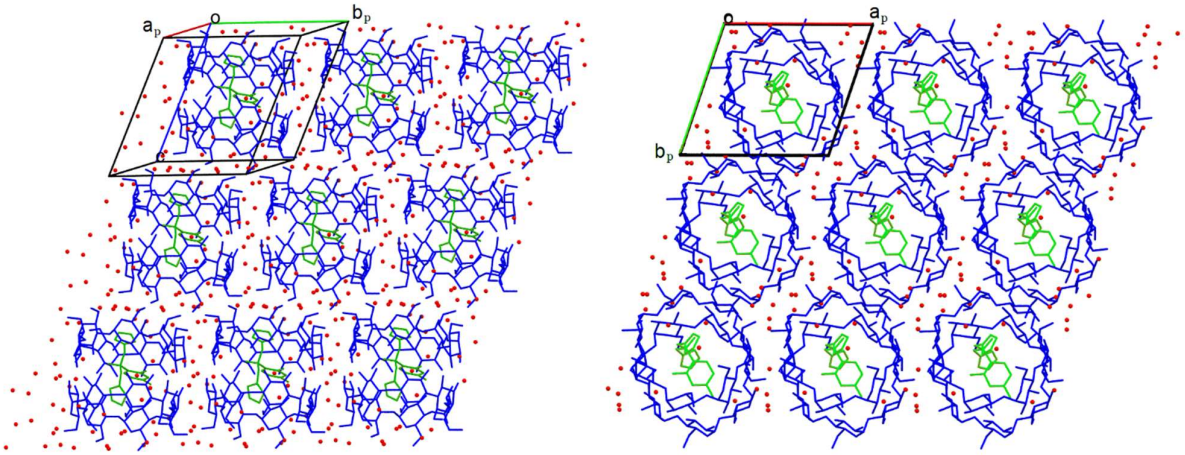

Figure 5.24: Two representations of TBCDFLU crystal packing. In green is reported the fluconazole molecule, in blue the cyclodextrin dimer and in red the oxygen atoms of the water molecules. On the left side is reported the view normal to the bc-face (from which the 'brick-cage' arrangement is very clear) and on the right side is reported the [001] projection of the crystal structure.

In *Figure 5.25* is reported the space-filling representation of a TBCDFLU cage which highlights the effective filling of the cavity by the guest. Several glucoside residues were removed to allow the visualisation of the fluconazole molecule.

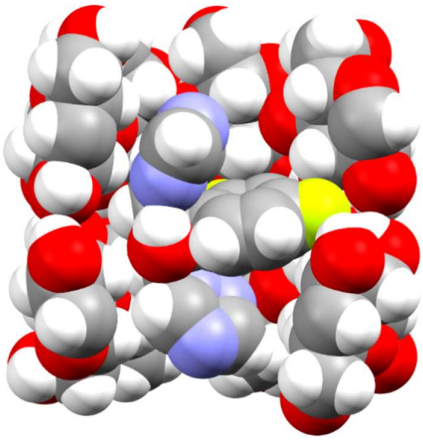

Figure 5.25: Space-filling representation of TBCDFLU (the upper cyclodextrin ring is the A molecule and the lower is the B molecule).

5.6.7) COMPARATIVE PXRD

The calculated PXRD trace from the refined model and the experimental pattern are reported in *Figure 5.26*. The degree of agreement is very high, corresponding peaks showing very similar profiles. However, it is also evident that several low-angle peak intensities in the experimental pattern have been adversely affected by preferred orientation effects in the sample.

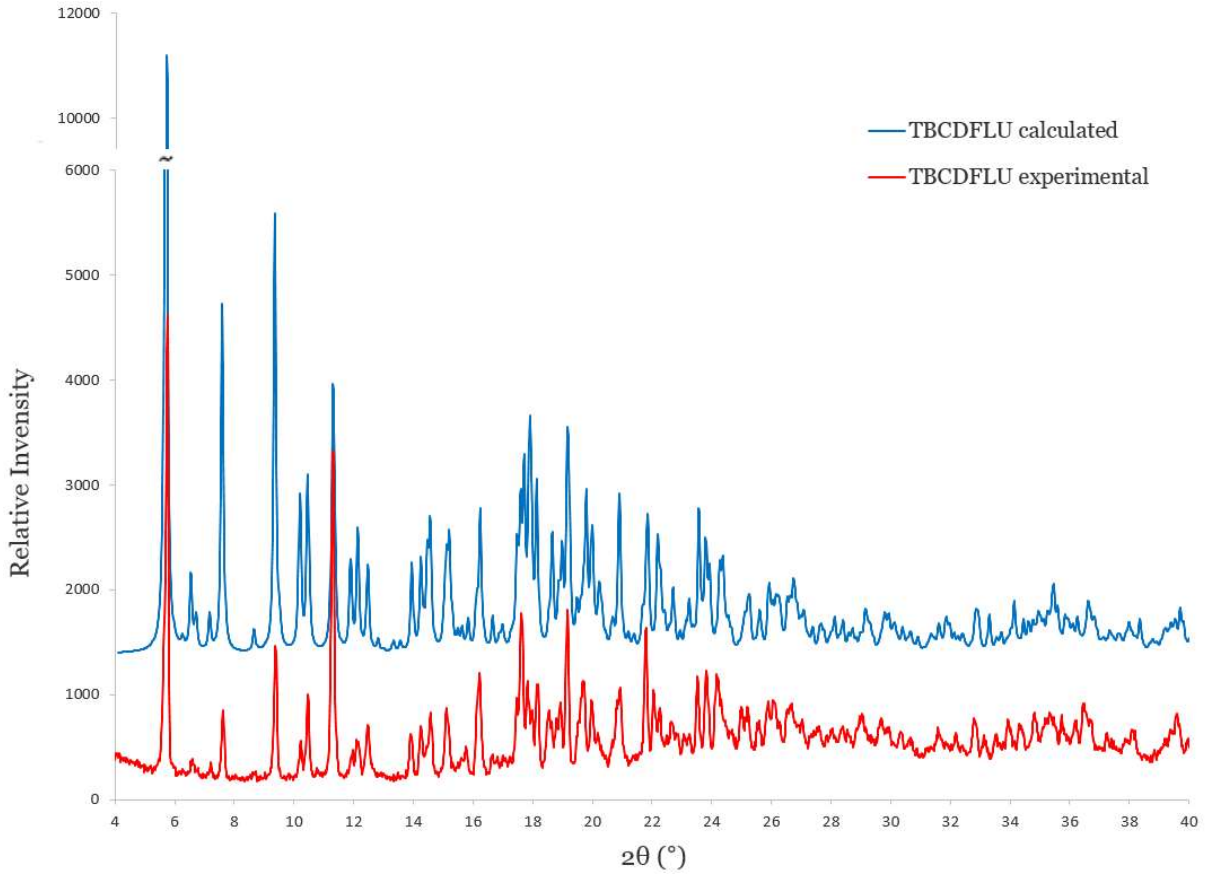

Figure 5.26: Calculated and experimental PXRD patterns for TBCDFLU.

5.7) PHASE SOLUBILITY ANALYSIS

The phase solubility studies were carried out only with fluconazole and β-CD and were performed according to the method described by Higuchi and Connors.[11] These authors

classified phase solubility profiles into two broad types, each with more than one sub-type, as follows:

A. The A-type presents an increase in the solubility of the drug with an increase in CD concentration and it can be divided into three sub-types. A_L has a linear increase, A_P deviates positively from linearity and A_N has a negative curve deviation due to a change in the physical nature of the solution.
B. The B-type profile indicates the formation of an insoluble complex in the solution. The sub-types (B_L and B_S) indicate, respectively, the formation of a completely insoluble complex and a complex with limited solubility.

Several series of dilutions of β-CD solutions (2, 4, 8, 12, 16, 20 mM) in water:EtOH (99:1 v/v) were prepared and an excess of fluconazole was added to a set of vials, each containing 3 ml of solution. The contents of the vials were magnetically stirred at 500 rpm for 36 h at the temperature of 299 ± 1 K. Each solution was then filtered through a 45 μm nylon filter and analysed by UV-Vis spectrophotometry. Measurements were performed in triplicate and average values of the absorbances at λ_{max} = 260 nm were recorded. The concentration of API was determined from the calibration curve in *Figure 5.27* (details of the procedures for obtaining the calibration data are provided in Chapter 2).

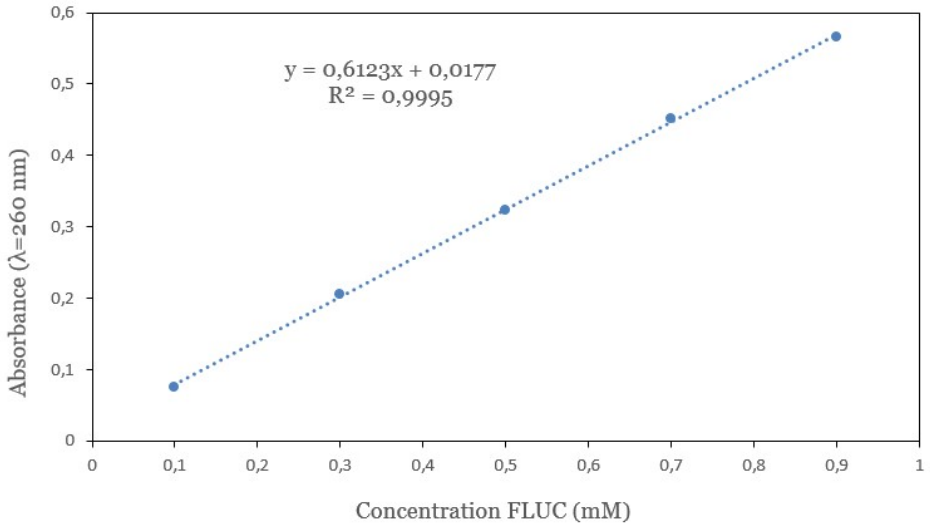

Figure 5.27: Calibration curve for the complex of β-CD and fluconazole (2:1).

With the Beer-Lambert equation (10), the extinction coefficient (ε_0) of fluconazole was found to be 627.85 M^{-1} cm^{-1}. This means that the API is strongly UV-active.

$$A = \varepsilon_0 cl \quad (10)$$

Each β-CD solution containing the fluconazole was filtered into a clean vial and rapidly diluted 1:20 with a solution of water:EtOH (99:1 v/v). The phase solubility profile (*Figure 5.28*) was based on the average of three different absorbance measurements per solution.

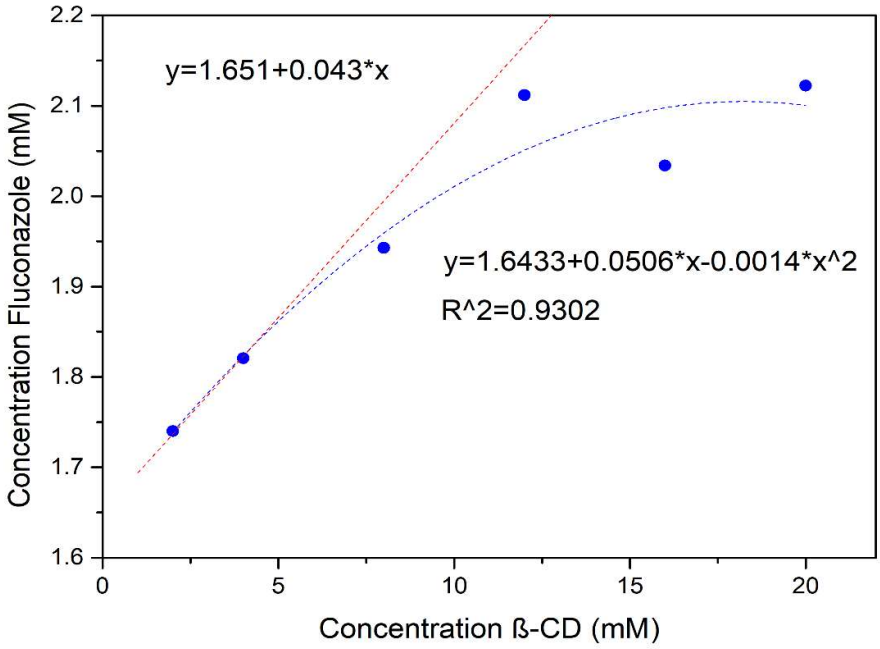

Figure 5.28: Phase solubility profile for the complex of β-CD and fluconazole. Notice that the requirement of linearity (in which the stoichiometric host-guest ratio is 1:1), useful for the calculation of the association constant K_c, is present only at a low concentration of host and guest.

The profile of phase solubility had a linear trend at low concentration, revealing a 1:1 complexation ratio between β-CD and fluconazole in solution. At high concentrations, there was a negative deviation from linearity with a second order polynomial trend. It indicated the formation of a complex with limited solubility. This result may be compared with results reported in a previous paper[12] where the phase solubility of fluconazole in β-CD using the same experimental procedure in pure water was investigated. The data were significantly different due to the change of solvent but the trend was very similar. The intrinsic solubility

(S_0) of the API at 299 ± 1 K (whose value is 1.651 mM) was extrapolated from the phase solubility profile. With these data it was possible to calculate the association constant (K_c) for the complex. This parameter was evaluated using the equation (11), which is applicable if the concentration is low and the stoichiometry of the CD-drug complex is 1:1.

$$K_C = \frac{slope}{S_0\,(1-slope)} \qquad (11)$$

The calculated value of K_c is 27.2 M^{-1}.

The association constant value reported in the previous paper[12] was very close to this result (22.2 M^{-1}). It is also necessary to bear in mind that the experimental conditions were very close to those employed in this work. The solutions were stirred in pure water for 48 h at 298 ± 1 K and they were analysed with a UV-Vis spectrometer (λ = 261 nm). The only difference was the concentration range spanned by the sets of solutions: in this work, the range was 2 mM to 20 mM, while in the previously reported one it was only 0 mM to 4 mM. The tendency of the complex is overall towards a B type, according to the Higuchi and Connors method. This means that at high concentrations the complex formed is less soluble than the one at low concentrations and for this reason the sub-type is Bs.

In the 20 mM β-CD solution, the concentration of fluconazole was 3.04 mM. The solubility of fluconazole in the 20 mM solution of β-CD was 0.9317 g/l. This result was compared with the fluconazole solubility in pure water (~1 mg/l)[1] and a ratio was calculated. The solubility enhancement factor of fluconazole was thus ~900. For this reason, it was possible to confirm a very significant improvement in the solubility of the API in the β-CD solution although the host-guest binding is very weak in solution. This result could be used in a future application to drug delivery. The β-CD was not the best solubiliser possible for a phase solubility experiment, since other types of cyclodextrins are more adapted for this analysis (e.g. HPBCD). The whole work in this chapter focuses on the host compound β-CD and therefore also the phase solubility analysis was carried out with the same type of solubiliser for completeness.

5.8) REFERENCES

1. Fluconazole, http://www.pubchem.ncbi.nlm.nih.gov, (accessed October 2017).
2. Z. Hoossen, Chemistry Honours project report, University of Cape Town, 2016.
3. Bruker AXS Inc., Program SAINT, Version 7.60a, Bruker AXS Inc., Madison, WI, USA, 2006.
4. G. M. Sheldrick, Program SADABS, Version 2.05, University of Göttingen, Germany, 2007.
5. Bruker AXS Inc., XPREP, Version 5.1, Bruker AXS Inc., Madison, WI, USA, 1997.
6. Cambridge Structural Database and Cambridge Structural Database system, Version 5.36 (updates to May 2017), Cambridge Crystallographic Data Centre, University Chemical Laboratory; Cambridge, England, 2014.
7. G. M. Sheldrick, *Acta Crystallogr. A.,* 2008, **64**, 112-122.
8. L. J. Barbour, *J. Supramol. Chem.,* 2001, **1**, 189-191.
9. K. Yvon, W. Jeitschko and E. Parthé, *J. Appl. Crystallogr.*, 1977, **10**, 73-74.
10. D. Mentzafos, I. M. Mavridis, G. Le Bas, G. Tsoucaris, *Acta Crystallogr.*, 1991, **B47**, 746.
11. T. Higuchi and K. A. Connors, *Adv. Anal. Chem. Instrum.,* 1965, **4**, 117-212.
12. J. Li, S. Zhang, Y. Zhou, S. Guan, L. Zhang, *J. Incl. Phenom. Macrocycl. Chem.*, 2016, **84**, 209–217.

CHAPTER 6

γ-CYCLODEXTRIN INCLUSION OF FLUCONAZOLE

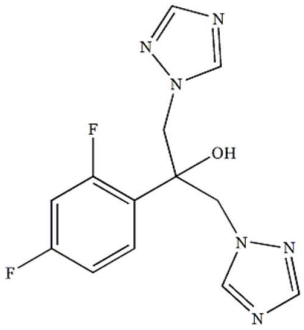

Fluconazole

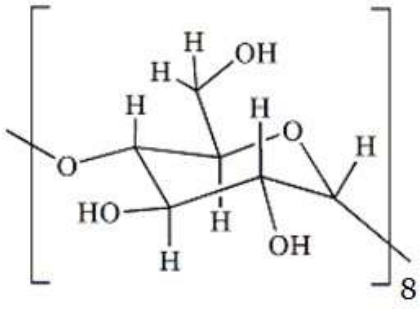

γ-cyclodextrin

6.1) EXPERIMENTAL

2 mg (6.53×10^{-6} mol) of fluconazole were kneaded for ~15 minutes with 9.31 mg (7.18×10^{-6} mol) of γ-cyclodextrin. A minimum amount of water (~25 μl) was added to minimise the quantity of solvent inside the system. The white powder which resulted from kneading was analysed using PXRD. A calculated trace from the isostructural series for γ-CD complexes[1] was compared with the trace experimentally recorded and it was concluded that the product was an authentic γ-CD complex containing fluconazole, hereafter referred to as GCDFLU. In *Figure 6.1* are reported comparative PXRD traces of GCDFLU and an isostructural γ-CD inclusion complex[1,2] to emphasise the effective success of the current kneading experiment. The close match of the common PXRD peaks not only indicates formation of an inclusion complex between γ-CD and FLU but enables assignment of its crystal system (tetragonal), space group ($P42_12$) and prediction of its unit cell dimensions as a ~ 23.8 Å, c ~ 23.1 Å. This illustrates the utility of exploiting isostructurality using the PXRD technique.

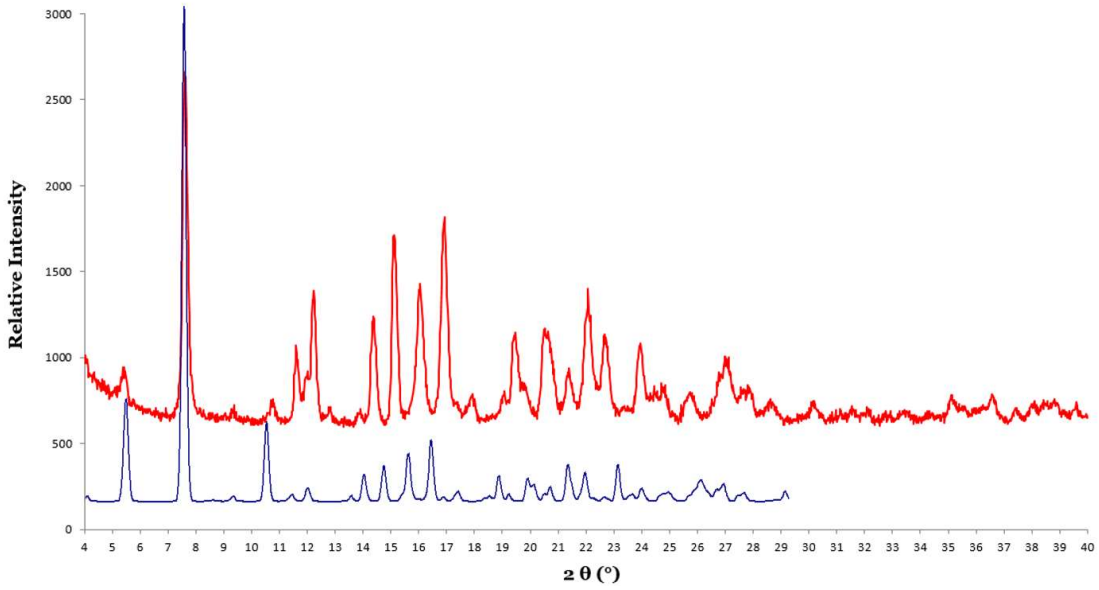

Figure 6.1: PXRD traces of GCDFLU (red) and an isostructural γ-CD inclusion complex (blue).[1, 2] *The two complexes belong to the space group $P42_12$.*

The same quantities of raw material were used for a co-precipitation attempt. The γ-CD was dissolved in ~400 µl of water at 60 °C with a gentle stirring. The fluconazole was added in small aliquots (~0.5 mg every hour) and the solution was maintained at 60 °C and stirred overnight (~12 h). The solution was filtered through a 0.45 µm nylon filter into a pre-heated vial and it was immediately incubated in a Dewar flask filled with water at 60 °C. The system was covered with alternate sheets of tinfoil and cotton wool to ensure the longest duration of incubation possible (~2 days). After this period, very small, tetragonally-shaped colourless crystals with square cross-section were obtained. The vial was exposed to the open air for two more days to permit the evaporation of solvent and the consequent enlargement of these crystals.

Referring to the situation found in *Paragraph 5.1* (Chapter 5), a comparison might be done here. Two more attempts with different temperatures of incubation were carried out to determine the dependence of the crystalline form of the new complex on the experimental conditions. A vial prepared for a co-precipitation attempt was cooled to an incubation temperature of 45 °C and a second replica was placed directly in water at ~ 20 °C. The results of all the experiments, independently of the temperature, yielded the same type of crystal complex. For this reason, it was possible to conclude that the incubation temperature was

not critical for isolating the single crystals of complex GCDFLU. The incubation procedure was used only to promote an enlargement of the size of the crystals.

6.2) NUCLEAR MAGNETIC RESONANCE SPECTROSCOPY

The stoichiometric ratio between γ-CD and fluconazole in the complex crystals was determined by ^{1}H-NMR spectroscopy. The ^{1}H-NMR spectrum of GCDFLU in DMSO-d_6 is reported in *Figure 6.2* and in *Table 6.1* all the peak integrations are presented.

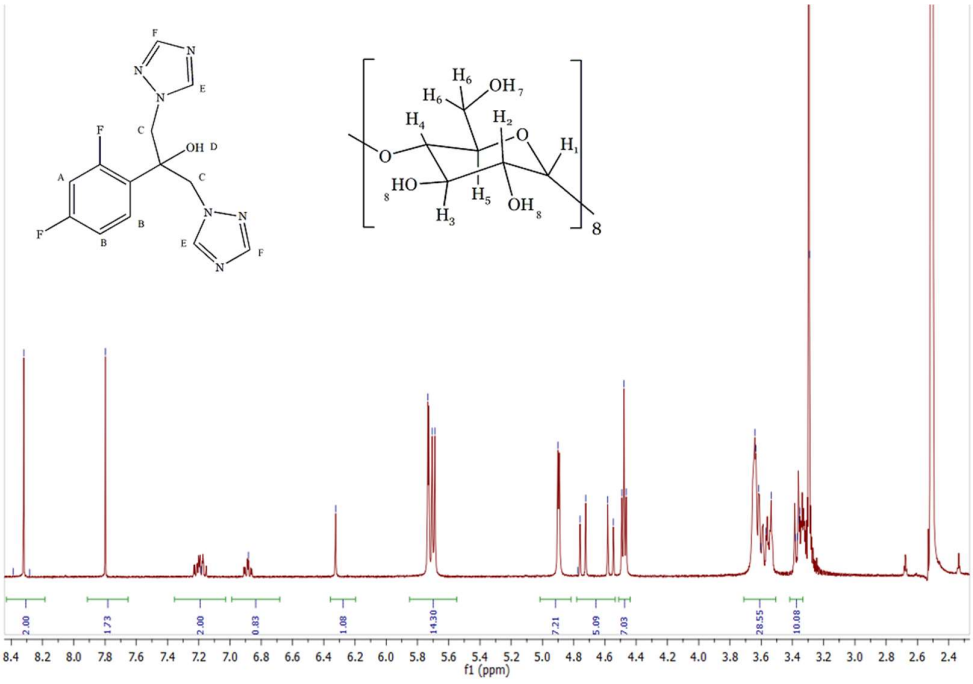

Figure 6.2: ^{1}H-NMR spectrum of GCDFLU in DMSO-d_6.

Table 6.1: ^{1}H-NMR peak integrations for GCDFLU.

Proton	δ (ppm)	Multiplicity	J (Hz)	Integration	Experimental/ Theoretical
H_E	8.32	s	/	2.00*	1.00
H_F	7.79	s	/	1.73	0.87
H_B	7.14-7.24	m	/	2.00	1.00
H_A	6.85-6.91	t of d	6.30; 1.50	0.83	0.83
H_D	6.32	s	/	1.08	1.08

H_8	5.66-5.76	d (x 2)	5.40; 2.10	14.30	0.89
H_1	4.85-4.94	d	3.00	7.21	0.90
H_C	4.53-4.78	q	42.30; 10.80	5.09	1.27
H_7	4.43-4.51	t	4.20	7.03	0.88
H_3, H_5, H_6	3.50-3.71	m	/	28.55	0.89
H_4	3.33-3.41	t	7.5	10.08	1.26

*reference integral

From the data above, it is evident that the integration of H_E (for the fluconazole) and the sum of the principal CD signals (H_3, H_4, H_5 and H_6) were in a 1:1 ratio. It was, however, difficult to assign certain signals. For the H_8 protons there was the presence of two different doublets; the proton assignment was not totally clear. The signal for H_2 completely overlapped with the one of water (3.2-3.3 ppm) and for this reason it was impossible to include it in the analysis. For accuracy, the last group of signals in the range 2.4-2.6 ppm was not analysed because it originated from the solvent (DMSO-d_6).

6.3) THERMAL ANALYSIS

Hot Stage Microscopy (HSM), Thermogravimetric Analysis (TGA) and Differential Scanning Calorimetry (DSC) were carried out on GCDFLU to evaluate all the possible behaviours at elevated temperatures.

6.3.1) HSM

A HSM experiment was conducted with a heating rate of 10 °C/min to establish the thermal stability of the complex GCDFLU. In *Figure 6.3* is reported the HSM experiment described above; the crystal was removed from mother liquor, put on a clean slide and covered with a small drop of silicone oil.

23.2 °C

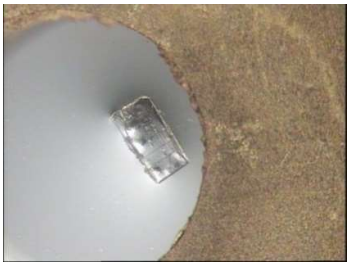

31 °C

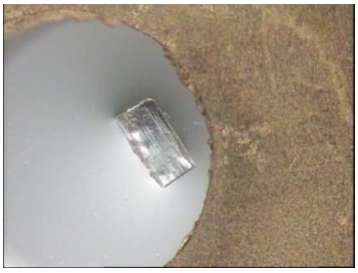

87 °C

122 °C

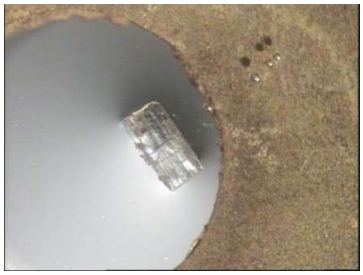

200 °C

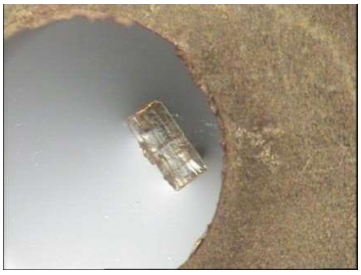

287.2 °C

305 °C

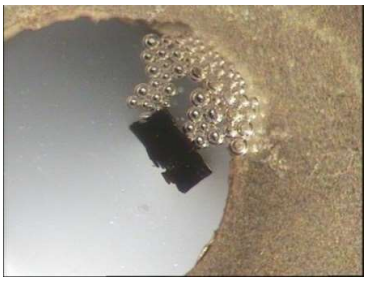

332.5 °C

Figure 6.3: HSM on GCDFLU (in red the temperature of commencement of degradation).

The crystal presented parallel cracks at low temperature (31 °C) that increased in number until 122 °C, the point at which the crystal began to dehydrate, as indicated by the appearance of bubbles. After the dehydration (122-200 °C) the crystal was stable until 278.2 °C (degradation point). It was possible to confirm that GCDFLU is thermally stable because the temperature of degradation of the complex was higher than both the melting point of fluconazole (138-140° C) and that of the degradation point of γ-cyclodextrin (267 °C).

6.3.2) TGA AND DSC

Thermogravimetric analysis was the only technique that was capable of measuring the exact number of water molecules per complex molecule in the crystal. Both TG and DSC traces are reported in *Figure 6.4*. The two curves confirmed the HSM test, showing only the dehydration event as a mass loss (TGA) and an endothermic peak (DSC). The decomposition peak was not recorded since the associated high temperature zone was not of practical interest.

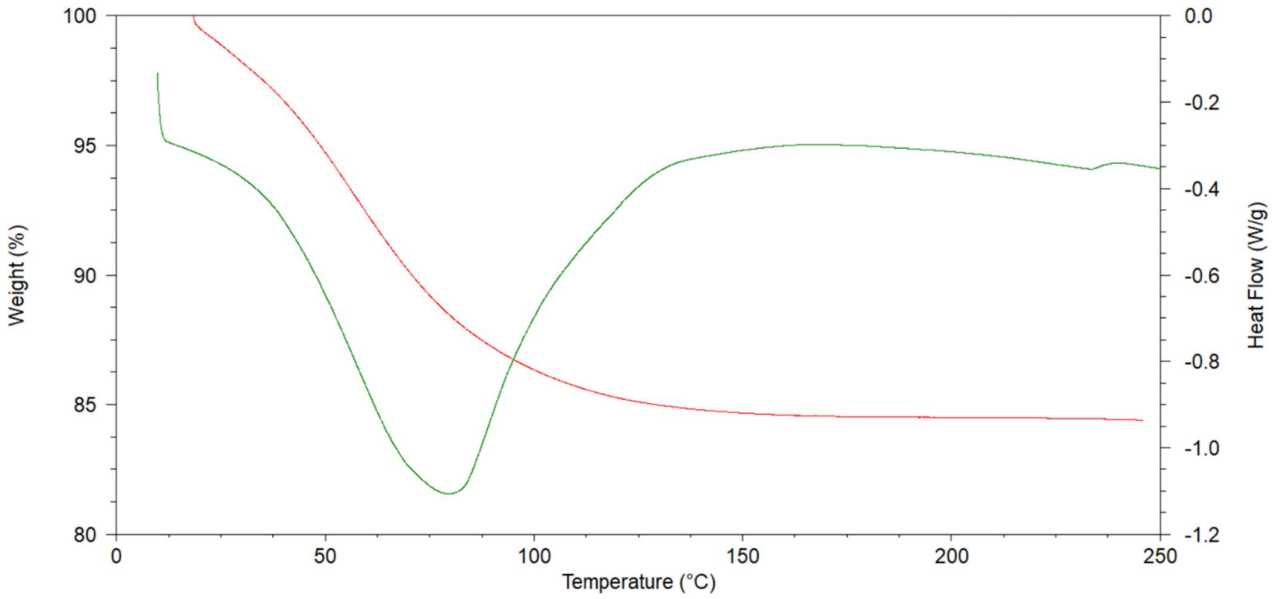

Figure 6.4: TG (red) and DSC (green) curves for GCDFLU.

The two curves shown in *Figure 6.4* were obtained from an average of five different analyses per technique. To establish the average number of water molecules per complex unit,

expression (12) was used. The percentage mass loss is 15.0 % ± 0.5 % and the stoichiometric ratio between host and guest from ^{1}H-NMR data is 1:1.

$$mass\ loss\ \% = \frac{n \times MW_{H_2O}}{MW_{\gamma-CD} + MW_{FLU} + (n \times MW_{H_2O})} \times 100 \quad (12)$$

The average number of water molecules was n = 15.7 ± 0.5. Thus, the formula for the complex GCDFLU can be expressed as γ-CD·FLU·15.7H_2O.

6.4) FOURIER TRANSFORM INFRARED SPECTROSCOPY

The FT-IR technique was not a diagnostic test but was useful to verify the complexation of the API by γ-CD. In *Figure 6.5* the FT-IR spectra of GCDFLU and its components are reported.

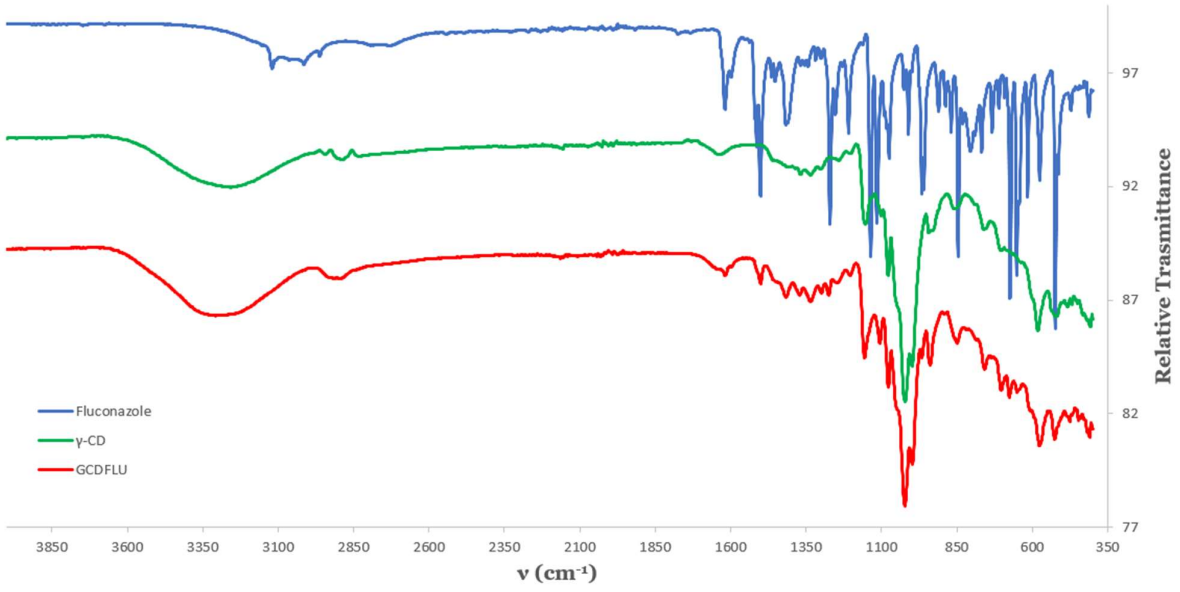

Figure 6.5: FT-IR spectra of the GCDFLU inclusion complex (red trace), γ-CD (green trace) and fluconazole (blue).

Notable observations include:

- the glycosidic bond stretching peak at ~1030 cm^{-1} occurred at the same frequency in both the host spectrum and the GCDFLU complex spectrum (also the relative transmittances were equal);
- the triazole aromatic bond stretching in the fluconazole spectrum (~1620 cm^{-1}) was present, with a lower intensity and it overlapped a signal of the γ-CD, also in the GCDFLU spectrum;
- the broad signal of water at 2990-3675 cm^{-1} had a bigger relative intensity in the complex spectrum than in the γ-CD spectrum;
- the signals in the range 632-873 cm^{-1} and the aromatic peaks at 1170-1500 cm^{-1} in the complex spectrum had a bigger relative transmittance than their counterparts in the γ-CD spectrum due to the API influence.

With some exceptions listed above, the GCDFLU spectrum might easily be superimposed on the γ-CD spectrum (*Figure 6.6*). This was a very important result because it was a clear signal of the complexation of the API.

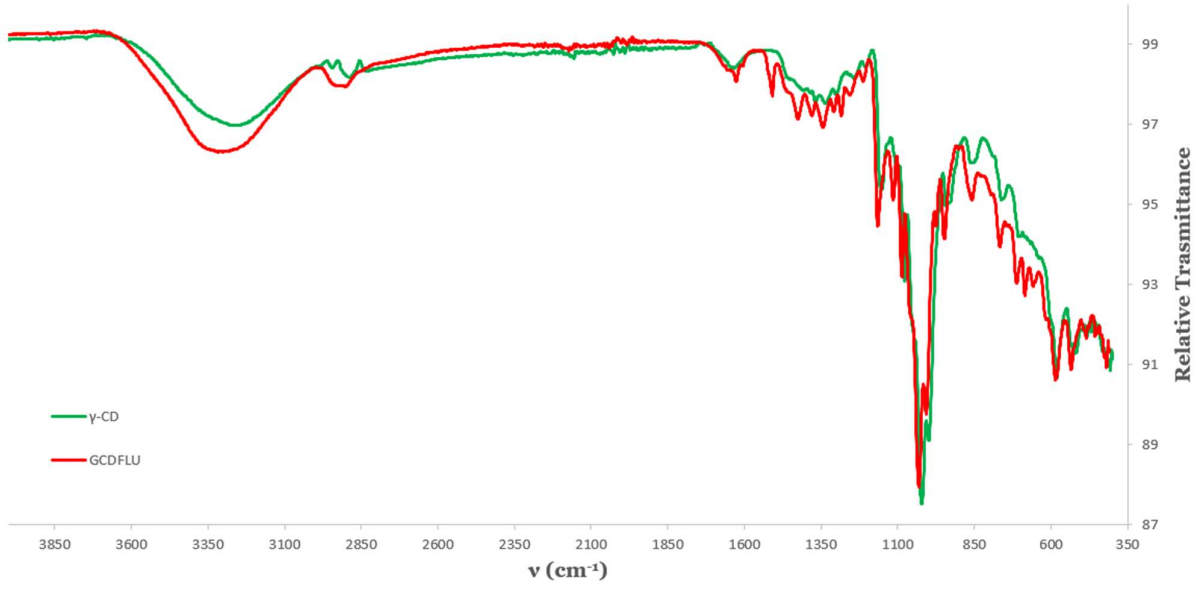

Figure 6.6: Overlay of the FT-IR spectra of the GCDFLU inclusion complex (red line) and the γ-CD (green line).

6.5) X-RAY ANALYSIS

The instrument used for the collection of the crystal reflection intensities was a Bruker KAPPA APEX II DUO single crystal X-ray diffractometer. The frames were integrated with the Bruker SAINT[3] software package and the data were corrected for absorption effects using the multi-scan method (SADABS).[4] The crystal system was found to be tetragonal and the space group $P42_12$ (as predicted using the PXRD technique) and subsequently confirmed by the program XPREP.[5]

The data-collection was performed at 100(2) K in order to obtain the best resolution, as it is known that the guest is frequently not discernible in γ-CD complex structures analysed at higher temperatures. The latter is due to the large size of the γ-CD cavity and its requirement of fourfold crystallographic rotational symmetry (and hence that of the guest molecule as well). These features thus promote guest disorder. The host structure was solved using isomorphous replacement with a CSD[6] structure as a trial model (SIBJAO). The refinement was carried out with SHELXL-97[7] though the X-Seed interface.[8] The asymmetric unit of the complex consists of three, crystallographically independent host fragments (each comprising two glucose units, guest and water molecules). When the fourfold rotation operation is applied to the three host fragments, three independent host molecules (A, B, C) are generated.

The water molecules are principally located between the host molecules. The guest was physically complexed by the host but the electron density inside the cavity was very low (maximum ~ 1.03 $eÅ^{-3}$). The peaks had poor intensity values and they were severely fragmented. This was associated with the effect of the high symmetry (a fourfold rotation axis along the crystallographic *c*-axis) and it led to a classical situation for γ-CD complexes structures: the impossibility of resolving the structure to a satisfactory level of refinement. Another problem was the total count of water molecules inside the structure. Although the number of water molecules contained in the structure was calculated from TGA to be 15.7 molecules, the total sum of the s.o.f.s (site-occupancy factors) for the oxygen atoms related to water molecules was calculated to be 11.7. Due to these typical shortcomings, all the existing data for GCDFLU (including the complex formula in *Table 6.2*) were obtained from the analysis described above. The evidence for the difference between the thermal analysis estimate and that for the refined model is recorded in the checkCIF report file, located in the Appendix section. Consequently, an important (but expected) "A alert" refers to a significant

discrepancy between the calculated and the experimental formula weights. In the electronic Appendix are provided all the files related to the current structure for the sake of completeness.

In *Table 6.2* are reported the data-collection and refinement parameters for the GCDFLU complex.

Table 6.2: Data-collection and refinement parameters for GCDFLU.

Abbreviated formula	γ-CD · FLU· 15.7 H_2O
Complex formula	$C_{48}H_{80}O_{40} \cdot C_{13}H_{12}F_2N_6O \cdot 15.7H_2O$
Formula weight (g mol^{-1})	1886.3
Data collection temperature (K)	100(2)
Crystal system	Tetragonal
Space group	$P42_12$
a (Å)	23.737(3)
c (Å)	23.155(3)
V ($Å^3$)	13047(5)
Z	6
ρ_{calc} (g/cm^3)	1.440
μ (mm^{-1})	0.131
F (000)	6018.0
Crystal size (mm)	0.22 x 0.24 x 0.26
Radiation (Mo Kα)	λ = 0.71073
Range scanned θ (°)	1.23 – 24.98
Index ranges ±*h*, ±*k*, ±*l*	$-11 \leq h \leq 28$, $-27 \leq k \leq 19$, $-27 \leq l \leq 27$
Reflections (total)	48809
Independent reflections	11480
Reflections with $I > 2\sigma(I)$	8100
Parameters	644
R_{int}	0.0518
R_1 [$I > 2\sigma(I)$]	0.1286

wR_2 [$I > 2\sigma(I)$]	0.3546
Goodness-of-fit, S	1.477
a, b in $w = 1/[\sigma^2(F_o^2)+(aP)^2+(bP)]$	a = 0.2, b = 0.0
$\Delta\rho_{min,\ max}$ (e Å^{-3})	-0.96 and 1.03

The PART command was used extensively to remove false atom connectivities on guest and water molecules. In *Table 6.3*, the primary oxygen atoms disordered over two positions are reported (with their relative s.o.f.s). The C-O bond lengths for these pairs of atoms were fixed with a DFIX restraint at 1.440(1) Å (except for C6G1-O6G1) whereas the distances between the oxygen atoms of water molecules were fixed with a DFIX restraint at 2.80(5) Å. Two pairs of water molecules affected by disorder were O9···O11 and O6···O12 (with s.o.f.s of 0.85 and 0.67, respectively). For the O9···O11 pair it was necessary to impose a DFIX restraint. All the disordered oxygen atoms are shown graphically in *Figure 6.7*.

The hydrogen atoms of the host molecules were placed geometrically with the 'generate HFIX' command of the X-Seed interface[8] and their U_{iso} values were maintained in the range 1.2-1.5 times the thermal parameters of their parent atoms. The residual positive electron density peak of 1.03 Å^{-3} was located near O7G5.

Table 6.3: Primary oxygen atoms disordered over two positions with relative s.o.f.s and indication of the imposition of a restraint on the C-O bond.

C atom	O atom	DFIX	s.o.f.
C6G1	O6G1	no	0.53
	O7G1	yes	0.47
C6G3	O6G3	yes	0.68
	O7G3	yes	0.32
C6G5	O6G5	yes	0.69
	O7G5	yes	0.31

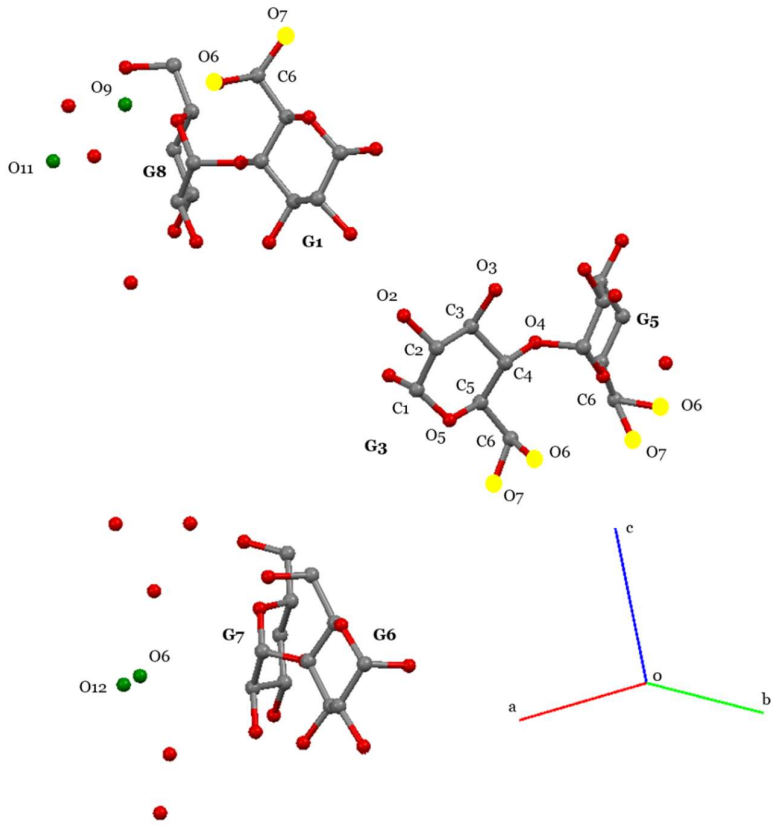

Figure 6.7: Graphical representation of disordered primary oxygen atoms in GCDFLU host structure (yellow spheres). Green spheres represent disordered water molecules. For simplicity, only the asymmetric unit is shown and all hydrogen atoms have been omitted.

The three independent molecules (A, B and C) form a channel packing arrangement. Each channel is centred on the fourfold rotation axis (in turn parallel to the crystallographic *c*-axis). When the structure is viewed along the *b*-axis it is possible to notice a slight vertical shift between the channels. This arrangement is typical of the space group $P42_12$ for γ-CD complex crystal structures and it is reported in *Figure 6.8*. The typical interactions that maintain the host molecule arrangement are O-H···O hydrogen bonds. In *Figure 6.9* a schematic representation of the host channels along the crystallographic *b*-axis is shown. The O-H···O hydrogen bond interactions occur between the respective cyclodextrin rims in the order tail-to-tail, head-to-head, and tail-to-head (respectively for A-B, B-C, C-A).

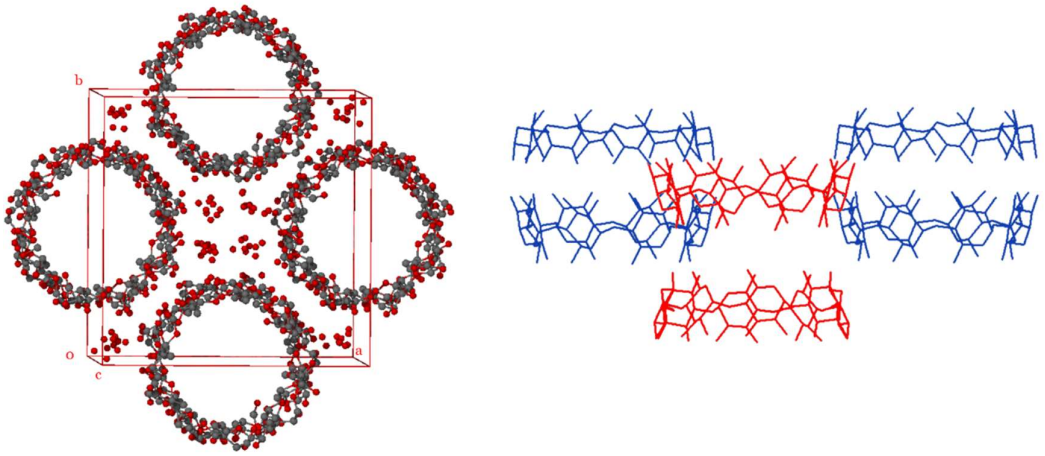

Figure 6.8: Channel structure of γ-CD in GCDFLU viewed nearly parallel to the c-axis (left) and along the b-axis (right). The image on the right has been coloured in order to emphasize the shift between channels.

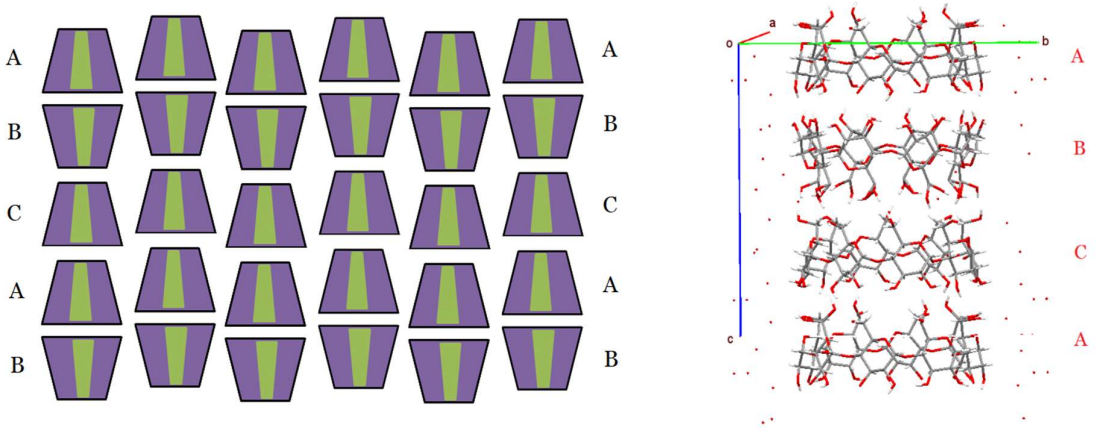

Figure 6.9: Schematic ABC packing motif of γ-cyclodextrin molecules for GCDFLU viewed along the a-axis. (On the right side the red dots represent the oxygen atoms of water molecules).

Due to the absence of a complete model from the single crystal X-ray analysis, it was not justified to compare a calculated PXRD pattern with the one obtained from the complex prepared by kneading, the latter being reported in *Figure 6.10*. This figure shows the traces for the starting components of the kneading experiment and that of the complex product.

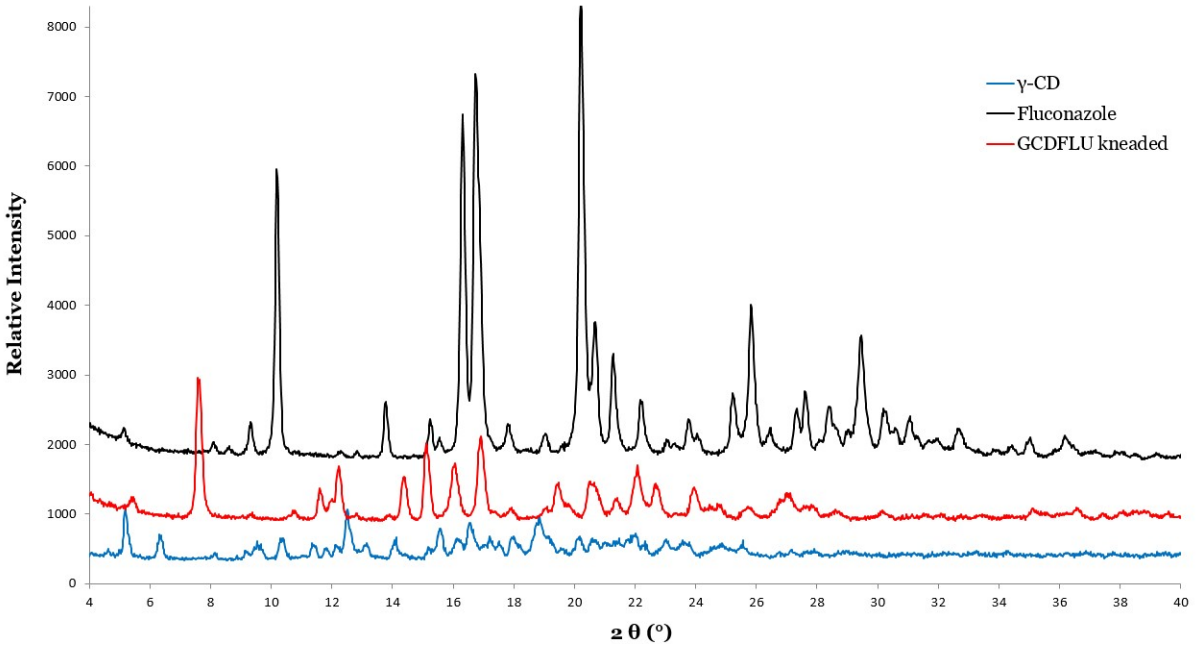

Figure 6.10: PXRD pattern of GCDFLU obtained by kneading (red), compared with pure γ-CD (blue) and fluconazole (black) PXRD patterns. Traces have been mathematically rescaled to facilitate the comparison.

Although the guest molecule cannot be visualised, the analyses carried out have revealed the complete stoichiometric formula of the hydrated inclusion complex and, from single crystal X-ray data, it was possible to be able to describe completely the host arrangement in the crystal and the role of the water molecules. From a pharmaceutical point of view, the data accumulated are very valuable since the complex has potential application for drug delivery. However, the data collected are not sufficient to fully express this potential. For this reason, more tests would need to be done in the future (e.g. solubility measurements and/or bioavailability studies).

6.6) REFERENCES

1. M. R. Caira, *Rev. Roum. Chim.*, 2001, **46**, 371-386.
2. S. Lubhelwana, Crystal isostructurality and X-ray diffraction studies of cyclodextrin inclusion compounds, 2005, MSc dissertation, University of Cape Town, South Africa, p.79. (https://open.uct.ac.za/handle/11427/6324, accessed Nov 2017).
3. Bruker AXS Inc., Program SAINT, Version 7.60a, Bruker AXS Inc., Madison, WI, USA, 2006.
4. G. M. Sheldrick, Program SADABS, Version 2.05, University of Göttingen, Germany, 2007.
5. Bruker AXS Inc., XPREP, Version 5.1, Bruker AXS Inc., Madison, WI, USA, 1997.
6. Cambridge Structural Database and Cambridge Structural Database system, Version 5.36 (updates to May 2017), Cambridge Crystallographic Data Centre, University Chemical Laboratory; Cambridge, England, 2014.
7. G. M. Sheldrick, *Acta Crystallogr.*, 2007, **64**, 112-122.
8. L. J. Barbour, *J. Supramol. Chem.*, 2001, **1**, 189-191.

CHAPTER 7

CONCLUSIONS

A summary of all the results obtained in this study together with further comments are presented in this chapter. Two known active pharmaceutical ingredients (APIs) of widespread use were modified *via* crystal engineering and supramolecular derivatization techniques. Four cyclodextrin (CD) inclusion complexes were isolated. A full characterization, including single crystal X-ray structures, was carried out for two CD complex crystals. In the other cases, limitations of molecular disorder prevented full structural characterization, but under these conditions the best possible X-ray analyses were performed.

7.1) SULFASALAZINE

This anti-inflammatory drug presented the phenomenon of tautomerism. It was possible to prepare and exploit an amine (A-SSZ) and an imine (I-SSZ) form of the drug. Both forms were isolated via re-crystallization in a proper solvent. A-SSZ (CCDC refcode QIJZOY) was stable in absolute ethanol 98% (EtOH) or pure 2-butanone (methyl ethyl ketone, MEK) and I-SSZ (CCDC refcode QIJZOY01) was stable in acetone and tetrahydrofuran (THF). Both tautomers were orange crystalline powders (I-SSZ had a darker colour than A-SSZ).

Several attempts were made to study the co-crystallization of both SSZ tautomers with a large number of co-formers. Attempts with lidocaine (an anaesthetic API), urea and citric acid turned out to be the most relevant. Only the products from experiments with A-SSZ were analysed by PXRD (due to their crystalline character) since products obtained using I-SSZ were all amorphous. The results showed an uncommon effect derived from LAG (Liquid-Assisted Grinding) that induced A-SSZ to transform into I-SSZ during the grinding process (the latter was conducted in a solvent appropriate to each tautomer). During this process, the specific co-former being employed for possible co-crystallization became amorphous. This unexpected effect undermined efforts to achieve the desired reactions, and for this reason no new co-crystal phases were obtained with SSZ. Certainly, further

experiments such as mechanochemical co-grinding would be appropriate for understand this SSZ behaviour. To obtain a single crystal, many attempts were carried out with very slow crystallization techniques in solution (low temperatures or evaporation rates of solvents) trying to avoid the formation of the amorphous phase observed with the mechanochemical approach. A large number of experiments, with compounds listed above, were carried out for a total of 68 attempts. These processes required some months of work and, for this reason of time constraints, further experiments were not performed and they should be carried out in the future.

A cyclodextrin inclusion complex of γ-CD with SSZ was isolated when the CD was reacted with the tautomer I-SSZ. From thermogravimetric (TG) analysis it was possible to obtain the water mass loss (13.4% ± 0.1 %) and hence calculate the number of water molecules contained in each complex structural unit (n = 15.0 ± 0.3). The stoichiometric ratio between host and guest was confirmed as 1:1 by ^{1}H-NMR analysis. Due to the lack of single crystals of the complex it was possible to determine only the full stoichiometric chemical formula of the complex, namely $C_{48}H_{80}O_{40} \cdot C_{18}H_{14}O_5N_4S \cdot 15\ H_2O$. The degradation point of this crystal was found to occur at a temperature of 240 °C.

7.2) FLUCONAZOLE

Due to the presence in the literature of several reports of co-crystals of this antifungal API, only attempts to include the drug in CDs were carried out. Three CD inclusion complexes were isolated and fully characterized: two with β-CD and one with γ-CD.

The two inclusion complexes with β-CD were obtained simply by changing the concentration of the drug or the temperature of the medium in which the crystallization was performed. Two distinct single crystals were analysed using SCXRD and two different structural models were elaborated. The first structure (partially analysed in a previous study[2] in 2016), was found to be triclinic (TBCDFLU) and it was re-modelled and completely refined. The second was found to be monoclinic (MBCDFLU). The packing arrangements in these crystal forms were completely different, namely a brick-cage packing for TBCDFLU and head-to-head channel packing for MBCDFLU. The thermogravimetric analysis was problematic due to the relatively rapid loss of water of crystallization from these complexes. As a preliminary study, a timed dehydration test was carried out. MBCDFLU dehydrated spontaneously in 12 seconds while TBCDFLU was stable. In order to prevent the loss of water from MBCDFLU

and to obtain consistent results, all TGA experiments were carried out with the samples immersed in silicone oil. The percentage mass loss was 16.6% ± 1.6% for MBCDFLU and 15.3% ± 0.8% for TBCDFLU. From *^{1}H-NMR* spectroscopic analysis of dissolved crystals the stoichiometric ratio CD:API for the two complexes was established as 2:1. With this information, it was possible to determine the chemical formulae for the two complexes, namely $(C_{42}H_{70}O_{35})_2 \cdot C_{13}H_{12}ON_6F_2 \cdot 21.3\ H_2O$ for MBCDFLU and $(C_{42}H_{70}O_{35})_2 \cdot C_{13}H_{12}ON_6F_2 \cdot 27.3\ H_2O$ for TBCDFLU. It was thus possible to confirm the distinct nature of the two crystal forms in terms of their molecular and crystal structures, water contents and tendencies for dehydration. Following dehydration, the final degradation temperatures of the resulting anhydrous complexes were also different, namely 308 °C and 320 °C respectively. A phase solubility study was performed according to the method described by Higuchi and Connors[3] to determine the formation constant of the complex in solution. A value of 27.2 M^{-1} was obtained.

In the literature a similar case to that found with TBCDFLU and MBCDFLU was reported previously: a methylparaben molecule was included in β-CD and two structurally different complexes were isolated.[4] It is remarkable that the procedures of isolation and the structures of the crystals are very similar to those for the fluconazole complexes, described in this dissertation. The latter complexes may be considered more relevant for two reasons. The first is the potential pharmaceutical application: fluconazole is a common antifungal drug, whereas methylparaben is an excipient used in drug and other formulations. The second reason relates to the operational time for isolating the crystals: in the paper describing the methylparaben complexes[4] the times varied from one week to one month, whereas in the case of the fluconazole complexes, it was possible to isolate both forms in 2-3 days.

The third and last complex of fluconazole was obtained with γ-CD as host. The preparative procedure was the same as that for the β-CD complex. The single crystal obtained was subjected to X-ray analysis and was found to be tetragonal (space group $P42_12$). The refined model comprised the host molecules and water molecules only, because it was impossible to find the significant difference electron density peaks of the guest inside the cavities of the host molecules (a common occurrence with γ-CD complexes). The crystal packing was organized in channels constructed from repeating units of three stacked crystallographically independent host molecules. The thermal analysis with HSM indicated the degradation point at 278 °C. The water mass loss of a sample analysed by TGA was 15.0 % ± 0.5 %. The stoichiometric ratio between the CD and the API, determined by *^{1}H-NMR* spectroscopic

analysis, was found to be 1:1. The combined data yielded the chemical formula for the complex, namely $C_{48}H_{80}O_{40} \cdot C_{13}H_{12}F_2N_6O \cdot 16H_2O$.

7.3) FUTURE WORK

Due to the lack of time phase solubility studies were carried out with fluconazole and only one cyclodextrin, namely β-CD. In the future, more extensive phase solubility experiments using a wide variety of CD hosts are envisaged. Further tasks would include also the completion of the refinement of the MBCDFLU model by the addition of hydrogen atoms to the water molecules and the drafting of a manuscript for publication on the topic presented in Chapter 5.

Although the GCDFLU X-ray model is incomplete due to severe guest disorder, the inclusion complex is nevertheless well characterized chemically, and from a pharmaceutical point of view the results obtained are very valuable for possible applications in drug delivery. In future, further assessment (e.g. solubility and stability measurements, bioavailability studies) would be required to evaluate its potential in this regard.

7.4) REFERENCES

1. G. M. Sheldrick, *Acta Crystallogr. A.,* 2008, **64**, 112-122.
2. Z. Hoossen, Chemistry Honours Project Report, University of Cape Town, 2016.
3. T. Higuchi and K. A. Connors, *Adv. Anal. Chem. Instrum.,* 1965, **4**, 117-212.
4. M. R. Caira, E. J. C. de Vries, L. R. Nassimbeni, *Chem. Commun.*, 2003, 2058-2059.

APPENDIX

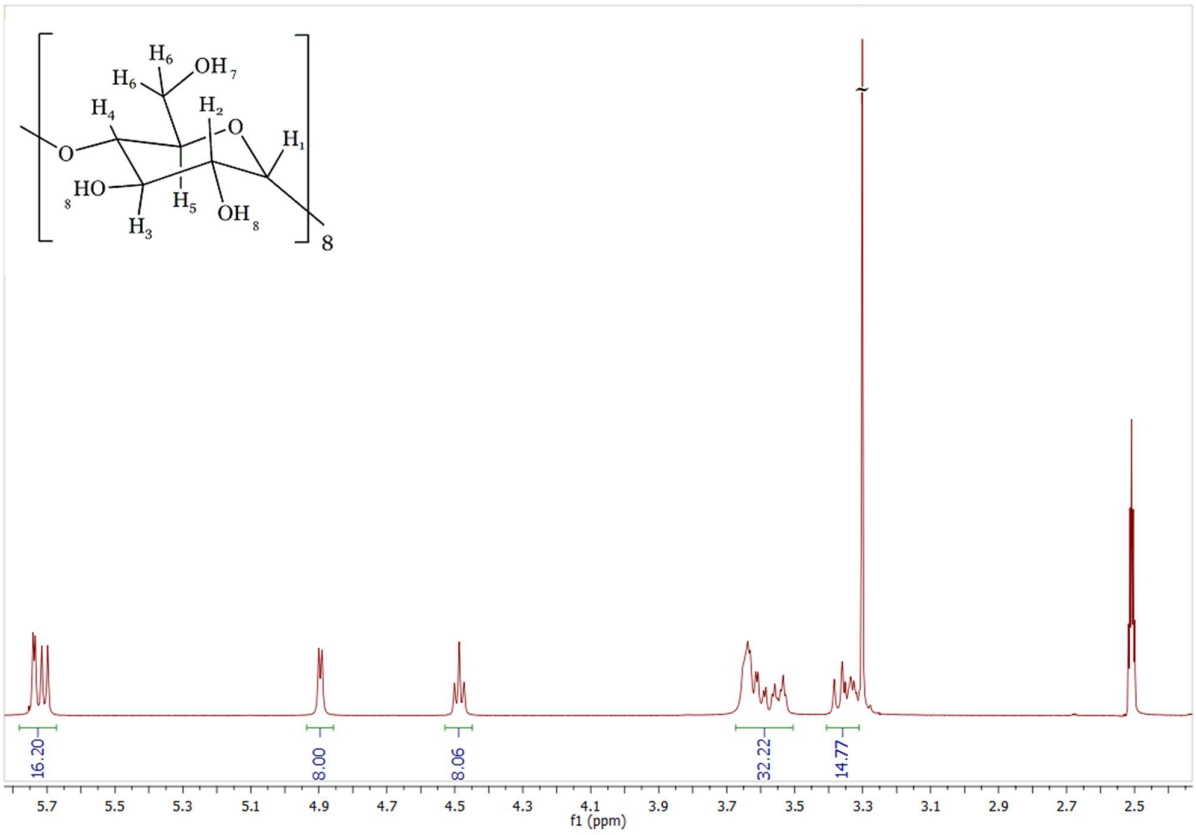

Figure A1: ^{1}H-NMR spectrum of pure γ-CD in DMSO-d_6.

Table A1: ^{1}H-NMR integration peaks for pure γ-CD.

Proton	δ (ppm)	Multiplicity	J (Hz)	Integration	Experimental/ Theoretical
H_8	5.67-5.76	d (x 2)	2.1; 5.1	16.20	1.01
H_1	4.87-4.92	d	2.7	8.00*	1.00
H_7	4.45-4.52	t	2.1	8.06	1.01
H_3, H_5, H_6	3.51-3.68	m	/	32.22	1.01
H_2, H_4	3.31-3.40	m	/	14.77	1.06

*reference integral

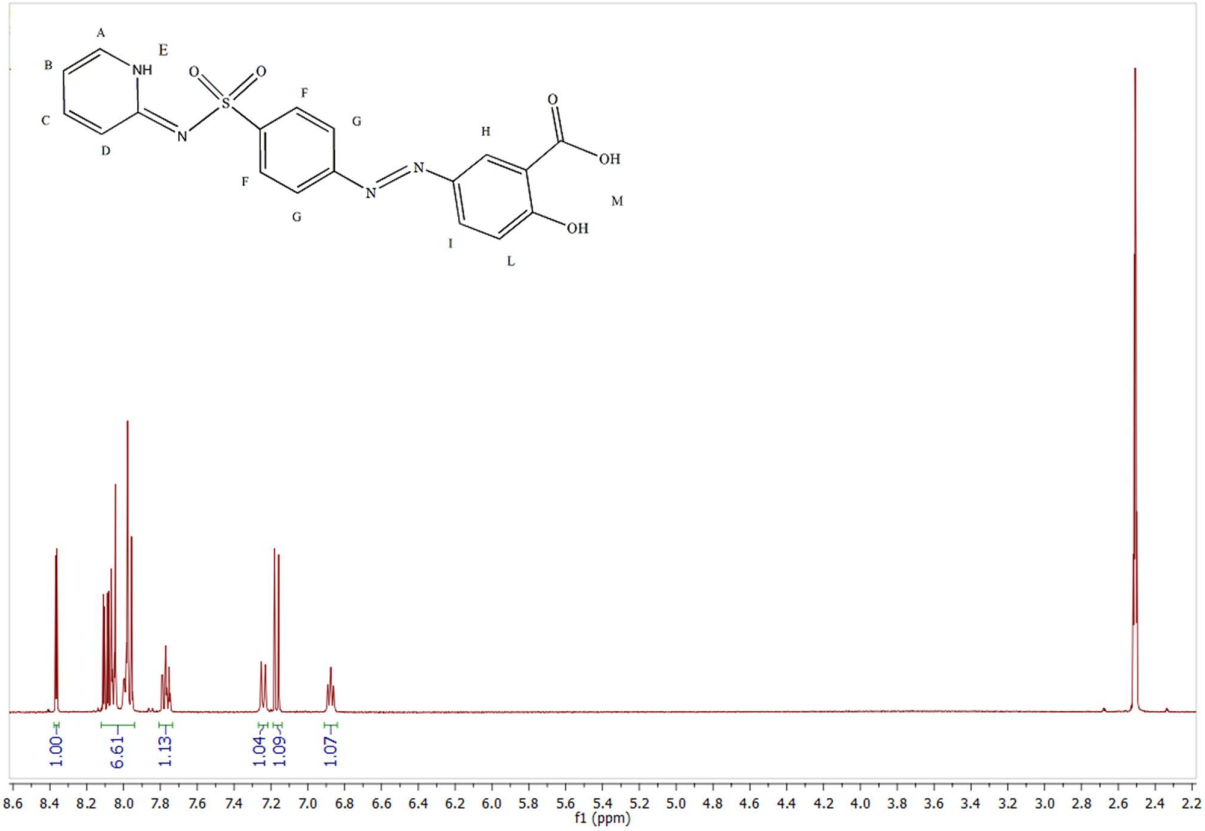

Figure A2: ^{1}H-NMR spectrum of pure I-SSZ in DMSO-d_6.

Table A2: ^{1}H-NMR integration peaks for pure I-SSZ.

Proton	δ (ppm)	Multiplicity	J (Hz)	Integration	Experimental/ Theoretical
H_H	8.35-8.38	d	1.8	1.00*	1.00
H_A, H_F, H_G, H_I, H_L	7.93-8.12	m	/	6.61	0.94
H_C	7.74-7.80	m	/	1.13	1.13
H_E	7.22-7.27	d	3.3	1.04	1.04
H_D	7.15-7.19	d	6.6	1.09	1.09
H_B	6.85-6.91	m	/	1.07	1.07

*reference integral